THEME [ENERGY.2012.7.1.1] Integration of Variable Distributed Resources in Distribution Networks

(Deliverable 3.3)

Advanced Local Distribution Grid Monitoring / State-Estimation

Lead Beneficiary:

INESC Porto

Table of Contents

List of Figures

List of Tables

List of Acronyms and Abbreviations

AANN	Auto-associative neural networks
AMI	Advanced Metering Infrastructure
AMM	Advanced Metering Management
CB	Circuit Breaker
CC	Control Centre
CL	Controllable Load
DG	Distributed Generation
DMS	Distribution Management Systems
DoW	Description of Work
DSE	Distribution State Estimation
DSM	Demand Side Management
DSO	Distribution System Operator
DT	Distribution Transformer
DTC	Distribution Transformer Controller
EB	Smart Meter
EMS	Energy Management Systems
EPSO	Evolutionary Particle Swarm Optimization
GPS	Global Positioning Systems
HLRR	Hidden Layer Reduction Rate
HMI	Human-Machine Interface
HV	High Voltage
IED	Intelligent Electronic Device
LV	Low Voltage
MV	Medium Voltage
PCA	Principal Component Analysis
PMU	Phasor Measurement Units
POCS	Projection Onto Convex Sets
PV	Photovoltaic Unit

RPROP	Resilient Back-Propagation
RTU	Remote Terminal Unit
SCADA	Supervisory Control and Data Acquisition
SAS	Substation Automation System
SE	State Estimation
SM	Smart meter
SSC	Smart Substation Controller
TSO	Transmission System Operator
WF	Wind Farm
WLS	Weighted Least Square

AUTHORS:

Authors	Organization	Email
Jorge Pereira	INESC Porto	jpereira@inesctec.pt
Pedro Pereira Barbeiro	INESC Porto	pedro.p.barbeiro@inesctec.pt
Henrique Teixeira	INESC Porto	henrique.s.teixeira@inesctec.pt
George Korres	ICCS/NTUA	gkorres@cs.ntua.gr
Xygkis Themistoklis	ICCS/NTUA	txiggs@hotmail.com
Manousakis Nikolaos	ICCS/NTUA	manousakis_n@yahoo.gr
Despina Koukoula	ICCS/NTUA	kdespina@power.ece.ntua.gr
Panayotis Moutis	ICCS/NTUA	Pmoutis@power.ece.ntua.gr

Access:		
	Project Consortium	
	European Commission	
	Public	X

Status:		
	Draft version	
	Submission for Approval	
	Final Version	X

1 Introduction

Description of the Task 3.3 "Advanced Local Distribution Grid Monitoring / State-Estimation" from the DoW (section 3.3.1)

Task 3.3 Advanced local distribution grid monitoring / state-estimation (Task leader: INESCP; ICCS)

In this task, a robust approach to distribution state estimation will be developed with enough robustness to face lack of information collected from the smart meters or RTU located in the grid by using additional historical information stored in the system data base.

The following sub-tasks are envisaged:

• Sub-Task 3.3.1 – MV grid topology identification using multiple data sources (including namely the information collected from the smart metering support infrastructure)

The correct network topology will be identified by using status information of switching devices, real-time analogue measurements, pseudo measurements (forecasted or historical load data) and virtual measurements (zero injection nodes, operational constraints of open/closed switching devices, radiality constraints), and any available information from smart metering equipment. A generalized probabilistic optimization formulation will be used to identify network topology. Statistical tests will be made to identify inconsistencies among analogue and digital information and eliminate any bad data. Opening switching operations may cause network splitting and the state variables in all the resulting islands will be determined by adding appropriate operating constraints in the state estimation formulation. The proposed approach will eliminate the need of repeated state estimation runs for alternative hypothesis evaluation.

• Sub-Task 3.3.2 – MV grid state estimation in distribution grids using smart metering information

Different state estimation formulations will be investigated for the best exploitation of the information from Advanced Metering Infrastructure (AMI) and Smart Global Positioning Systems (GPS) and synchronized Phasor Measurement Units (PMU) devices. Smart meters connected to a node, make time synchronized measurements of the active and reactive loads at predefined time intervals. These measurements will be transmitted to a database server periodically. This makes sure that the state estimator will have, at least, previous day's measurements of all the loads.

To facilitate the computation burden of the enormous volumes of data produced from the smart meters and the load forecasting algorithms, distributed processing will be implemented, by dividing the network into several zones. The zones will perform local estimation that leads to global estimation through information exchange, coordination and communication among them.

To assure accurate distribution voltage estimations and minimize the estimated voltage uncertainty, identification of the minimum number and location of additional voltage and current sensors in the network is needed.

In each of these subtasks, a pre-prototype of the software tool will be developed and validated. A specification of the database and data communications requirements will be established and will feed the operational phase.

The advanced local distribution grid monitoring / state estimation will be based at the top level of the system architecture (central systems) and also at the HV/MV substation having as input information gathered from lower levels of the architecture.

Hence, equipment deployed must not only have a great deal of processing capability but also be able to collect data from local sensors. Also, an adequate and flexible communication link must be guaranteed. For this functionality, several data acquisition points are required so that enough redundancy is assured to make the state estimation function converge and have accurate results.

The main objective of the state estimation (SE) functionality is to find the values for a set of variables (states) that adjust in a more adequate way to a set of network values (measurements) that is available in real-time [1], [2]. The state variables are such that all the other network variables can be evaluated from them, and the operation state is obtained. The calculation of the state variables considers the physical laws directing the operation of electrical networks and is typically done adopting some criteria. The Distribution State Estimation (DSE) is implemented at the functional level of the HV/MV primary substation and only the MV level state variables are calculated [3]–[7]. It is assumed that the state estimation functionality will be installed at the central management level, i.e., at the SCADA/DMS. The following issues should be considered in distribution networks:

- Instrumentation: no (or only a few) sensors in the distribution networks.
- Algorithmic: long radial feeders with heterogeneous lines and cables may result in ill conditioned matrices.
- Large number of nodes: long calculation times.
- Active and reactive power cannot be decoupled: decoupled transmission state estimation algorithms cannot be applied.

2 MV grid state estimation in distribution grids using smart metering information (sub-task 3.3.2)

In order to derive consistent and qualified state estimates, it is necessary to use all the information available for the network and not only real-time measurements, because their availability is very limited. Therefore, the DSE functionality includes information coming from different sources, namely: AMI, DTC acting as Remote Terminal Units (RTUs), and Phasor Measurement Units (PMUs) synchronized by the Global Position System (GPS) signal, if available [8]–[11]. Smart meters (EBs) connected to LV nodes can make time-synchronized measurements of active (*P*) and reactive (*Q*) loads, as well as voltage magnitudes, at predefined time intervals (usually every 15 minutes). These measurements are transmitted to a database server periodically (for instance, daily). This ensures that the DSE will have, at least, measurements from the previous day of all the loads [6].

Based on these measurements a set of pseudo-measurements will be generated and used together with near real-time information, for instance from distributed generators (DG) [6], to make the network fully observable and guarantee an adequate degree of redundancy for running the state estimator. This can be accomplished by an autoregressive load estimation model [12], which utilizes previous day metered LV consumption data as well as same day dependent variables, such as temperature, day type (weekday or weekend), humidity, etc. The upstream MV/LV substation load will be estimated by aggregating all the downstream LV loads, using an expert system trained specifically for this purpose [13], [14]. This expert system will be located at the central management level, where historical information is available.

The MV/LV substations that require generation of these pseudo-measurements, are those without DTC or substations where the transmission of real time DTC measurements has failed. When a MV/LV substation has a DTC with measurements that are available in real-time, the generation of pseudo-measurements is not necessary.

The structure of the state estimation module is shown in Figure 1.

The following **input** information should be available to state estimator: network parameters and configuration (topology) as well as analog measurements, such as ***actual*** *(telemetered)* measurements subject to errors, due to metering inaccuracies, communication system etc (active and reactive power flows, branch currents, active and reactive injections - loads and generations - node voltage magnitudes, statuses of switching devices, and position of transformer taps), ***pseudo*** measurements subject to errors (forecasted load injections or manually entered measurements of any type), and ***virtual*** measurements which contain no error (zero injections at network nodes that have neither load nor generation, zero voltage drops at closed switching devices, and zero active and reactive power flows at open switching devices).

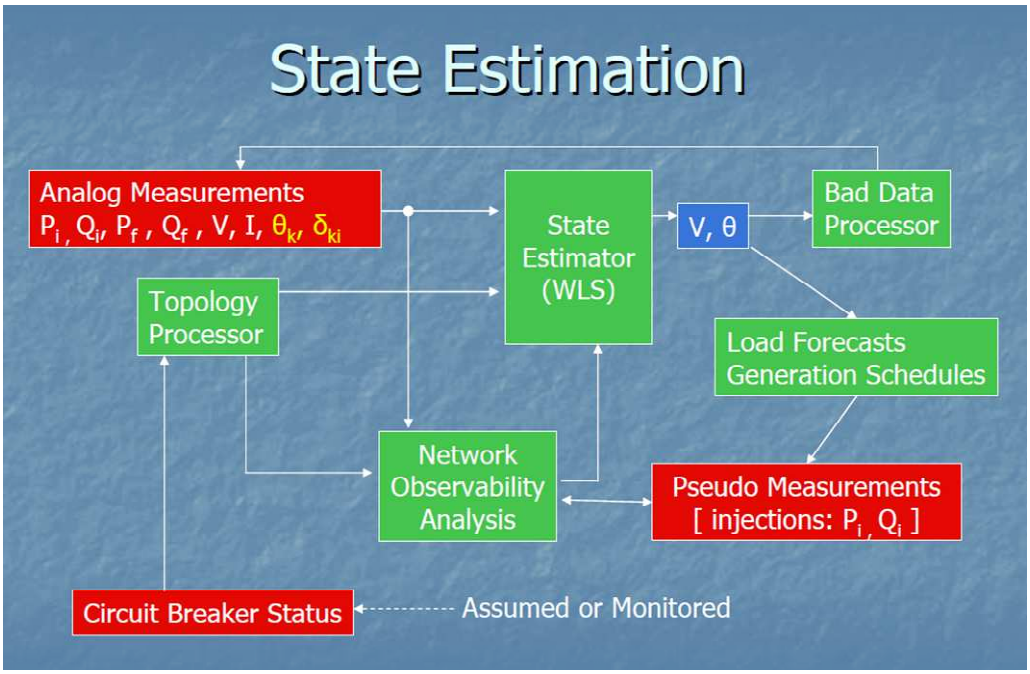

Figure 1 - Structure of the state estimation module.

After the execution of the SE algorithm, the voltage magnitudes and phase angles of the network nodes are estimated. The following **output** information is provided:

- Voltage magnitudes and phase angles at all nodes.
- Active and reactive injected power at each generation and load node.
- Active and reactive power flows at both sides of each line, transformer, and switch.
- Current flows at both sides of each line, transformer, and switch.
- Detection and removal of bad and conflicting data.
- Status of the switching devices with unknown or wrong status.
- Critical and noncritical measurements.
- Performance metrics and confidence indices for the computed solution.

2.1 State Estimation Algorithm

Although distribution systems are unbalanced in nature, in order to avoid modelling complexities, the network is assumed to be balanced and the single phase equivalent network model is considered for power flow and state estimation analysis. In this research, the following nonlinear measurement model is used:

$$z = h(x) + e \qquad (1)$$

where z is the measurement vector, $h(x)$ is the vector of nonlinear functions relating measurements to states, x is the true state vector consisting of nodal voltages

(magnitudes and phase angles), and e is the vector of measurement errors. The class of estimators discussed in this section are based on the maximum likelihood theory and rely on a priori knowledge of the distribution of the measurement error (normally distributed, with $E(e)=0$ and $E(ee^T)=R=diag(\sigma_i^2)$, where σ_i^2 is the variance of the ith measurement error). A node is arbitrarily selected as the reference node and its voltage angle is set to zero.

Measurements can be classified as *critical (nonredundant)* and *noncritical (redundant)*. A critical measurement is the one whose elimination from the measurement set makes the network unobservable [2]. Critical measurements have zero residuals and therefore their errors cannot be detected. If these measurements are inaccurate no action can be taken. Noncritical measurements have nonzero residuals, allowing detection and possibly identification of their errors. A minimally dependent set of measurements has the property that elimination of any measurement from this set, makes the remaining measurements critical. All the measurements of a minimally dependent set have equal absolute values of their normalized residuals [30]. As a consequence, gross error on one or more measurements of a minimally dependent set can be detected but not identified. The critical measurements and minimally dependent sets of measurements are determined by method [30]. Since the measurement redundancy is low in distribution networks, few critical measurements and minimally dependent sets may occur, making the error filtering process rather difficult. This is the reason why forecasted load (pseudo) measurements should be as accurate as possible.

Since distribution systems have limited or no measurement redundancy, the suitability of the state estimation algorithms that have been suggested for transmission systems needs further investigation [5]. The available measurements are predominantly of pseudo type (statistical in nature), so the performance of SE should be based on some statistical measures, such as bias, consistency and quality. These statistical measures are explored by investigating three of the most common transmission system state estimation approaches [5] with regard to their suitability for the DSE problem under stochastic behaviour of the measurements and limited or no redundancy [3], [4].

The problem is to find an estimate $\hat{x}$ of the state vector which minimizes the following objective function:

$$J(x)=\sum_{i=1}^{m}\rho(r_i) \tag{2}$$

where $r_i:\ \mathcal{N}(0,1)$ is the weighted residual of the ith measurement:

$$r_i=\frac{z_i-h_i(x)}{\sigma_i} \tag{3}$$

Table 1 summarizes the adopted SE approaches. The different estimators can be characterized based on the choice of the ρ function.

Table 1 - State estimation approaches.

Approach	$\rho(r_i)$	Solution method
Weighted Least Squares (WLS)	$\frac{1}{2}r_i^2$	Newton iterative
Weighted Least Absolute Value (WLAV)	$\lvert r_i \rvert$	Linear Programming (LP) or Interior Point (IP)
Schweppe-Huber Generalized-M (SHGM)	$\begin{cases} \frac{1}{2}r_i^2 & \text{if } \lvert r_i \rvert \le \alpha w_i \\ \alpha w_i \lvert r_i \rvert - \frac{1}{2}\alpha^2 w_i^2 & \text{otherwise} \end{cases}$ where w_i is the iteratively modified weighting factor and α is a tuning parameter	Iteratively Reweighted Least Squares (IRLS)

The performance evaluation of the above SE techniques have showed that WLAV and SHGM methodologies cannot be applied to distribution systems [5]. The WLS method gives consistent and better quality performance when applied to distribution systems. Hence, WLS is found to be the suitable solver and is used in this project.

The solution $\hat{x}$ can be found by the normal equations (NE) iterative procedure as follows:

$$G(x^k)\Delta x^k = H^T(x^k)R^{-1}\Delta z^k \qquad (4)$$

where, $\Delta x^k = x^{k+1} - x^k$, $\Delta z^k = z - h(x^k)$, $H = \partial h / \partial x$ is the Jacobian matrix evaluated at $x = x^k$, $G = H^T R^{-1} H$ is the gain matrix evaluated at $x = x^k$, and k is the iteration index.

2.2 Required Data for State Estimation Execution

The SE algorithm will run at pre-defined time intervals (i.e. every 15 minutes or every hour). Accurate load models are critical for state estimation. Innovative techniques will identify load models and load compositions (i.e. demand profiles), using standard available measurement data at network buses, individual demand component signatures and general information about demand composition.

Load modeling in the distribution network will have the following characteristics:

- For unmeasured nodes, load profiles will be developed for each type of customer (such as residential, commercial, industrial etc), based on some monitoring and

energy bill data. Historical samples obtained for different seasons, days and times, will be stored separately for different load types (residential, industrial and commercial).

- For measured nodes, the consumed P, Q power will be provided.

It is assumed that domestic smart meters connected to a node, take synchronized measurements of active and reactive consumption of the loads at predefined time intervals. These measurements are transmitted to a database server periodically, i.e. AMR data in the PCC's MV distribution system for the current day are transmitted from 00.00 hrs to 06.00 hrs of the next day. In any case, state estimator will have the previous day's measurements of all the loads. The proposed state estimator will estimate reliably the node voltages of a distribution network by using the previous day's measurements (while considering whether the day is a weekday, Saturday and Sunday). The AMR meters installed at distributed generators (DG) will measure net P, net Q and V at predefined time intervals and communicate immediately to the server. The SE will also read P/Q consumption of the loads connected to each transformer which will summed up (as the measurements are time synchronised) to calculate the load of the transformer (and the node). The previous day's loads of the nodes and near real-time power measurements from distributed generators will be used as power injection measurements.

Summarizing, the required data for state estimation execution are shown below.

LV network	– P/Q power consumption and V magnitude at every LV load bus – P power production and V magnitude at every LV production bus.
MV network	– P/Q power consumption at MV consumption bus, if available – P/Q power production and V magnitude and phase at MV production bus, if available. – P/Q power flow in the MV lines with RTU or PMU.
MV/LV (secondary) substations	P/Q power consumption, V magnitude and/or I magnitude and power factor, in the primary or secondary of the transformer, if available.
HV/MV (primary substation)	P/Q power consumption, V magnitude and/or I magnitude and power factor, in the primary or secondary of the transformer, if available. These measurements could also be available for each MV feeder;

The transmission frequency for each data level is shown below.

Past data of the LV network	It should be available once a day with 24 hours of delay (i.e., from d-1).
Dynamic data of the LV	The data of some reference DG and load units (by

network	DTC) should be available every 15 minutes with a maximum delay of 1 minute.
MV network	It should be available in real time (e.g., on a 1 minute time basis).

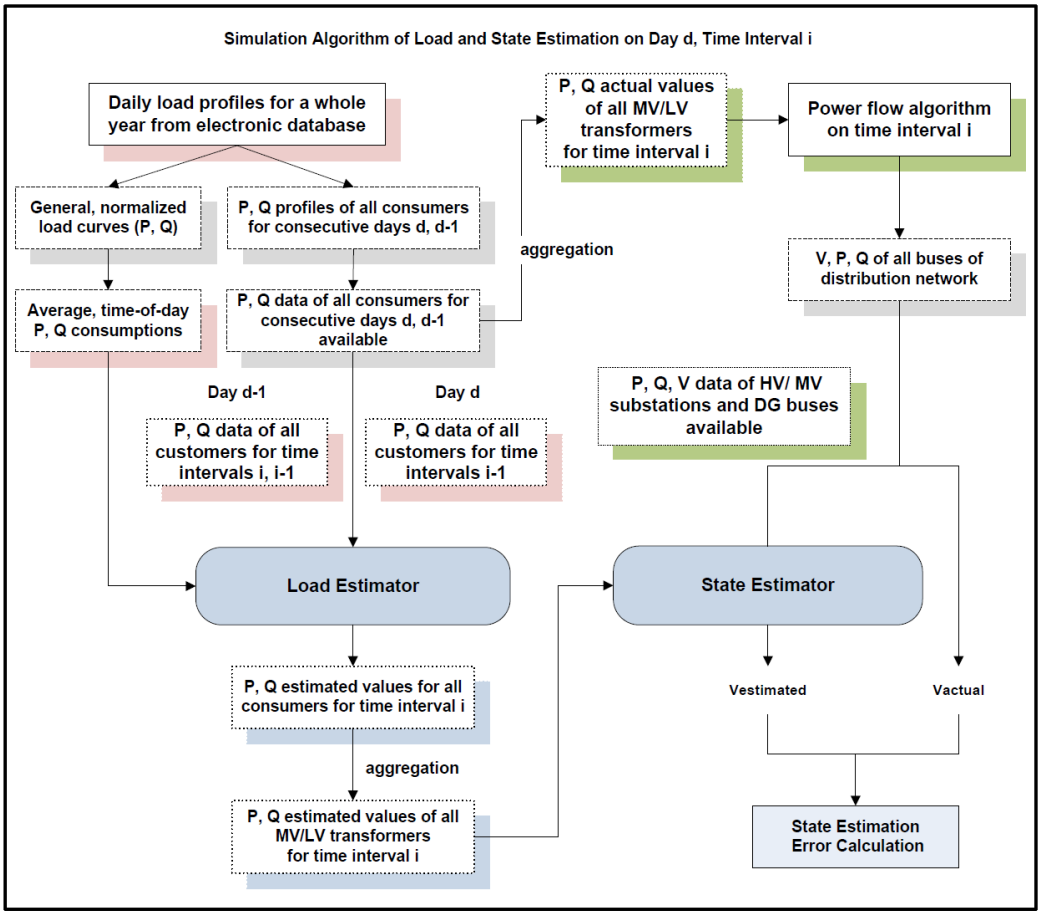

Figure 2 - Data flow chart of the load and state estimation

A general framework for the combined simulation of load and state estimation is presented in Figure 2. The load estimation algorithm is using data provided by LV or MV smart meters. It deploys a simple time series model [8] using basic class-specific load curves associated to each consumer type (e.g. domestic, commercial etc.) to improve the accuracy of individual customer load estimates. Load estimates can be obtained hourly, half-hourly or less. Then, all individual load estimates are aggregated, based on topology and connectivity data, to extract load estimates per MV/LV distribution transformers. These values are treated as pseudo-measurements and used as inputs to state estimation algorithm along with (near) real-time data collected from other points of the power network. Time delay in data transmissions from smart meters to data management centers is a parameter which affects significantly the load estimation algorithm performance.

2.3 Pseudo-measurement generation with autoencoders

In order to derive consistent and qualified state estimates, it is necessary to use all the information available for the network and not only real-time measurements, because their availability is very limited. Smart meters (EBs) connected to LV nodes can make time-synchronized measurements of active (P) and reactive (Q) loads, as well as voltage magnitudes (V), at predefined time intervals (usually every 15 minutes). These measurements are transmitted to a database server periodically (for instance, daily).

Based on these "historical" measurements and with some real-time information from LV network, a set of pseudo-measurements for the secondary substations will be generated and used together with near real-time information for MV network, to make the network fully observable and guarantee an adequate degree of redundancy for running the state estimator at the MV network. This can be accomplished by an Auto-associative neural networks (AANN) or autoencoders [14], which utilizes historical metered LV data to be properly trained. The pseudo-measurements generation consists of running the autoencoder, already trained, incorporating an optimization procedure for reconstructing the missing variables of the secondary substations [15].

This expert system will be located at the central management level, where historical information is available.

The MV/LV substations that require generation of these pseudo-measurements, are those without DTC or substations where the transmission of real time DTC measurements has failed. When a MV/LV substation has a DTC with measurements that are available in real-time, the generation of pseudo-measurements is not necessary.

2.3.1 The Autoencoder Concept

Auto-associative neural networks (AANN) or autoencoders are feedforward neural networks that are built to mirror the input space S in their output. The size of the output layer is the main difference between an autoencoder and a traditional neural network – in an autoencoder the size of its output layer is always the same as the size of its input layer. Therefore, an autoencoder is trained to display an output equal to its input. This is achieved through the projection of the input data onto a different space S' (in the middle layer) and then re-projecting it back to the original space S. In other words, the first half of the autoencoder approximates the function *f* that encode the input space to the space compressed S' while the second half approximates the inverse function f-1that projects back the set of values in space S' to the original space S. The detailed mathematical formulation can be found in [16]. With adequate training, an autoencoder learns the data set pattern and stores in its weights information about the training data manifold. The

typical architecture of an autoencoder is a neural network with only one middle layer – Figure 3 This simple architecture is frequently adopted because networks with more hidden layers have proved to be difficult to train [17], although allowing increasing accuracy. An autoencoder with one hidden layer and linear activation functions performs the same basic information compression from space S to space S' as Principal Component Analysis (PCA) [18]. With nonlinear activation functions and multiple layers, autoencoders chart the input space on a non-linear manifold in such a way that an approximate reconstruction is possible with less error [19]. Plus, PCA does not easily show how to do the inverse reconstruction, which is straightforward with autoencoders.

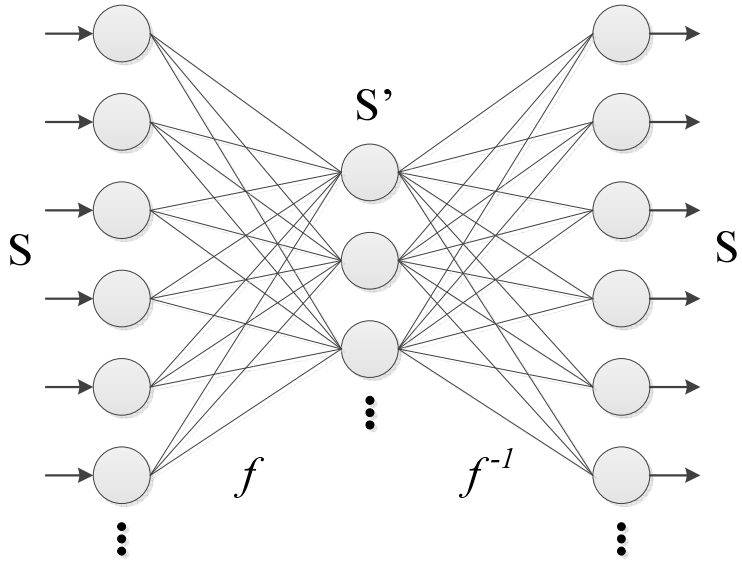

Figure 3 - Architecture of an autoencoder with a single hidden layer

There is no *a priori* indication of an adequate hidden layer reduction rate (measured as the ratio between the number of neurons in the smallest middle layer and the number of neurons in the input/output layer) to be adopted. This decision on the reduction rate is dictated in present-day practice by trial and error and by characteristics of the problem.

Autoencoders with thousands of inputs have been proposed for data or image compression, using the signals available in the middle layer, which maps the input to a reduced dimension space. Reconstruction is then performed using the second half of the autoencoder [20-22].

Once the autoencoder is trained, if an incomplete pattern is presented, the missing components may be replaced by random values producing a significant mismatch between input and output. Typically three different approaches can be followed in order to find the missing values on the way to minimize that error (convergence is reached). The approach called Projection Onto Convex Sets (POCS) [23] consists basically in iteratively reintroducing the output value in the input such that it will converge to a value that minimizes the input-output error (Figure 4). This convergence method uses alternating linear projections on the input and output space to converge to the assumed

missing values. The two other approaches are based on an optimization algorithm in order to discover the values that should be introduced in the missing components such that the input-output error becomes minimized. In the process denoted unconstrained search, the convergence is controlled only by the error on the missing signals (Figure 5), whereas in the constrained search it is controlled by the error on all the outputs of the autoencoder (Figure 6). Any of these optimization procedures may be used, but according to some related works in the state estimation area [14, 24], constrained search appears to the most suitable method to search a missing signal.

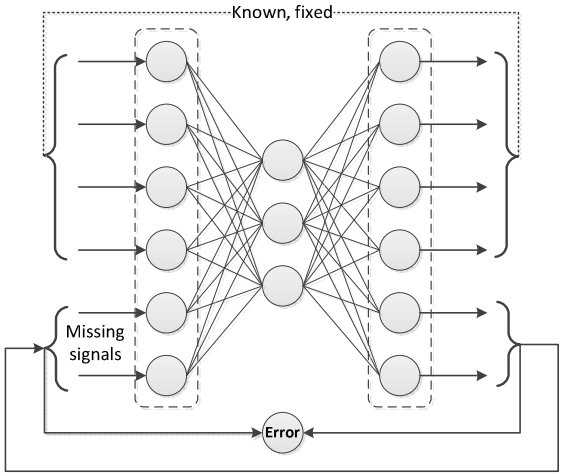

Figure 4 - Illustration of the POCS algorithm

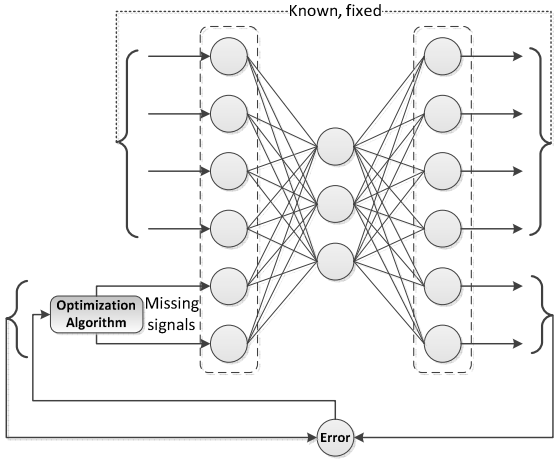

Figure 5 - Illustration of the unconstrained algorithm

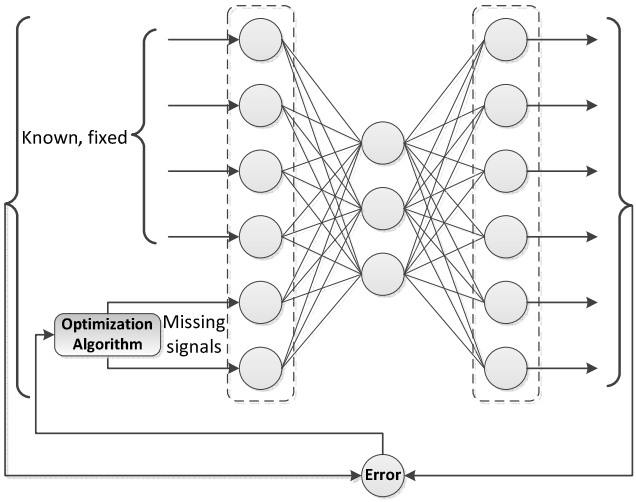

Figure 6 - Illustration of the constrained algorithm

Autoencoders are frequently applied in areas related with pattern recognition and reconstruction of missing sensor signals [20, 25]. However, their application in the power systems area is not very common. In [14] one can find the proposal of offline trained autoencoders for recomposing missing information in the SCADA of Energy/Distribution Management Systems (EMS/DMS). Also in [24], a model for breaker status identification and power system topology estimation is presented. More recently, in [26] is proposed a concept of transformer fault diagnosis and in [15] one can find an innovative method to perform state estimation in distribution grids, both applications using autoencoders.

2.3.2 Methodology

In the present work it is expected to estimate the MV network operation state using data of the real-time measurements available on the MV network and also pseudo-measurements and/or other measurements taken from smart meters and other equipment installed in the LV network.

In order to turn the MV network observable will be used a pseudo-measurement generation method for MV/LV secondary substation without real-time measurements. The LV measurements will be considered to generate pseudo-measurements for the upstream MV/LV substation load, which aggregates all downstream LV loads and LV generation. This will be done using an autoencoder properly trained and located at the central management level or at DTC level, where historical information is available.

A constrained search approach is applied for finding the missing signals (see Figure 6). In the context of this approach, to generate pseudo-measurements for the MV/LV secondary substation without real-time measurements, missing signals have to be the active and reactive injected power and also the voltage magnitude value, all calculated at the bus of the secondary level of the correspondent substation.

Within the constrained search approach, the optimization algorithm used to reconstruct the missing signals was a meta-heuristic method called Evolutionary Particle Swarm Optimization (EPSO). The EPSO algorithm has been successfully applied already in several problems in the power systems area [27-29]. The fitness function of the EPSO was defined to minimize the square error between the input and the output of the autoencoder.

2.3.2.1 Historical Data

An effective pseudo-measurements generation through the use of autoencoders requires inevitably a large historical database, which needs to contain data about the variables that are passed to the autoencoder (missing signals and measurements recorded). Additionally, the amount of data for each time instant/operating point should be available in enough number. This is crucial for a successful and effective training process since it is what enables the autoencoder to learn the necessary patterns/correlations between the electrical variables of a given network. There is no rule of thumb regarding the quantity of data in the historical database. However, it is known that few or too much data will lead to an inaccurate autoencoder. A trial and error approach can be followed to identify the optimal quantity of data in the historical database to be passed to the autoencoder.

2.3.2.2 The Standardization Procedure

A standardization procedure is run with the goal of pre-treating the input and output train data set. In this scale adjustment process, the range of the input and output values is transformed to a normalized interval of [-1, 1]. This procedure increases the performance and efficiency of the autoencoder training, once it allows a better adjustment of the input variables to the range of the activation function and also allows the autoencoder to be less affected by the different ranges of the variables in the training data set.

There are three main methods to standardize the data: Z-Score method, Decimal Scaling method and Min-Max method. The last one is the best standardization procedure when the minimum and maximum values of the data set are known. Therefore this is the method applied here to perform the standardization once that looking to the historical database, the minimum and maximum values of the variables that compose the input vectors can be easily obtained.

$$y' = \frac{y - \min_a}{\max_a - \min_a} \times (\max_A - \min_A) + \min_A \qquad (5)$$

Where:

y' – Standardized value for the considered variable;

y – Variable value in the original representation interval;

$\min_a$ – Minimum value of the "original" range of values;

$\max_a$ – Maximum value of the "original" range of values;

$\min_A$ – Minimum value of the standardized range of values (-1);

$\max_A$ – Maximum value of the standardized range of values (1).

2.3.2.3 Training Process

As any learning process in life, this learning procedure is no more than a trial and error method, where for several scenarios or input data the autoencoder will produce an output vector that will be compared to the desired output. If the actual output is too far from the desired one, it will be submitted to the input data again, adjusting its internal parameters, in order to produce a good approximation of the actual output to the desirable one.

With the purpose of training the autoencoder properly, an adaptive gradient-based algorithm called Resilient Back-Propagation (RPROP) algorithm was adopted. This algorithm belongs to the most widely used class of algorithms for supervised learning of neural networks and is an update of the Back-Propagation. Differently of the basic version of the Back-Propagation algorithm, which considers a fixed learning rate to determine how the weights should evolve, the RPROP has an adaptive gradient-based algorithm that makes it more efficient. In general terms, individual step sizes are used for updating the weights in order to minimize oscillations and maximize the length of the step size. In this way the learning process during the neural network training is speed-up while local optimums are avoided.

The RPROP algorithm works in much the same way as the name suggests: after propagating an input through the autoencoder neural network, the error is calculated and then it is propagated back through the network while the weights are adjusted in order to make the error smaller.

Another training particularity of this algorithm is that instead of training on the combined data, the training data set is executed sequentially one input at a time, minimizing the mean square error for the entire training data set and at the same time providing a very efficient way of avoiding getting stuck in a local minimum.

Besides the training algorithm, there are a set of important parameters that must be defined to successfully complete the training stage. Some of them are typical values, while others are case dependent (influenced by the characteristics of the problem, type of networks, etc.), such as the activation functions, the hidden layer reduction rate (HLRR) and the number of training epochs. Experimental training tests were carried out in order to select the most appropriate activation function for the hidden and output layers. These

activation functions can be modelled by different types of mathematical functions, being the most common the threshold, the sigmoid and step wise function. For the specific problem under analysis, results have shown that when non-linear activation functions are used in both layers the autoencoder performance is better than with any other combination that includes linear functions. Therefore, in the studies performed, a symmetric sigmoid was adopted as the activation function for both the middle and the output layer. This activation function is illustrated in equation (6).

$$\begin{cases} \varphi(\upsilon) = \dfrac{1}{1+e^{(-a\upsilon)}} \\ -1 \leq \varphi(\upsilon) \leq 1 \end{cases} \quad (6)$$

Where:

$\varphi(\upsilon)$ – Output of the respective neuron;

υ – Sum of all the inputs of the respective neuron, which correspond to the outputs from the neurons of the previous layer;

a – Slope parameter of the sigmoid function.

Regarding the hidden layer reduction rate, as it was already mentioned, there is no *a priori* indication of an adequate hidden layer reduction rate to be adopted. With relation to the number of training epochs, it is also an important parameter to fine-tune the weights of the autoencoder. An overstated number can lead to overfitting, while the opposite is very likely to lead to underfitting. This effect can be overcome by analysing the evolution of mean square error of a test data set through the use of cross-validation methods.

In the view of the above, a trial and error approach was followed to find the most adequate parameters in order to have the autoencoder properly tuned.

2.3.2.4 Autoencoder Performance Evaluation for Pseudo-Measurements Generation

After having an autoencoder properly trained, one can advance to the testing phase. This stage consists on running the autoencoder, while incorporating the EPSO for the purpose of reconstruct the missing variables: active and reactive injected power and also the voltage magnitude value. An evaluation data set specifically defined to meet this purpose will be used. Then, based on the results achieved the performance of the autoencoder is evaluated.

The ideas previously depicted are presented on the flowchart in the Figure 7.

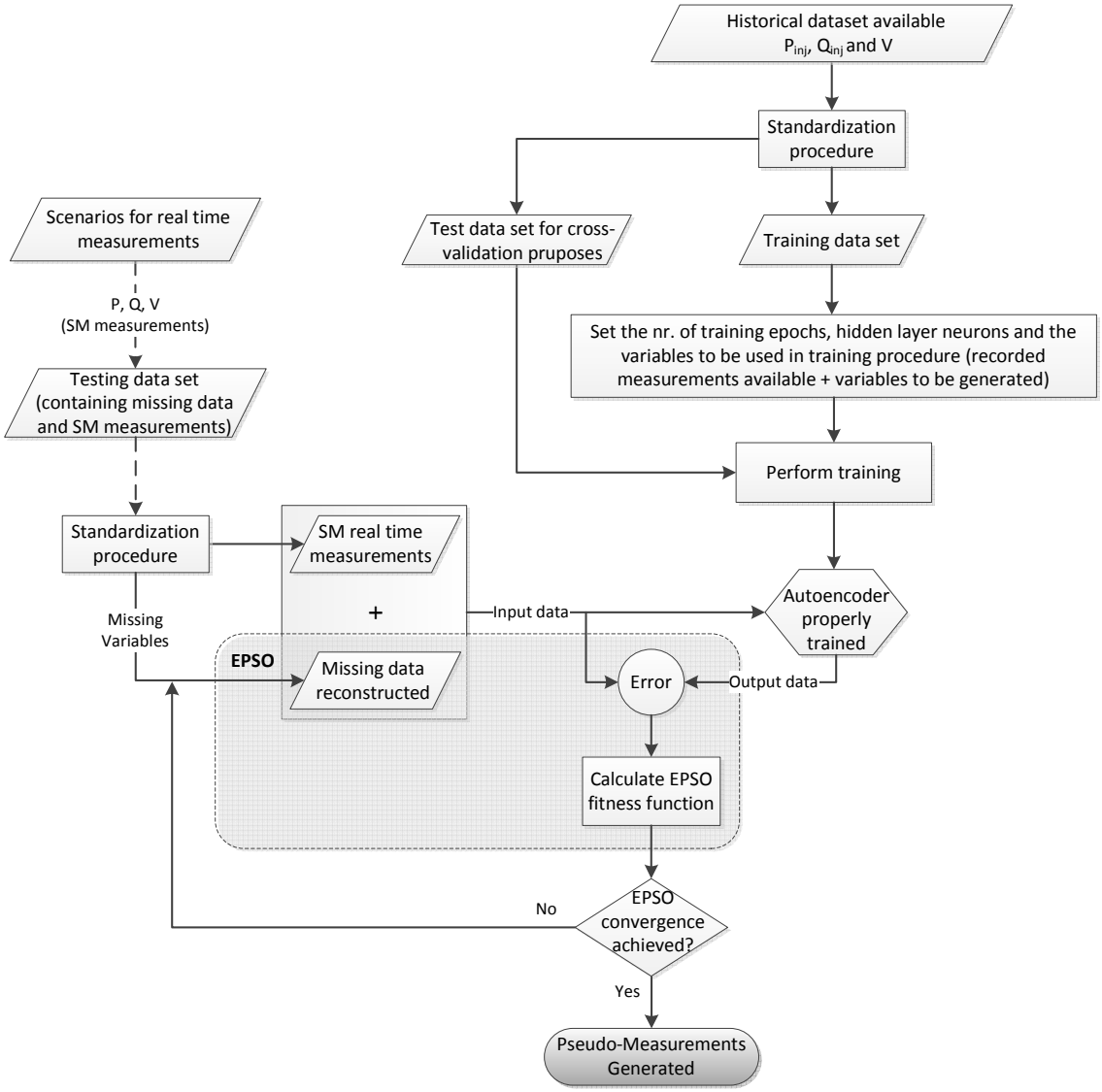

Figure 7 - Flowchart of the main steps of the pseudo-measurements generation methodology

2.4 Measurement Observability

The linear equations (4) are uniquely solvable and the gain matrix is nonsingular, iff the matrix H has full column rank [1], [2] that is:

$$nullity(H) = 0 \tag{7}$$

Under the condition (7) the network is said to be observable, otherwise it is unobservable. If the network is not observable, it is still useful to know which parts of the network have measurements to estimate their state. These parts of the network are called *observable islands*. The observability analysis has three main functions [2]:

- determine if the network is observable or not
- if the network is not observable, identify the observable islands
- make the network observable by introducing additional pseudo-measurements (from load forecasting or load allocation applications)

The sparse linear system of equations (4) can be efficiently solved for Δx^k by Cholesky factorization, according to the following steps [2]:

- **Ordering:** Symmetrically reorder rows and columns of matrix G so Cholesky factors LDL^T of G, where D is positive diagonal matrix and L is unit lower triangular matrix, suffer relatively little fill.
- **Symbolic factorization:** Determine locations of all fill entries and allocate data structures in advance to accommodate them.
- **Numeric factorization:** Compute numeric values of entries of Cholesky factors.
- **Triangular solution:** Compute solution Δx^k of (4) by forward and backward substitution.

2.5 Bad Data Identification

The state estimation results are reliable only if the available measurements are affected by random errors. If measurements with gross errors are present, then the resulting state estimation may be unreliable. Bad measurements are identified by performing statistical tests on the normalized residuals [2]. The normalized residuals are defined as:

$$\hat{r}_N = (diagP_r)^{-\frac{1}{2}}\hat{r} \tag{8}$$

where,

$$\hat{r} = z - h(\hat{x}) \tag{9}$$

and P_r is the residual covariance matrix, defined as:

$$P_r = Cov(r) = R - HG^{-1}H^T \tag{10}$$

Random vector $\hat{r}_N$ has unit normal distribution. A detection threshold of $N_p = 3$, corresponding to $(1-p) = 0.003$ false alarm probability, is adopted for bad data identification. Let the ith measurement have the largest normalized residual (in absolute value) $\left|\hat{r}_{N,i}\right|_{max}$. If $\left|\hat{r}_{N,i}\right|_{max} > N_p$, the measurement i is flagged as bad data, is eliminated from the measurement set and state vector $\hat{x}$ and normalized residuals $\hat{r}_N$

are recalculated. If the new $\left|\hat{r}_{N,i}\right|_{max} < N_p$, all bad data have been eliminated, else the process is continued until all bad data are identified.

2.6 Parallel Processing

In order to reduce the computational burden of the enormous volumes of data produced by the smart meters and the load estimation algorithms that generate the pseudo measurements, a parallel multi-area state estimator (MASE) will be implemented, processing in parallel the data gathered from each area (zone) on multiple CPUs (cluster) or multicore CPUs and coordinating the zone border information to compute the system-wide state [31]-[37].

In this project the overall system is decomposed into a certain number of predefined non-overlapping areas and each area independently executes its own state estimator based on local measurements. A central coordinator receives the estimated values of boundary measurements and states, and computes the system-wide solution. The basic criterion of partitioning a power system into several control areas is to have areas as equal in size as possible, so that the workload on each area processor is as balanced as possible, and interconnections between distinct areas be limited, as much as possible, to reduce the amount of inter-process communication necessary**.** There are several graph partitioning packages available. The most common are yED [38], Metis [39], Chaco [40], Jostle [41], Scotch [42] and Ralpar [43].

Two processing techniques are used to solve the MASE problem: **parallel** and **distributed**. A widely accepted distinction between them is that the parallel processing employs a number of closely coupled processors, using several threads created by an executable and sharing the same physical memory, while distributed processing employs a number of loosely coupled and geographically distributed computers, using several executables having their own memory and communicating between them using messages [31]. For a large power system, distributed processing can bring more flexibility and reliability in monitoring and control and can save on large investment in communication networks. Two computer architectures have been proposed for the MASE problem: the **hierarchical** and the **decentralized**. In *hierarchical* MASE, a master processor distributes the work among slave computers performing local area SE and, subsequently, coordinates the local estimates [34] repeatedly after each iteration. In *decentralized* MASE, the central coordinator computer is missing and each local processor communicates only with processors of neighbouring areas, exchanging border information [34].

A measured power system, comprising n buses, may be partitioned in r non-overlapping observable control areas A_i connected via tie-lines ending at border buses, as shown in Figure 8. Each area has n_i buses such that $n = \sum_{i=1}^{r} n_i$.

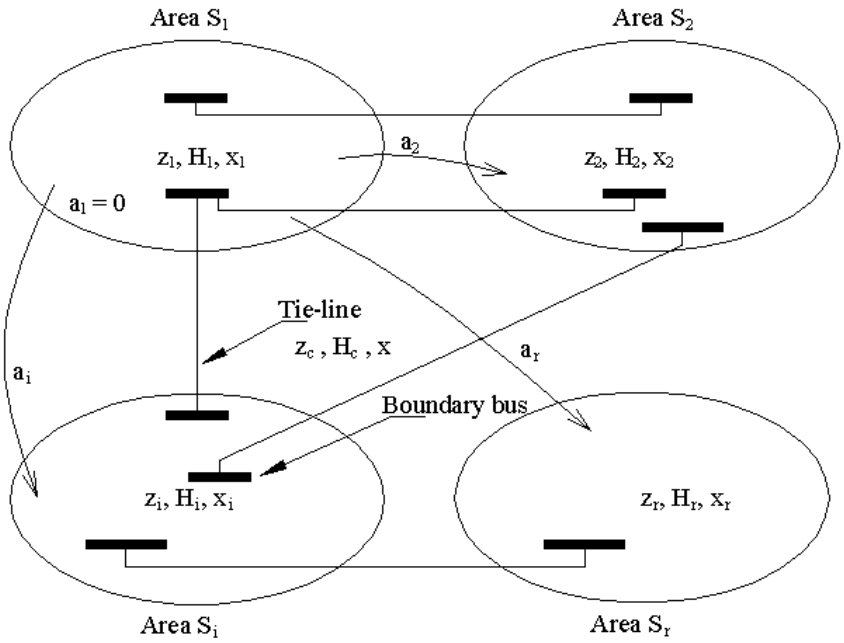

Figure 8 - Network partitioning in r non-overlapping areas

Each area is governed by its own *local* computer, that is responsible for estimating its own state, and is connected by communication links to a *coordination* computer. Let $A(i)$ be the set of all buses in area A_i. A bus $k \in A(i)$ is internal in area A_i if all its neighbors $l \in A(i)$. A bus $k \in A(i)$ is boundary at area A_i if some of its neighbors $l \in A(j), j \neq i$. If $I(i)$ and $B(i)$ are the sets of internal and boundary buses of area A_i, respectively, then $A(i) = I(i) \cup B(i)$. According to measurement classification of Figure 9:

- A power injection measurement at a bus $k \in I(i)$, a voltage measurement at a bus $k \in A(i)$, and a power or current flow measurement at end k of a branch $k-l$ ($k, l \in A(i)$) are *internal* in area A_i.
- A power injection at a bus $k \in B(i)$ and a power or current flow at end k of branch (tie-line) $k-l$ ($k \in B(i)$, $l \in B(j), j \neq i$), are *boundary measured buses* at area A_i. We define by $C(i) \subseteq B(i)$ this set of boundary measured buses and by $E(j) \subseteq B(j)$ the set of *external* buses $\in B(j), j \neq i$ and connected with buses $\in C(i)$.

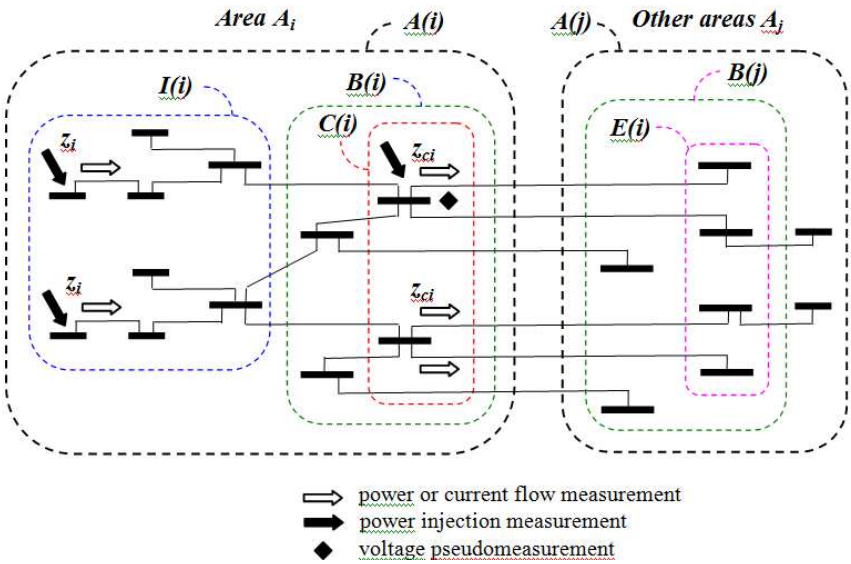

Figure 9 - Classification of buses and measurements in a multi-area power system.

The SE model establishes a relationship between measurements and states, as:

$$\begin{pmatrix} z_1 \\ \mathrm{M} \\ z_r \\ z_c \end{pmatrix} = \begin{pmatrix} h_1(x_1) \\ \mathrm{M} \\ h_r(x_r) \\ h_c(x) \end{pmatrix} + \begin{pmatrix} e_1 \\ \mathrm{M} \\ e_r \\ e_c \end{pmatrix} \tag{11}$$

where, $z_i, i=1,\ldots,r$ is the $m_i \times 1$ vector of internal measurements in area A_i, z_c is the $m_c \times 1$ vector of boundary measurements, $x_i = \begin{pmatrix} \delta_i \\ V_i \end{pmatrix}$ is the $2n_i \times 1$ local state vector, composed of n_i voltage phase angles and magnitudes at all buses of area A_i, $x^T = \left(x_1^T, \cdots, x_r^T\right)$ is the $2n \times 1$ system-wide state vector, $h_i(.), i=1,\ldots,r$ and $h_c(.)$ are nonlinear vector functions relating measurements to states, $e_i, i=1,\ldots,r$ and e_c are Gaussian error vectors, with zero mean $E(e_i)=E(e_c)=0$ and covariance matrices $R_i = E\left(e_i e_i^T\right) = \left(\sigma_1^2, \ldots, \sigma_{m_i}^2\right)$ and $R_c = E\left(e_c e_c^T\right) = \left(\sigma_1^2, \ldots, \sigma_{m_c}^2\right)$ respectively, σ_i being the standard deviation of the error associated with measurement i.

The system-wide state estimator will minimize the quadratic objective function:

$$\min_x J(x) = \sum_{i=1}^{r} \left(z_i - h_i(x_i)\right)^T R_i^{-1} \left(z_i - h_i(x_i)\right) + \left(z_c - h_c(x)\right)^T R_c^{-1} \left(z_c - h_c(x)\right) \tag{12}$$

and the state estimate $\hat{x}$ will be obtained by iteratively solving the so-called Normal equations:

$$\left(\begin{array}{ccc|c} G_1(x_1(k)) & \cdots & 0 & H_{c1}^T(x_1(k)) \\ \vdots & \ddots & \vdots & \vdots \\ 0 & \cdots & G_r(x_r(k)) & H_{cr}^T(x_r(k)) \\ \hline H_{c1}(x_1(k)) & \cdots & H_{cr}(x_r(k)) & -\sum_{i=1}^{r} R_{ci} \end{array}\right)\left(\begin{array}{c} \Delta x_1(k) \\ \vdots \\ \Delta x_r(k) \\ \hline \lambda(k+1) \end{array}\right)=\left(\begin{array}{c} H_1^T(x_1(k))R_1^{-1}\Delta z_1(k) \\ \vdots \\ H_r^T(x_r(k))R_r^{-1}\Delta z_r(k) \\ \hline \Delta z_c(k) \end{array}\right) \quad (13)$$

where, k is the iteration index, $\Delta x_i(k)=x_i(k+1)-x_i(k)$, $\Delta z_i(k)=z_i-h_i(x_i(k))$, $\Delta z_c(k)=z_c-h_c(x(k))$, $H_i=\partial h_i/\partial x_i$ is the $m_i\times 2n_i$ Jacobian matrix of h_i evaluated at $x_i(k)$, $H_{ci}=\partial h_c/\partial x_i$ is the $m_c\times 2n_i$ Jacobian matrix of h_c evaluated at $x_i(k)$, $G_i(x_i(k))=H_i^T(x_i(k))R_i^{-1}H_i(x_i(k))$ is the $2n_i\times 2n_i$ gain matrix, and the $m_c\times m_c$ covariance matrix R_{ci} includes only those diagonal entries of R_c corresponding to the boundary measurements of area A_i. The coefficient matrix of (13) has doubly-bordered block diagonal (DBBD) form, composed of diagonal blocks G_i, bordered blocks H_{ci}, and cutset block $-R_c=-\sum_{i=1}^{r}R_{ci}$. The DBBD form of (13) is particularly suitable for a parallel solution [37].

If an area A_i has no voltage magnitude measurement, a voltage phase angle and magnitude pseudo measurement of arbitrary value is assigned to a boundary bus and appended both in z_i with an arbitrary positive weight and in z_c with an opposite negative) weight [35]. At least one conventional voltage magnitude measurement is necessary for observability and a phase angle (critical) pseudo measurement of arbitrary value and weight has to be introduced at a bus of an arbitrarily chosen area. Under the above assumptions, each gain matrix G_i will be positive definite and non-singular and its Cholesky factors will be:

$$G_i=L_iD_iL_i^T \quad (14)$$

where L_i is unit lower triangular matrix and D_i is diagonal matrix with positive diagonal entries. For each area A_i we define the following coefficient matrix:

$$F_i=\begin{pmatrix} G_i & H_{ci}^T \\ H_{ci} & -R_{ci} \end{pmatrix} \quad (15)$$

which has a signed-Cholesky factorization as:

$$\begin{pmatrix} G_i & H_{ci}^T \\ H_{ci} & -R_{ci} \end{pmatrix}=\begin{pmatrix} L_i & 0 \\ M_i & L_{ci} \end{pmatrix}\begin{pmatrix} D_i & 0 \\ 0 & -D_{ci} \end{pmatrix}\begin{pmatrix} L_i^T & M_i^T \\ 0 & L_{ci}^T \end{pmatrix} \quad (16)$$

where L_{ci} is unit lower triangular matrix and D_{ci} is singular diagonal matrix. Positive (negative) diagonal entries of R_{ci} correspond to boundary measurements (voltage

pseudo measurements) of area A_i. Zero diagonal entries of R_{ci} correspond to boundary measurements or voltage pseudo measurements of other areas $A_j, j \neq i$. Note that if $D_{ci}(k,k)=0$ then $L_{ci}(j,k)=0, j>k$ [37]. The indefinite non-singular matrix G_c and its signed Cholesky factors are:

$$G_c = \sum_{i=1}^{r} G_{ci} = \sum_{i=1}^{r} L_{ci} D_{ci} L_{ci}^T = L_c D_c L_c^T \tag{17}$$

where G_c is termed interface matrix, $G_{ci} = H_{ci} G_i^{-1} H_{ci}^T + R_{ci}$ is the local Schur complement for area A_i, L_c is unit lower triangular matrix and D_c is nonsingular diagonal matrix. The diagonal entries of D_c, which correspond to the boundary measurements and the voltage pseudo measurements, are positive and negative respectively [37]. Combining (13)-(17) the following iterative procedure is derived:

$$\begin{aligned}
&\Delta y_i(k) = (L_i D_i)^{-1} H_i^T R_i^{-1} \Delta z_i(k),\ i=1,\ldots,r \\
&\lambda(k+1) = \left(L_c^T\right)^{-1} \left[(L_c D_c)^{-1} \left(\Delta z_c(k) - \sum_{i=1}^{r} M_i D_i \Delta y_i(k) \right) \right] \\
&\Delta u_i(k) = M_i^T \lambda(k+1),\ i=1,\ldots,r \\
&\Delta x_i(k) = \left(L_i^T\right)^{-1} \left(\Delta y_i(k) + \Delta u_i(k) \right),\ i=1,\ldots,r
\end{aligned} \tag{18}$$

The mismatch $\Delta z_c(k)$ can be written as:

$$\begin{aligned}
\Delta z_c(k) = z_c - h_c(x(k)) &= \begin{pmatrix} z_{c1} \\ \vdots \\ z_{cr} \end{pmatrix} - \begin{pmatrix} h_{c1}(x_{a1}(k), x_{c1}(k), x_{e1}(k)) \\ \vdots \\ h_{cr}(x_{ar}(k), x_{cr}(k), x_{er}(k)) \end{pmatrix} \\
&= \begin{pmatrix} z_{c1} \\ \vdots \\ z_{cr} \end{pmatrix} - \begin{pmatrix} h'_{c1}(x_{a1}(k), x_{c1}(k)) + h''_{c1}(x_{c1}(k), x_{e1}(k)) \\ \vdots \\ h'_{cr}(x_{ar}(k), x_{cr}(k)) + h''_{cr}(x_{cr}(k), x_{er}(k)) \end{pmatrix} \\
&= \begin{pmatrix} \Delta z_{c1}(k) \\ \vdots \\ 0 \end{pmatrix} + \cdots + \begin{pmatrix} 0 \\ \vdots \\ \Delta z_{cr}(k) \end{pmatrix} - \begin{pmatrix} h''_{c1}(x_{c1}(k), x_{e1}(k)) \\ \vdots \\ h''_{cr}(x_{cr}(k), x_{er}(k)) \end{pmatrix}
\end{aligned} \tag{19}$$

where z_{ci} comprises the subset of measurements in z_c whose from end belongs to area A_i, $\Delta z_{ci}(k) = z_{ci} - h'_{ci}(x_{ai}(k), x_{ci}(k))$, x_{ai} comprises the subset of variables in x_i associated with first neighbors of buses $\in C(i)$, x_{ci} comprises the subset of variables in x_i associated with buses $\in C(i)$, and x_{ei} comprises the subset of variables in $\bigcup_{j \neq i} x_j$ associated with buses $\in E(i)$, as depicted in Figure 10.

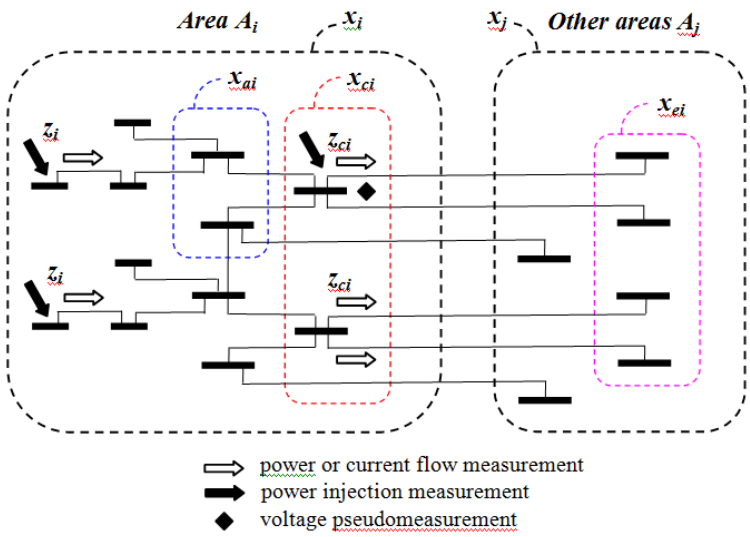

Figure 10 - Classification of states and measurements in a multi-area power system.

An example of multi-area partitioning for a distribution network is provided in Figure 11.

Based on the multi-area SE formulation presented before, the distributed iterative solution algorithm can be outlined as follows:

Step 1. Start iterations by setting the iteration index $k=0$.
Step 2. Initialize state vectors $x_i(k)$, $i=1,\ldots,r$, typically as the flat start.
Step 3. Each area A_i, $i=1,\ldots,r$ concurrently:

a) Calculates and factorizes the coefficient matrix $F_i=\begin{pmatrix} G_i & H_{ci}^T \\ H_{ci} & -R_{ci} \end{pmatrix}$ as

$$F_i=\begin{pmatrix} L_i & 0 \\ M_i & L_{ci} \end{pmatrix}\begin{pmatrix} D_i & 0 \\ 0 & -D_{ci} \end{pmatrix}\begin{pmatrix} L_i^T & M_i^T \\ 0 & L_{ci}^T \end{pmatrix}.$$

b) Calculates $\Delta y_i(k)=(L_i D_i)^{-1} H_i^T R_i^{-1}\Delta z_i(k)$, $\rho_i(k)=\begin{pmatrix} \vdots \\ \Delta z_{ci}(k) \\ \vdots \end{pmatrix}-M_i D_i \Delta y_i(k)$.

c) Transmits L_{ci}, D_{ci}, and $\rho_i(k)$ to the coordinator.

Step 4. The coordinator:

a) Calculates and factorizes the gain matrix $G_c=\sum_{i=1}^{r} L_{ci} D_{ci} L_{ci}^T$ as $G_c=L_c D_c L_c^T$.

b) Calculates $\rho_c(k)=\sum_{i=1}^{r}\rho_i(k)-\begin{pmatrix} h''_{c1}(x_{c1}(k),x_{e1}(k)) \\ \vdots \\ h''_{cr}(x_{cr}(k),x_{er}(k)) \end{pmatrix}$ and

$$\lambda(k+1)=\left(L_c^T\right)^{-1}\left[\left(L_c D_c\right)^{-1}\rho_c(k)\right].$$

c) Transmits $\lambda(k+1)$ to each area A_i, $i=1,\ldots,r$.

Step 5. Each area A_i, $i=1,\ldots,r$ concurrently:

a) Calculates $\Delta u_i(k)=M_i^T\lambda(k+1)$ and $\Delta x_i(k)=\left(L_i^T\right)^{-1}\left(\Delta y_i(k)+\Delta u_i(k)\right)$.

b) Determines $e_{i,max}(k)=max\left|\Delta x_i(k)\right|$.

c) Checks if $e_{i,max}(k)<e_{i,max}(k-1)$

– If yes, updates $x_i(k)$ by $x_i(k+1)=x_i(k)+\Delta x_i(k)$ and transmits

$$x_{ci}(k+1)\cup\left(\bigcup_{\substack{j=1\\ j\neq i}}^{r} x_{ej}(k+1)\right)$$ and $e_{i,max}(k)$ to the coordinator.

– If not, area i starts to diverge and is not further considered.

Step 6. The coordinator:

a) Calculates $e_{max}(k)=max\left[e_{i,max}(k)\right]$.

b) Checks if $e_{max}(k)<e_{max}(k-1)$

– If yes, checks if $e_{max}(k)<\varepsilon$, where ε is a predefined convergence tolerance. If yes, system wide state estimation has converged and algorithm stops. If not, sets $k=k+1$ and goes to step 3.

– If not, system wide state estimation starts to diverge and algorithm stops.

By the above distributed iterative scheme, the optimal solution is obtained in the same number of iterations as in the conventional centralized formulation. At each iteration, the required data exchanges between areas and the coordinator are:

- the unit lower triangular matrix L_{ci} and the diagonal matrix D_{ci}, of dimension $\frac{m_c^2-m_c}{2}$ and m_c respectively, and the vector $\rho_i(k)$, of dimension m_c, from each area A_i to the coordinator (step 3.c);

- the vector $\lambda(k+1)$, of dimension m_c, from the coordinator to each area A_i (step 4.c);

- the scalar $e_{i,max}(k)$ and the vector $x_{ci}(k+1)\cup\left(\bigcup_{\substack{j=1\\ j\neq i}}^{r} x_{ej}(k+1)\right)$, of dimension $l_i\leq|B(i)|$, where $|B(i)|$ is the cardinality of set $B(i)$, from each area A_i to the coordinator (step 5.c), where $\bigcup_{\substack{j=1\\ j\neq i}}^{r} x_{ej}(k+1)\subseteq x_i(k+1)$ (step 5.c).

Summarizing, each area sends to and receives from the coordinator $\frac{m_c(m_c+5)}{2}+l_i+1$ floating-point elements at each iteration. The number of floating-point data that have to be exchanged between the areas and the coordinator at each iteration, will be $\frac{m_c(m_c+5)}{2}+\sum_{i=1}^{r} l_i+r$. In practice, the number of boundary measurements and boundary buses involved with boundary measurements in each area is very limited compared to the number of area's local measurements, thus the amount of data exchange between areas and the coordinator is very small and possible time delays, and thus an increase in the total computational cost, are avoided.

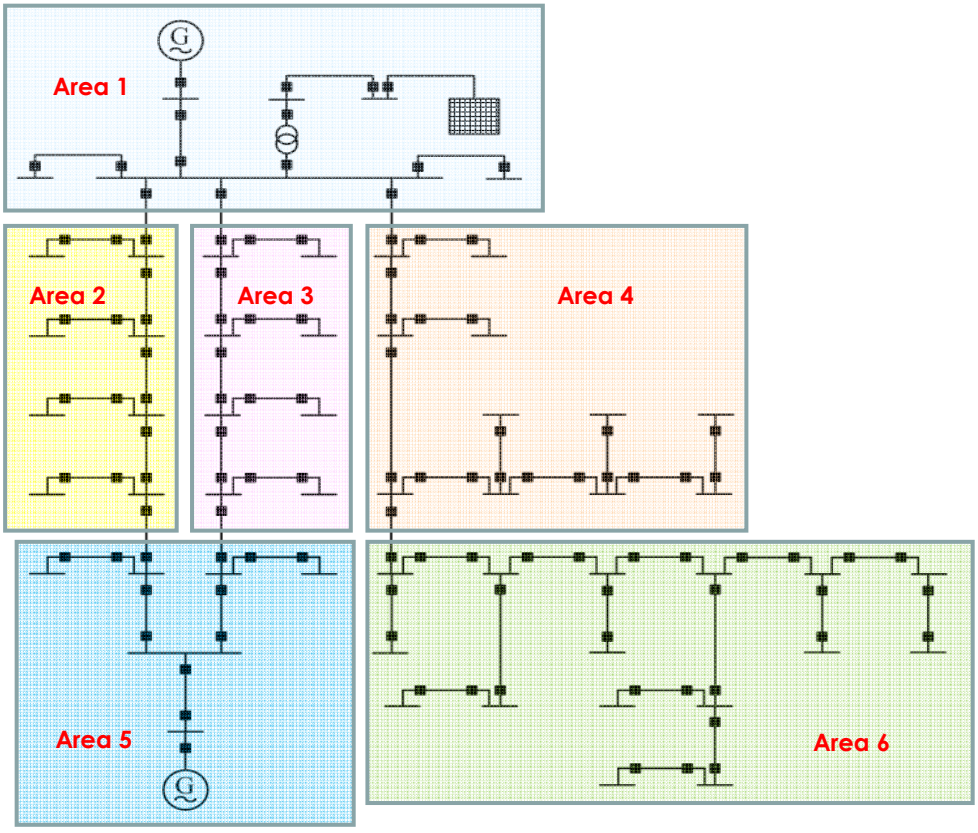

Figure 11 - Illustrative example of distribution network multi-zone partitioning.

2.7 Meter Placement

In order to assure accurate distribution voltage estimates and minimize the estimated voltage uncertainties, identification of the minimum number and location of additional voltage, current and power sensors in the network is included as a sub-function

of the state estimation functionality [53], [54]. A heuristic method will be applied using the uncertainty of each state as a metric to assess the accuracy of the state estimation solution [5]:

$$x_i^{uncertainty\%} = \left| \frac{300 \times \sqrt{C_x(i,i)}}{x_i^{true}} \right| \quad (20)$$

where

$$C_x = \left(H^T R^{-1} H \right)^{-1} \quad (21)$$

C_x is the state error covariance matrix, the ith diagonal entry $C_x(i,i)$ of C_x is the variance of the ith state, and x_i^{true} is the true state value (voltage or angle) of the ith bus. For the derivation of eq. (20), we have assumed that the region between $(\text{mean} - 3\sigma)$ and $(\text{mean} + 3\sigma)$ covers the full area under the Gaussian distribution.

An obvious choice to reduce the state uncertainties is to place voltage or/and active/reactive power meters on the nodes or close to the nodes having the largest diagonal elements $C_x(i,i)$, assuming that a predefined number of measurements are available.

3 MV grid topology identification using multiple data sources (including namely the information collected from the smart metering support infrastructure) (Sub-Task 3.3.1)

The traditional way of structuring state estimation in transmission networks relies on the assumption that the network parameters and topology are known beyond any doubt. The Network Topology Processor (NTP) converts the bus section/switch model in the bus/branch model, by processing the switching device (circuit breaker, isolator, bus-tie) statuses (logical data). The bus-branch model has proven to be effective for analog bad data analysis based on the *J(x)* and r_N statistical tests [44]-[46]. In case of logical bad data, this model does not provide means for explicit representation of switching devices and assignment of statistical values to them. It is to be noted that topology errors have a more dramatic influence on the measurement residuals than the parameter errors, causing state estimate to be significantly biased. As a result, several analog measurements appear as interacting bad data and may be erroneously eliminated, yielding unacceptable state. It is also possible to have serious convergence problems, in the presence of topology errors.

In distribution systems, the status of several switching devices may be unknown or suspicious, since reconfiguration actions are very frequent and the number of telemetered measurements is generally very limited. As a consequence, it is not possible to find and fix one topology beyond any kind of uncertainty. In any case, it must be considered one topology to initiate the SE process but the formulation should be flexible enough to identify topology changes [47]. In order to simulate an in service / out of service generator, load, or branch, the generalized state estimation model, reported in [1], [47] – [50] will be used.

In this project a probabilistic procedure is proposed for the topology identification, by augmenting the state vector with the statuses and the power flows across the switching devices and introducing “soft” operational constraints related to switching devices, with a degree of uncertainty. This means that topology will be estimated at the same time with analog information. Normalized residual test will be used to identify and correct bad switch statuses. An advantage over previous methods is that the proposed approach eliminates the need of repeated state estimation runs for alternative hypothesis evaluation.

3.1 Switching device modeling

The status of a switching device $k-l$ may be *open, closed or unknown*, as shown in Figure 12

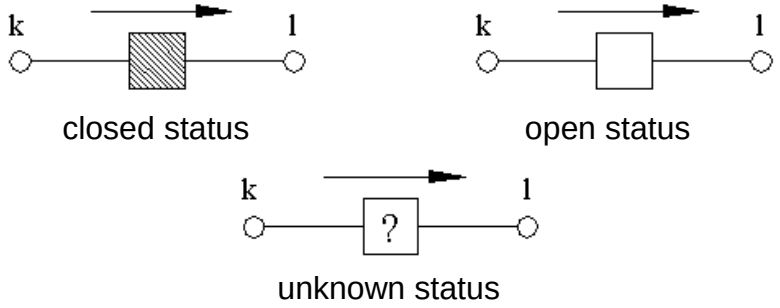

Figure 12 - Status of switching device $k-l$.

In order to examine the in/out operation of a branch *k-m* (Figure 13.a) and a generator or a load connected at bus *k* (Figure 14.a, Figure 14.c), a switching device is assigned to it and is explicitly modeled by introducing a virtual zero injection node *l*, as shown in Figure 13.b, Figure 14.b and Figure 14.d, respectively.

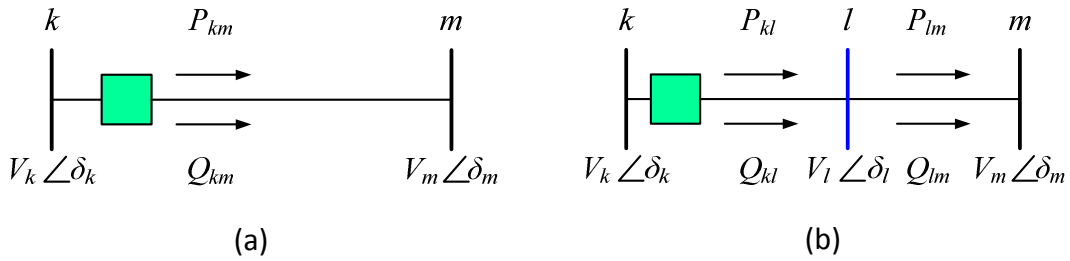

Figure 13 - Modeling switching device associated with a branch.

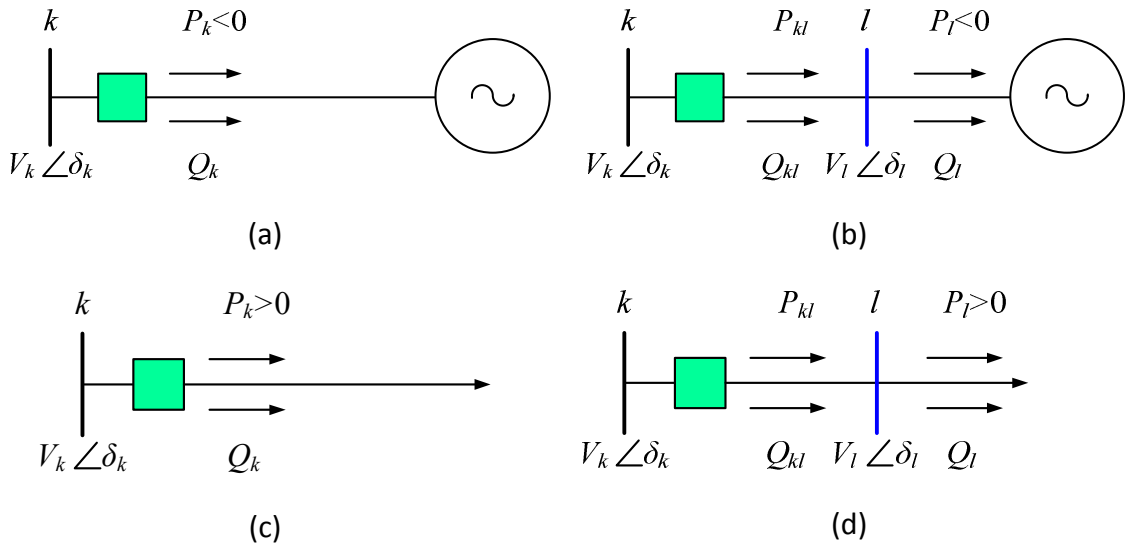

Figure 14 - Modeling switching device associated with a generator or load.

The state vector is augmented by the probabilistic status (continuous random variable) s_{kl} $(0 \le s_{kl} \le 1)$ of the switching device $k-l$ and the bus voltage angle δ_l and magnitude V_l of the virtual node l.

For a switching device $k-l$, the following measurements may be available:

- active and reactive power flow, written as:

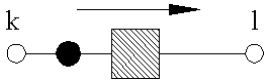

$$P_{kl}^{meas} = P_{kl} + e_{P_{kl}}, \qquad Q_{kl}^{meas} = Q_{kl} + e_{Q_{kl}} \tag{22}$$

- active and reactive injection, written as:

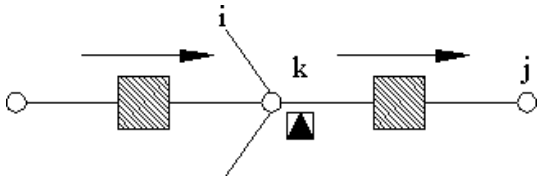

$$\begin{aligned} P_k^{meas} &= \sum_{i \in L_k} P_{ki}(\delta_k, \delta_i, V_k, V_i) + \sum_{j \in B_k} P_{kj} + e_{P_k} \\ Q_k^{meas} &= \sum_{i \in L_k} Q_{ki}(\delta_k, \delta_i, V_k, V_i) + \sum_{j \in B_k} Q_{kj} + e_{Q_k} \end{aligned} \tag{23}$$

where the superscript $meas$ stands either for assumed (manual) or measured (monitored) values and L_k (B_k) is the set of nodes connected to node k through conventional (switching) branches, P_{kj} (Q_{kj}) is the true active (reactive) power flow across switching device $k-j$, and $P_{ki}(\delta_k, \delta_i, V_k, V_i)$, $Q_{ki}(\delta_k, \delta_i, V_k, V_i)$ is the true active and reactive power flow across conventional branch $k-i$, calculated according to power flow equations of Appendix C.

- status, written as:

$$s_{kl}^{meas} = s_{kl} + e_{s_{kl}} \tag{24}$$

where $s_{kl}^{meas} = 0$ is for open and $s_{kl}^{meas} = 1$ is for closed status. If status information is unavailable, then the status is considered as unknown or uncertain and (24) is not used.

For each switching device $k-l$, soft operational constraints (pseudo measurements with uncertainty) are introduced:

$$0 = s_{kl}\delta_{kl} + e_{s\delta_{kl}}, \qquad 0 = s_{kl}V_{kl} + e_{sV_{kl}} \tag{25}$$

$$0=(1-s_{kl})P_{kl}+e_{P_{kl}}, \qquad 0=(1-s_{kl})Q_{kl}+e_{Q_{kl}} \tag{26}$$

where δ_{kl} (V_{kl}) is the angle difference $\delta_k-\delta_l$ (magnitude drop V_k-V_l) across switching device $k-l$.

From (25) we obtain zero estimated angle difference ($\hat{\delta}_{kl}\to 0$) and zero estimated voltage drop ($\hat{V}_{kl}\to 0$) if the estimated status $\hat{s}_{kl}\to 1$ (is closed). From (26) we obtain $\hat{P}_{kl}\to 0$ and $\hat{Q}_{kl}\to 0$ if the estimated status $\hat{s}_{kl}\to 0$ (is open).

A threshold value of $\varepsilon=10^{-4}$ is adopted for status identification. An estimated status $\hat{s}_{kl}\le\varepsilon$ ($\hat{s}_{kl}\ge 1-\varepsilon$) indicates that the switching device $k-l$ is open (closed) with probability $1-\varepsilon$ [48]. An estimated status $\varepsilon<\hat{s}_{kl}<1-\varepsilon$ indicates uncertain status due to model inconsistencies and bad data. Assuming that there is enough measurement redundancy around the location of the switching device under suspicion, the correct status of the switching device $k-l$ can be identified by testing its normalized residual against a detection threshold. It is worth to be noted that, even for large scale distribution networks with thousand of buses, the number of switching devices explicitly modeled will be relatively low, and thus the size of the augmented state and measurement vectors will not lead to prohibitive computational burden.

Two types of topology errors will be investigated in this project:

- ***Exclusion error:*** when a switching device actually in service, is inadvertently excluded in the model.
- ***Inclusion error:*** when a *switching* device is erroneously included in the state estimation model.

3.2 The Network Splitting Problem

When speaking about topology identification we are also addressing the problem of islanding. Depending on the unknown or suspicious status of some switching devices, a number of disconnected electrical islands may be formed. A local phase angle reference bus will be considered for each island. However, a problem will exist when the number of islands is not known a priori. In this case, the number of reference buses will be also unknown.

The splitting problem can be formulated as the problem of finding the state variables in all electrically disconnected islands. Traditional SE approach assumes that the topology is known and fixed a priori and the whole system consists of a unique connected island or a predefined number of islands. In this case, splitting is impossible since there is a unique bus for phase angle reference. When considering status uncertainties, the number of initial islands can be smaller or larger than those really existing in the system. If the network is split into two or more disconnected islands, the system becomes unobservable and the state vector cannot be computed.

The following approach is proposed to resolve this problem. Assume that the network is separated into a set of islands (subsystems) owing to switching devices $k-l$ being reported as open. Island S_1 is arbitrarily chosen to contain the global reference bus. For each island $S_i \neq S_1$, two soft constraints (pseudo measurements) are introduced as follows:

$$0 = \prod_{k \in S_i, l \in S_{j \neq i}} (1 - s_{kl})\, \delta_{ref,i} + e_{\delta_{ref,i}} \tag{27}$$

$$0 = \delta_{ref,i} + e_{\delta_{ref,i}} \tag{28}$$

where, $k-l$ are open switching devices connecting island S_i with islands $S_j \neq S_i$, buses k and l belong to islands S_i and S_j respectively, and $\delta_{ref,i}$ is the phase angle of an arbitrarily selected reference bus in the ith island with respect to that of island 1. Pseudo measurements of type (27) make the network observable and permit calculation of the state vector.

The way constraint (27) works is explained as follows:

- If all initially open switching devices $k-l$ invoked in (27) remain open ($s_{kl} = 0$) after all iterations, then $\delta_{ref,i} = 0$, which indicates that island S_i is actually isolated from the rest of the system and its own state variables are estimated with respect to local reference bus.
- When the status of an initially open switching device $k-l$ ($k \in S_i$ and $l \in S_j$), becomes closed ($s_{kl} = 1$) after some iterations, pseudo measurement (27) becomes $0 = 0.\delta_{ref,i}$ and has no influence on $\delta_{ref,i}$. In this case island S_i is merged with island S_j and pseudo measurement (27) for this island is eliminated by assigning to it a very small weight.

4 Simulations with Rhodes distribution network

In this section simulation results for all the relevant subtasks will be presented, using the Rhodes distribution network and the associated parameter and measurement data provided in Appendix B.

4.1 State estimation simulations and KPI calculations

The available measured data depend on the types and locations of the metering devices at the Rhodes network. The injected active and reactive power and voltage magnitude at the MV infinite bus are measured every hour by an RTU and transmitted in near real-time (with a small time delay i.e. 15 min or ½ hour). The injected power of the slack bus is shared among the two feeders in proportion to the total rated power of the DG units and distribution transformers associated to each feeder and results in two pairs of active and reactive power flow measurements at the receiving end of the two feeders R220 και R260. The power injections and voltage magnitudes at the two WF are recorded hourly but are transmitted once per day and are available the next day. For the power injections and voltage magnitudes of the PV units and the power consumptions of MV load buses no real-time data is available. HEDNO has provided the shape of the seasonal supply curves and the daily distribution of photovoltaics' (PV) generation. Based on this historical data and statistical information, hourly power generation curves were generated at DG buses. Using these hourly DG generation and hourly total feeder flow values, hourly power demand curves for the load buses were obtained. The general idea is to subtract the contribution of DG generation from the total feeder flows and get the total power consumption of each feeder as follows:

$$P_{flow}^{tot} = \left|P_{dem}\right| - \left|P_{gen}^{DG}\right|$$

where

P_{flow}^{tot} : power flow metered at the top of the feeder,

P_{dem} : total power demand of the feeder

P_{gen}^{DG} : power generation of DG units of the feeder.

The calculated total hourly power demand was allocated among the set of MV/LV distribution transformer buses connected to the feeders, by using the following ratios obtained from transformer capacities:

$$P_i = \frac{TC_i}{\sum_{i=1}^{NF} TC_i} P_{tot}$$

where

P_i : power demand at node i,

P_{tot} : power flow metered at the top of the feeder,

TC_i : transformer capacity at node i

NF : number of nodes served by each feeder.

In this way, 135 active and reactive power consumption curves were generated and randomly distributed fluctuation was added at each curve. Furthermore, typical active and reactive load demand values per load bus were calculated by assuming a specific loading level, approximately 90% of rated transformer capacity, and a flat power factor of 0.9. Based on the above load demand and generation injections, hourly power flow solutions were derived and used as inputs to the state estimator. Also, normally distributed random errors were added at the load flow results, in order to simulate the measured values.

State estimation is carried out at hourly intervals on daily basis for a period of one week. More specifically, a whole week of July 2013 was used for simulations, in order to assess the performance of the combined operation of the method of pseudo-measurements generation for load buses and state estimation algorithm. The index *Relative Percentage Error* (RPE) was deployed to quantify errors in voltage magnitude estimates for all network buses. It is a vector indicator whose calculation is based on the relative difference between measured and estimated voltage magnitudes of the full state vector, i.e. it consists of as many elements as the number of network buses.

$$RPE_V = \frac{V_m^{meas} - V_m^{est}}{V_m^{meas}} 100\%$$

where

V_m^{meas}: measured voltage magnitude vector,

V_m^{est} : estimated voltage magnitude vector.

The variations of the index RPE per network bus, using internal (contiguous) bus numbering, are shown in Figure 15 and Figure 16. Each figure is associated with a different day of the selected week and includes 24 RPE values for each bus (one per hourly state estimation execution). Since the test network consists of 374 buses, each daily diagram displays $24 \times 374 = 8976$ values, as follows: each diagram depicts 24 curves of RPE fluctuation and each curve consists of 374 values (one per network bus).

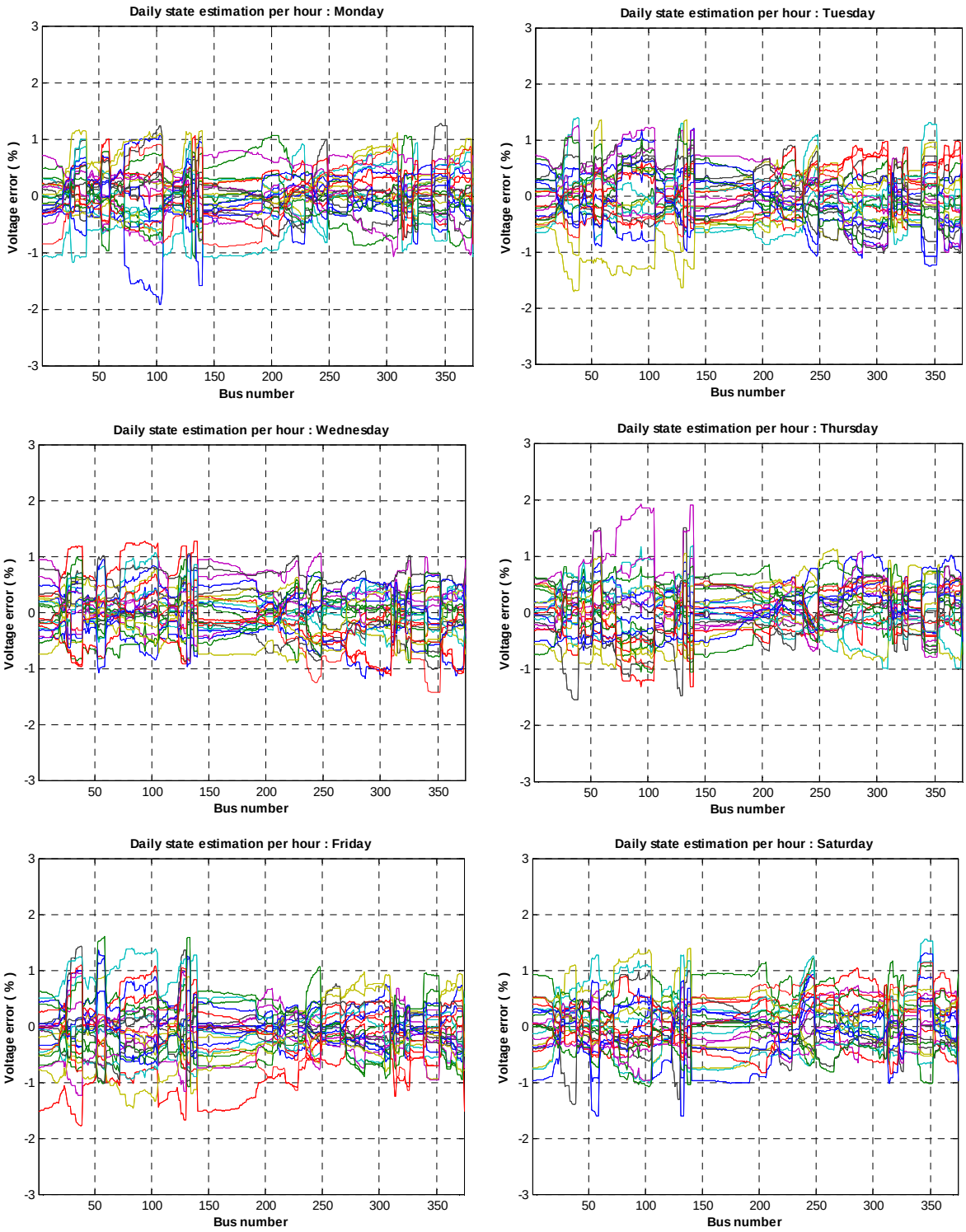

Figure 15 - Voltage magnitude relative percentage errors (RPE) per network bus (Monday-Saturday)

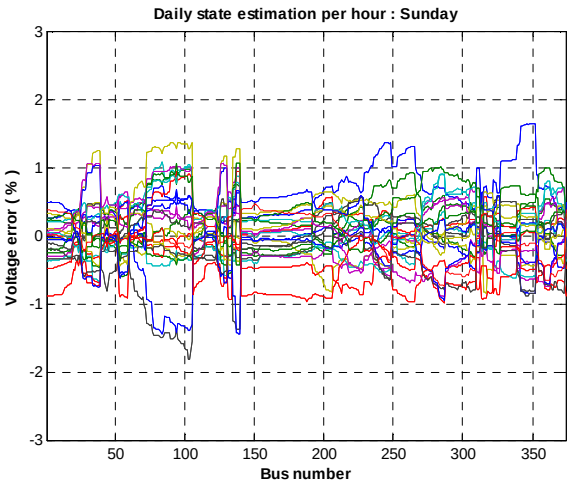

Figure 16 - Voltage magnitude relative percentage errors (RPE) per network bus (Sunday)

In general, $RPEs$ lie in a range of ±2%. Results of Friday and weekend show higher RPE values and most of the related curves tend to disperse along vertical axis more than respective curves of the other weekdays. Since these diagrams cannot be fully informative a statistical analysis of results is necessary. In Table 2 mean absolute values of voltage $RPEs$ are calculated and categorized according to the bus type they refer to: *load buses (PQ), photovoltaics (PV), wind farms (WF), zero-injection buses, capacitor buses (CP)* and *the slack bus (SB).*

Table 2 - Statistical results for weekly state estimation simulations.

Day	Max average error / Bus No	Average errors per bus type					
		PQ	PV	WF	ZI	CP	SB
Monday	0.5782 / 140	0.3304	0.3325	0.2233	0.3207	0.2897	0.3084
Tuesday	0.5891 / 140	0.3741	0.3861	0.2603	0.3376	0.3253	0.3562
Wednesday	0.5292 / 38	0.3354	0.3557	0.2205	0.3358	0.3306	0.3538
Thursday	0.6367 / 103	0.3568	0.3536	0.3001	0.3427	0.3061	0.3178
Friday	0.6526 / 38	0.3625	0.3576	0.3152	0.3417	0.3333	0.3575
Saturday	0.5910 / 286	0.3572	0.3650	0.2789	0.3387	0.3393	0.3366
Sunday	0.5950 / 139	0.3362	0.3478	0.2036	0.3251	0.2509	0.2529

Average errors, shown in Table 2, indicate that SE results are more accurate nearby wind farms, capacitor banks and zero injection buses. On the contrary, higher average errors are observed at load and PV buses. Wind farm power generations are based on actual measurement derived from previous day data, while zero injection measurements are treated as perfect data. Medium values result for slack bus voltage error. As mentioned before, all load demand data are pseudo-measurements and general solar

power generation curves were used to create hourly PV power generation values. In general, actual real-time or, even, historical data for power injection at certain buses, lead to lower errors than using pseudo-measurements or derivative data.

Error Estimation Index (EEI) and $Macc_V$ indicators were used to test the state estimation accuracy (Figure 17 and Figure 18).

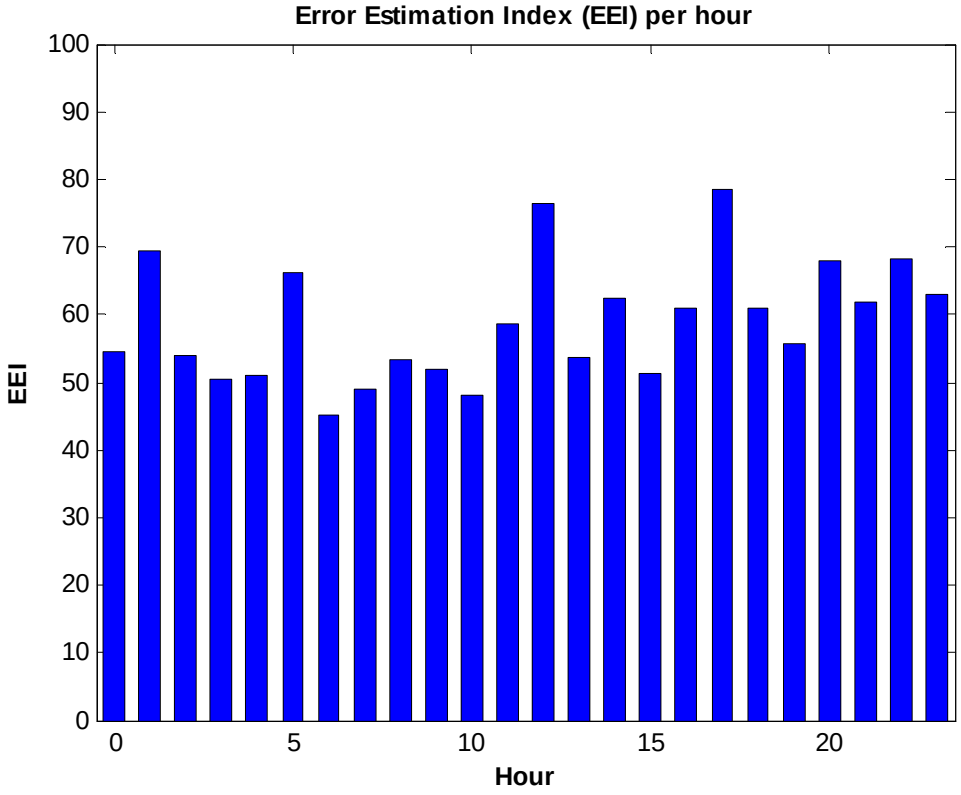

Figure 17 - Error Estimation Index (EEI)

The values of EEI, displayed in Figure 17, vary between 35 and 80. This index depends on the number of measurements and the range of values of the standard deviations. Assuming that each measurement i has a random Gaussian noise of $\pm 3\sigma_i$ deviation around the mean, the maximum (threshold) value for the index *EEI* would be $EEI_{max} = \sum_{i=1}^{m} \left(\frac{\pm 3\sigma_i}{\sigma_i} \right)^2 = 9m$. In our case, 807 measurements have been used for the SE process, meaning that $EEI_{max} = 9 \times 807 = 7263$, and all standard deviations are within the interval [0.01, 0.02]. It is evident that the values of index EEI, shown in Figure 17, are very low compared to the threshold value, which certifies the efficiency of the SE algorithm.

Concerning the index $Macc_V$, displayed in Figure 18, it is observed that its values lie between 0.03 and 0.14 p.u., which means that the state estimator has significant accuracy in terms of voltage phasor estimates for all network buses.

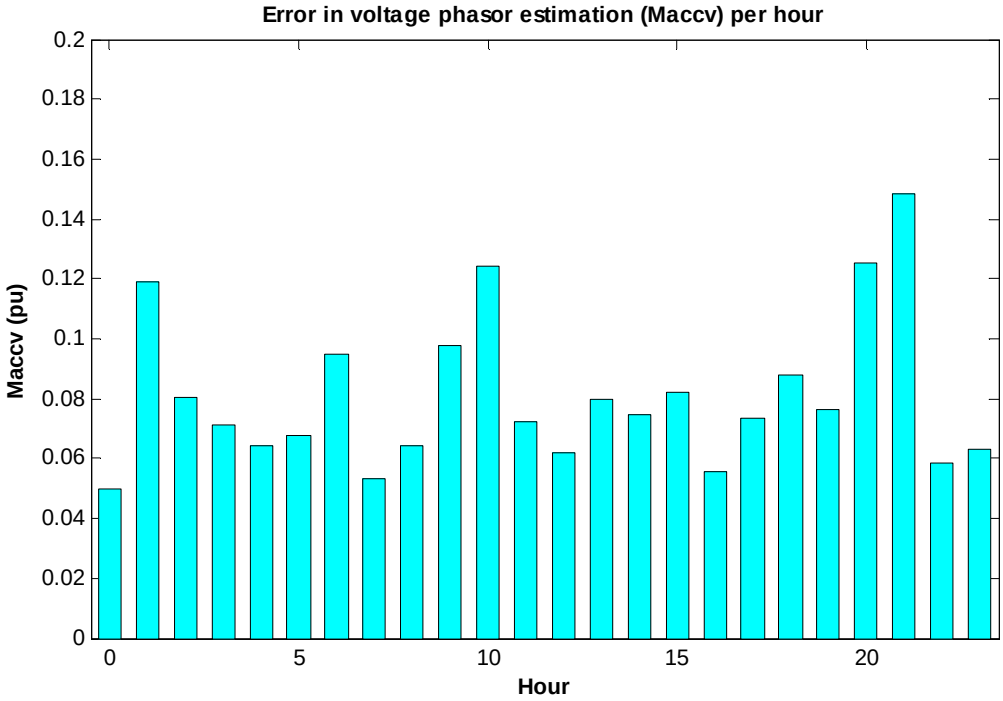

Figure 18 - 2-norm Voltage Error

Furthermore, certain KPIs were computed and depicted in diagrams, in order to evaluate the accuracy and performance of the state estimation algorithm (see Appendix D for definitions). For this task, hourly state estimation runs were carried out for one, randomly selected, day. As a consequence, 24 values per each KPI will be provided. Active and reactive power injection and flow estimates were checked. Measured, estimated and true values are used for each index of interest and computations are carried out based on a norm-like set of equations (see Appendix D for details). They are quantitative measures of the power measurement estimates precision.

As shown in Figure 19, Figure 20 and Figure 21, 1-norm and 2-norm KPIs for active and reactive power flows are higher than the power injections KPIs. The behavior of flow KPIs is approximately the same per norm and their values relatively low. The 1-norm injection KPIs are significantly higher, at least 10 times bigger, while 2-norm injection KPIs are 5 times bigger, on average, than equivalent flow KPIs. In general, 1-norm and 2-norm KPIs are within acceptable limits and confirm that state estimation is adequately accurate. With regard to infinity norm KPI, the resulting KPI flow values are very close to the corresponding 1-norm flow KPIs. On the contrary, the resulting injection KPI values are much smaller than the the corresponding 1-norm injection KPIs. This is anticipated, since flow measurements are only 2, while injections measurements are 373. In this way, maximum estimation errors of injections and flows per SE execution are relatively close, approximately 0.01 p.u. on average.

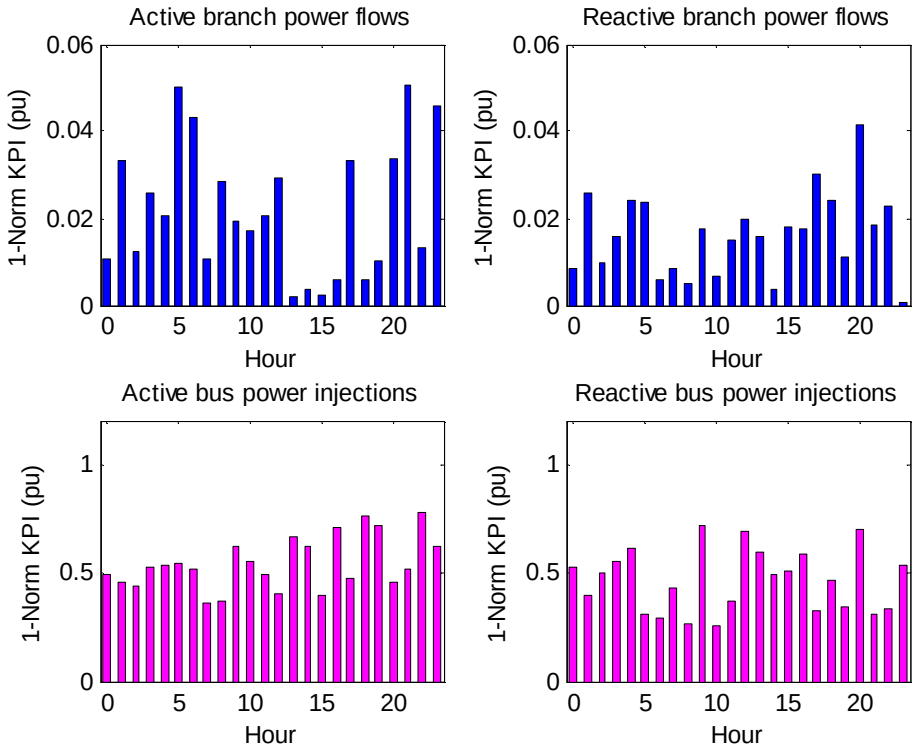

Figure 19 - 1-norm Power Flows and Injections Estimation Errors

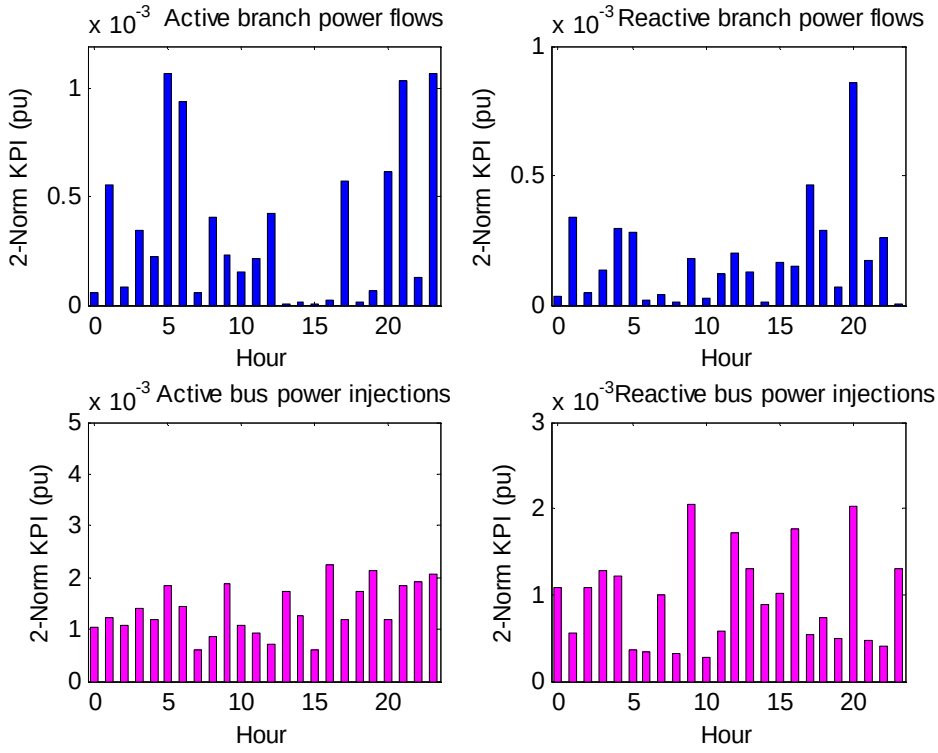

Figure 20 - 2-norm Power Flows and Injections Estimation Errors

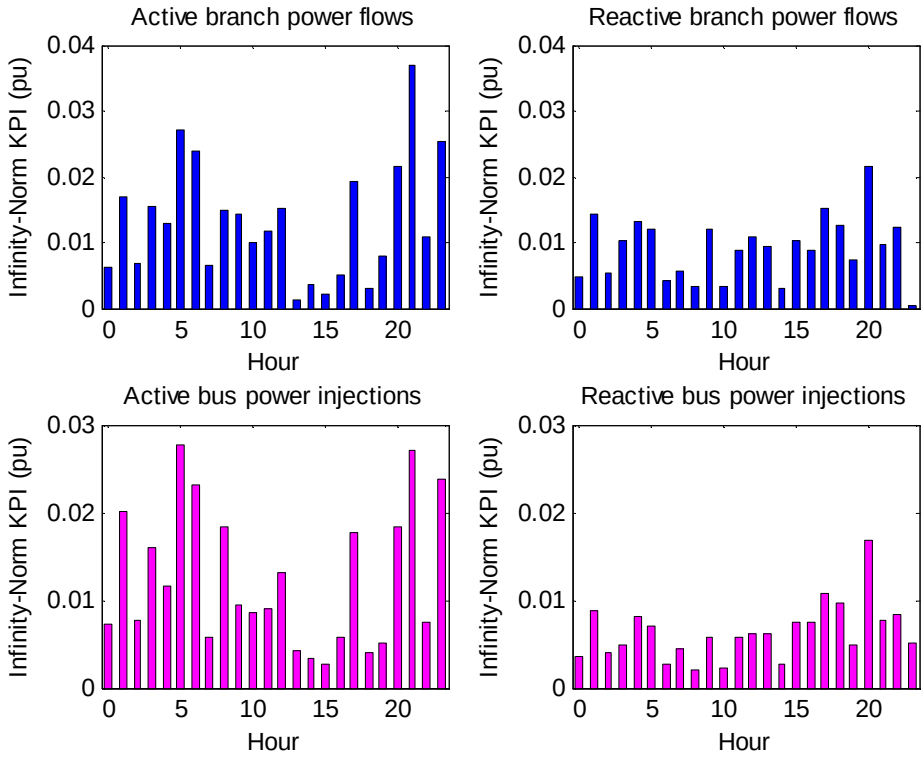

Figure 21 - Infinity-norm power flows and injections estimation errors

The last accuracy KPI is presented in Figure 22 and it is an estimation error ratio: 2-norm metric of the difference between true and estimated value to 2-norm metric of the difference between true and measured value. For a good estimation, the estimate of each power quantity should lie closer to the true than the measured value and the entire metric will be less than one. As can be seen, power injection KPIs, PIP_i, PIQ_i, meet this requirement except for 2-3 values. Power flow KPIs, PIP_f, PIQ_f, are rather worse (approximately 10% of the 48 flow values are higher than 1).

Finally, the performance of the state estimator was assessed by means of three KPIs related to the convergence of the algorithm: $Mconv_{obj}$, $Mconv_V$, $Mconv_\delta$. The first KPI uses the objective function value to check convergence capability, while the other two use voltage magnitude and angle estimates (see Appendix D for corresponding definitions). Their variation is shown in Figure 23.

Indices $Mconv_{obj}$ and $Mconv_V$ show almost identical variation per SE run. Index $Mconv_\delta$ tends to show the same behavior for about 50% of the cases (10th to 23th hour). Generally, all KPIs have relatively low values, as it is desirable. The value of $Mconv_V$ means that the ratio of two last successive voltage magnitude estimates is almost one, while the value of $Mconv_\delta$ shows that a precision of 3rd decimal digit is fulfilled concerning voltage angle estimation before the last algorithm iteration.

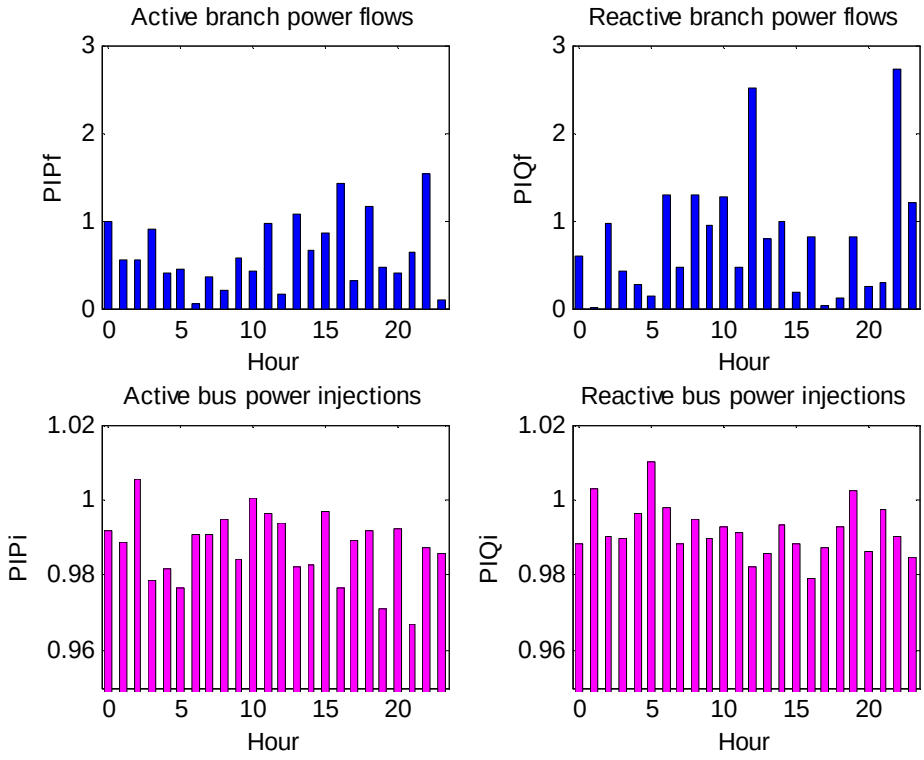

Figure 22 - Ratio of power flows and injections estimation errors

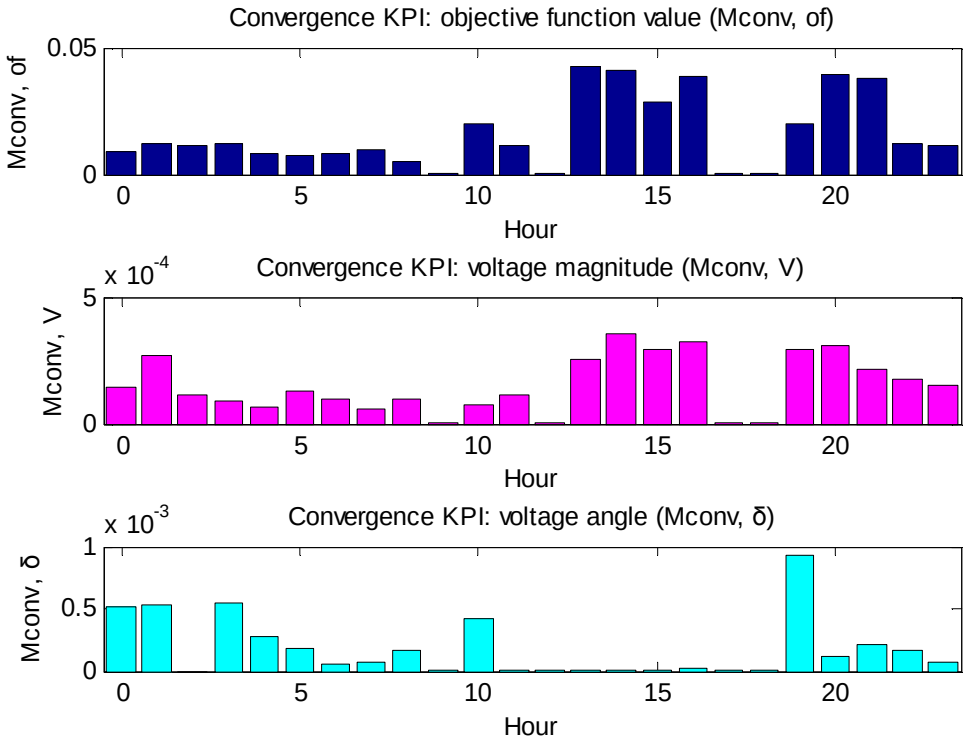

Figure 23 - Convergence KPIs

4.2 Bad data analysis

Three cases with single bad data are examined. Only the behavior of generation and load bus states is studied (zero injection buses are excluded). As a consequence, the set of buses shown in the horizontal axis of the following figures does not include the zero injection buses and the remaining buses are renumbered consecutively (for instance, node 121 corresponds to bus number 61 of feeder R220 due to exclusion of zero injection buses). Estimated values of the reference bus are given in the diagrams of feeder R220 (last value per each diagram, corresponding now to bus number 73). Each diagram is separated in two subplots, one per feeder.

Case 1: Single bad data at generation bus 121 (bus number 61) of feeder R220. The true and the measured generation is 0.22MW+0.07MVAr and 0.35MW+0.11MVAr respectively. The true and the estimated bus voltage magnitudes and active/reactive injections are shown in Figure 24 - Figure 27. As can be seen, the faulty generation value at bus 121 affects mainly the buses of feeder R220, where this bus belongs, and the reference bus, especially concerning estimates of active power injection and voltage magnitude. Additionally, as can be observed, a set of buses (40-50, 59-62) which are directly or closely connected to node 121, show the highest errors . The normalized residuals of the active and reactive injected generation measurements of bus 121 were 3.237>3 and 3.614>3 respectively, indicating gross errors. After removing these measurements and recomputing the state vector all the normalized residuals became<3.

Case 2: Single bad data at load bus 8 (bus number 4) of feeder R220. The true and the measured load is 0.15MW+0.05MVAr and 0.34MW+0.12MVAr respectively. The true and the estimated bus voltage magnitudes and active/reactive injections are shown in Figure 28 - Figure 31. As can be observed, the faulty load value at bus 8 affects mainly the nodes of feeder R220 and the reference node. As in the previous case, a set of buses (0-27) show remarkably higher errors than the others because of their direct connection with bus 8. The normalized residuals of the active and reactive load injection measurements at bus 8 were 4.171>3 and 3.621>3 respectively, indicating gross errors. After removing these measurements and recomputing the state vector all the normalized residuals became<3.

Case 3: Double bad data at load bus 324 (bus number 61) and generation bus 380 (bus number 92) of feeder R260. The true and the measured injections are 0.09MW+0.06MVAr and 0.21MW+0.13MVAr (bus 324) and 0.12MW+0.05MVAr and 0.17MW+0.08MVAr (bus 380) respectively. The true and the estimated bus voltage magnitudes and active/reactive injections are shown in Figure 32 - Figure 35. As can be seen, the faulty load and generation values at buses 324 and 380 affect mainly the buses of feeder R260 and the reference node and a set of neighboring buses (50-70). The normalized residuals of the active and reactive injection measurements for bus 324 were 3.564>3 and 3.89>3 and for bus 330 were 3.12>3 and 3.08>3 respectively, indicating gross errors. After removing these measurements and recomputing the state vector all the normalized residuals became<3.

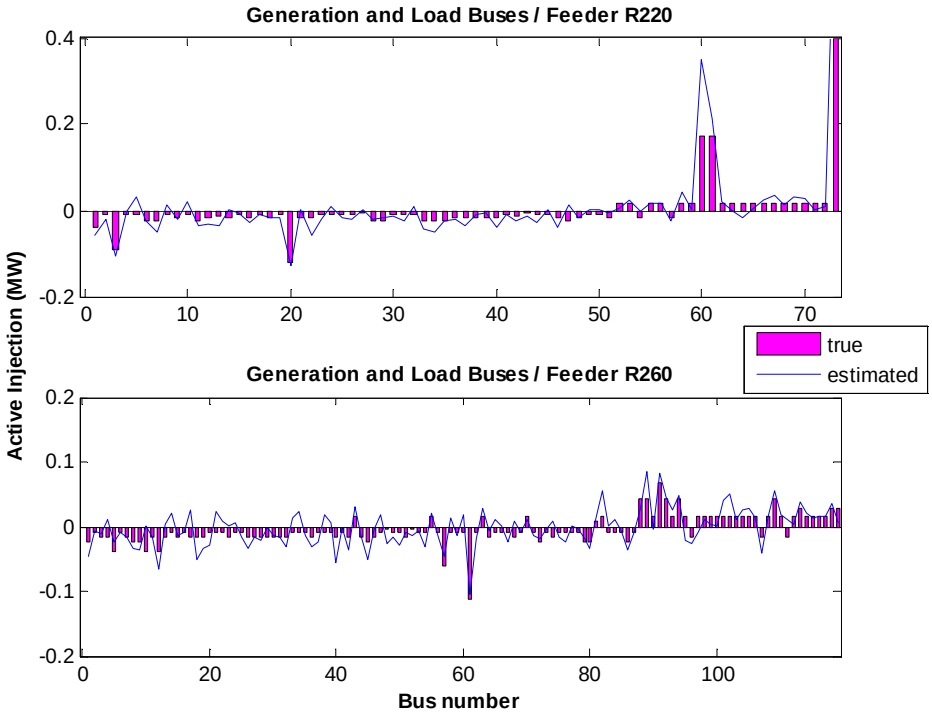

Figure 24 - True and estimated active bus injections (single bad data at generation bus 121).

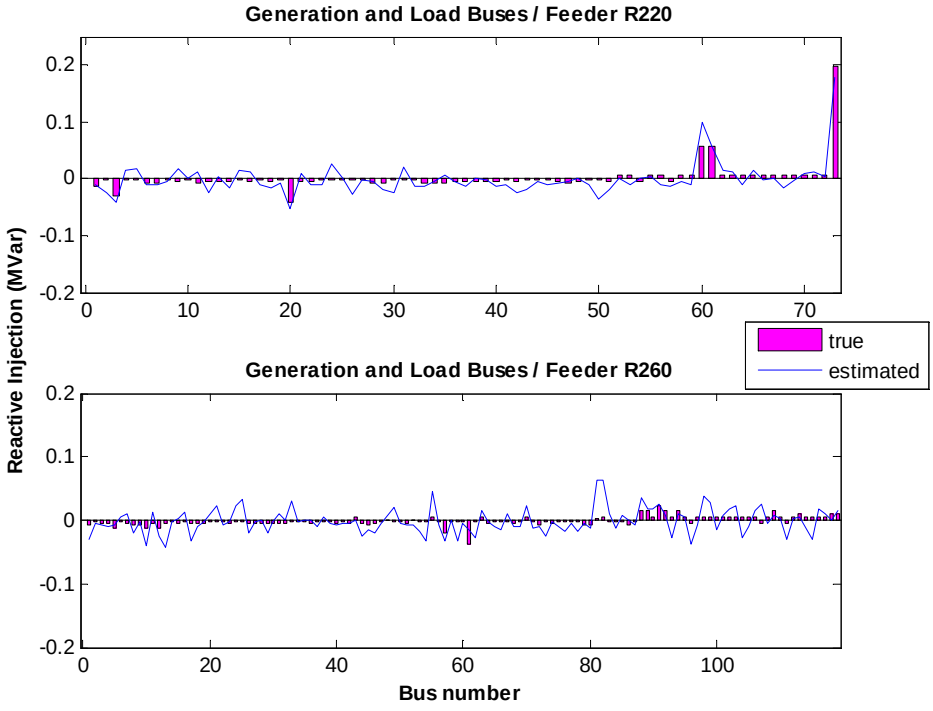

Figure 25 - True and estimated reactive bus injections (single bad data at generation bus 121).

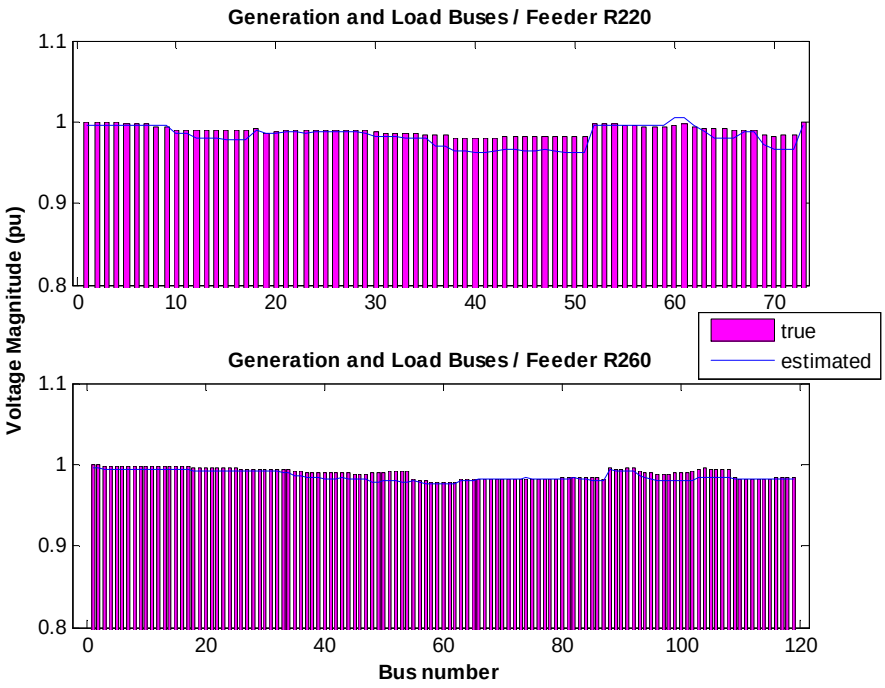

Figure 26 - True and estimated node voltage magnitudes (single bad data at generation bus 121).

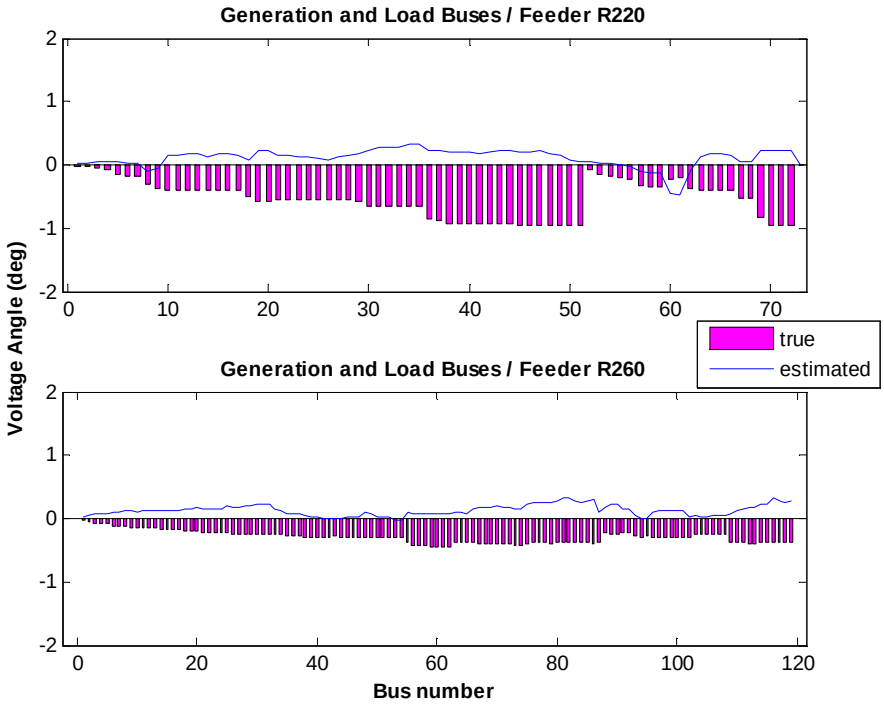

Figure 27 - True and estimated node voltage angles (single bad data at generation bus 121).

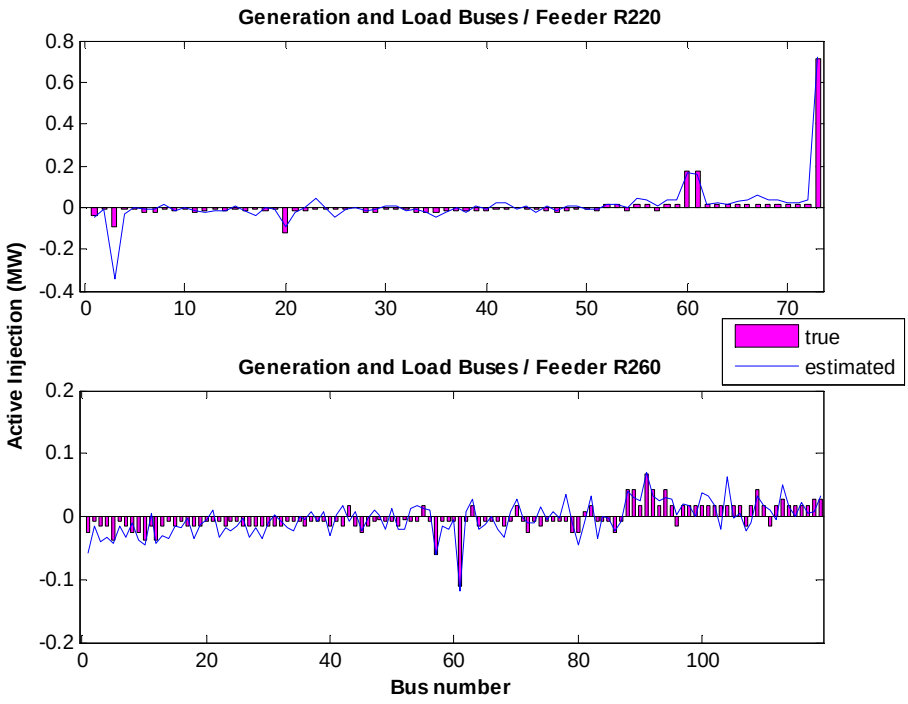

Figure 28 - True and estimated active bus injections (single bad data at load bus 8).

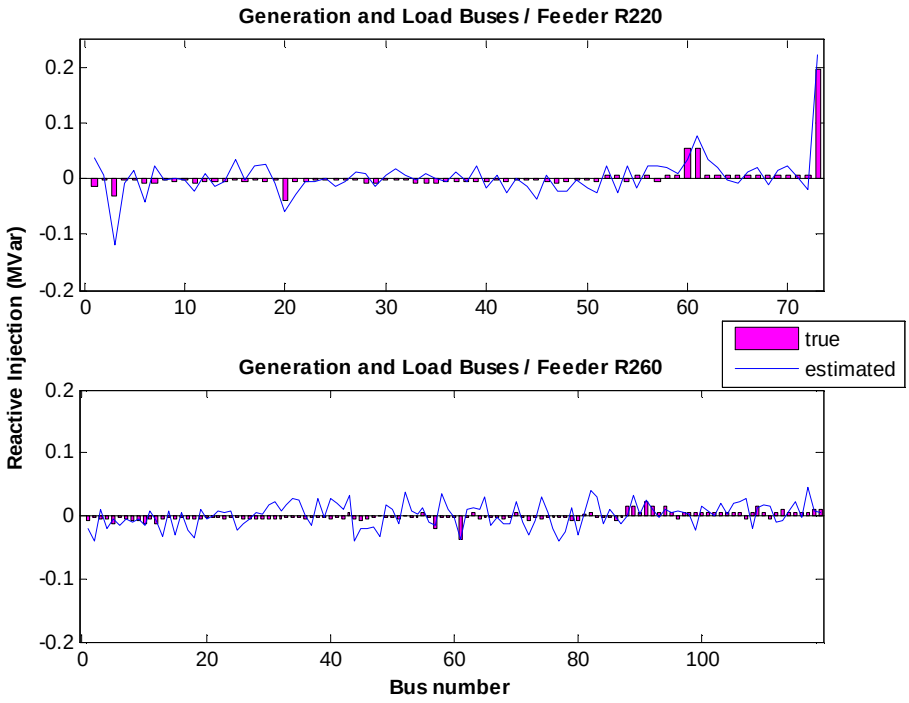

Figure 29 - True and estimated reactive bus injections (single bad data at load bus 8).

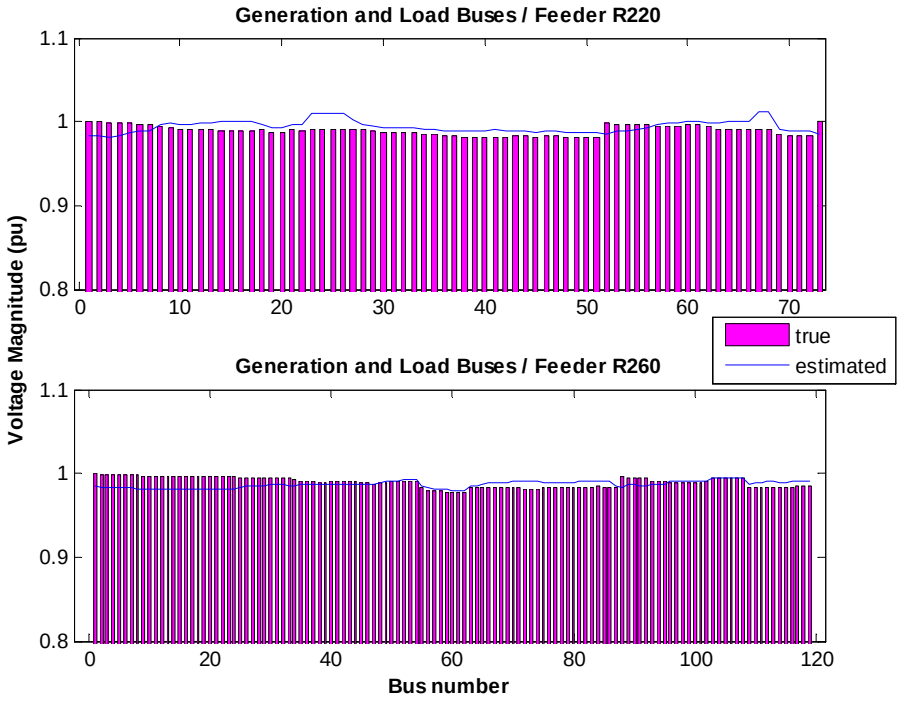

Figure 30 - True and estimated node voltage magnitudes (single bad data at load bus 8).

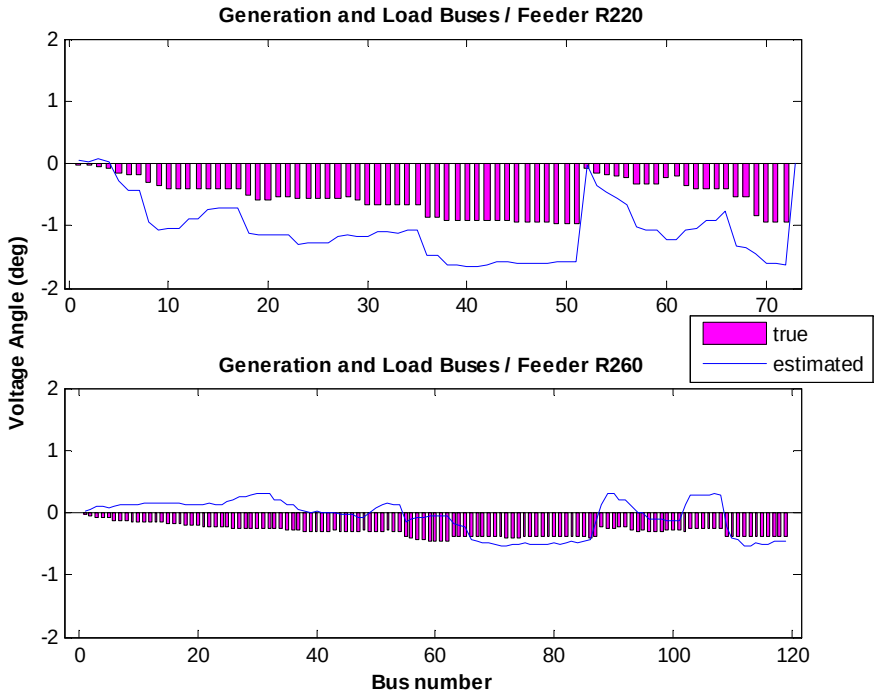

Figure 31 - True and estimated node voltage angles (single bad data at load bus 8).

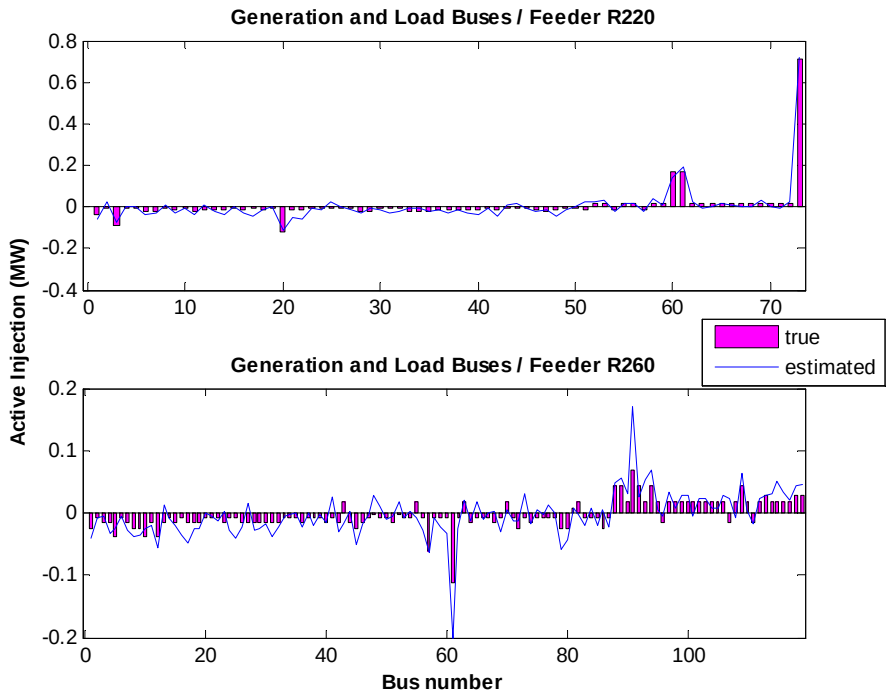

Figure 32 - True and estimated active bus injections (bad data at generation bus 380 and load bus 324).

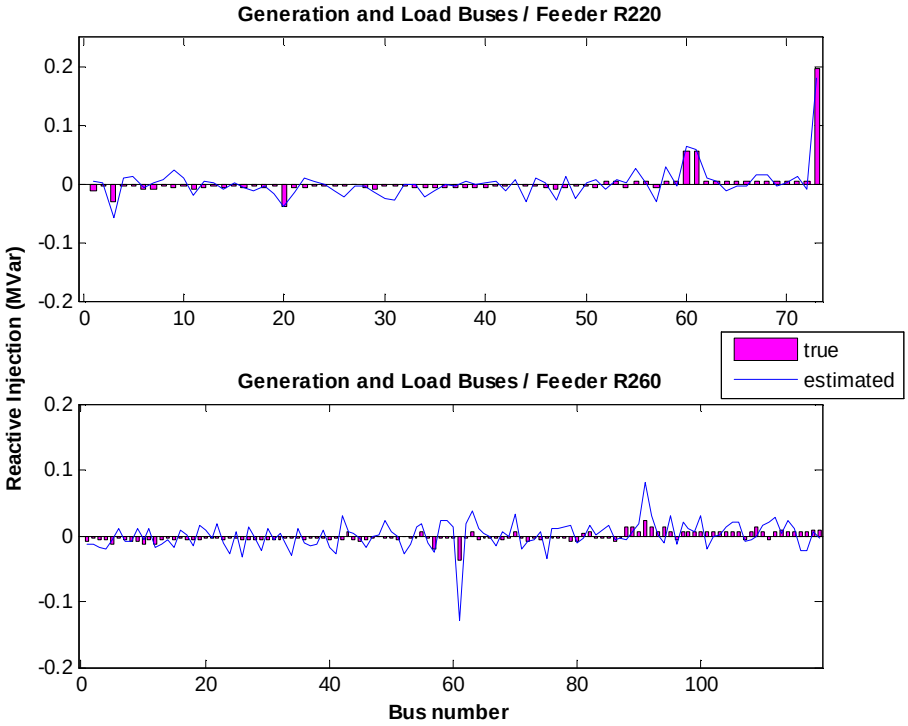

Figure 33 - True and estimated reactive bus injections (bad data at generation bus 380 and load bus 324).

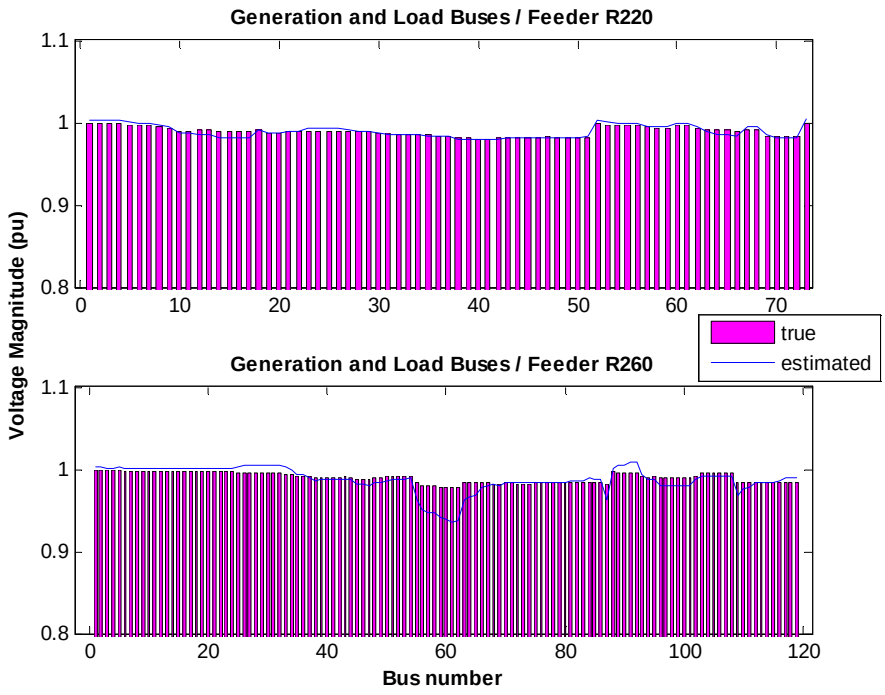

Figure 34 - True and estimated node voltage magnitudes (bad data at generation bus 380 and load bus 324).

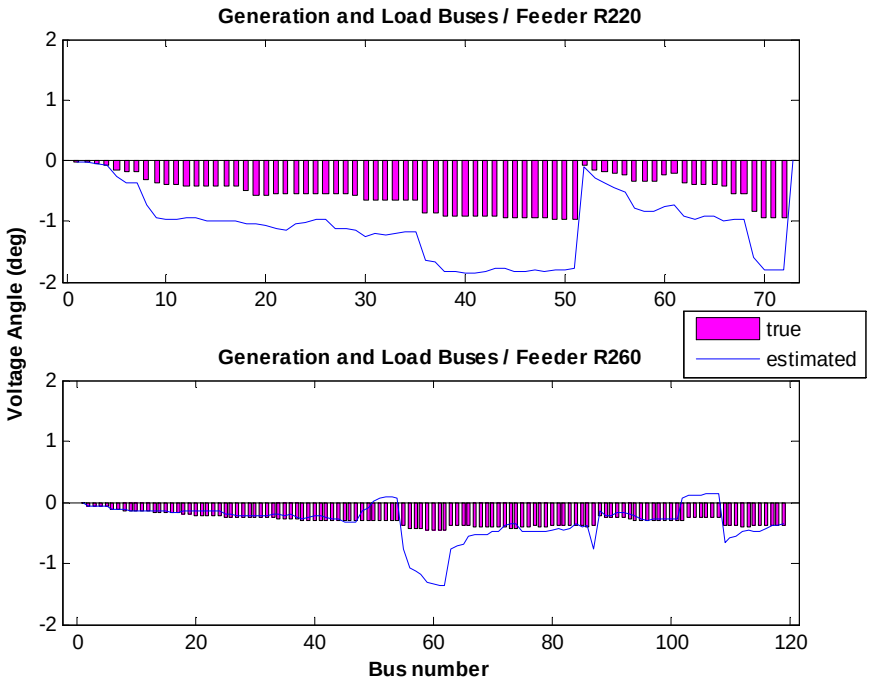

Figure 35 - True and estimated node voltage angles (bad data at generation bus 380 and load bus 324).

State estimation simulations show that a gross error in a load or generation bus injection affects mainly the node voltages of the feeder where this load or generation bus belongs. Additionally, estimated errors in voltage angles are higher than those of voltage magnitudes. The primary MV substation at the slack bus acts as a burden to the error spread from one feeder to another. The reason is the relatively low measurement redundancy at each feeder (groups of minimally dependent sets of measurements are formed), which restricts the error propagation at a narrow region around the contaminated measurements.

4.3 Multi-area state estimation simulations

In this section, the computation time requirements for the local and the coordination levels of the proposed distributed state estimator are analyzed. The proposed distributed algorithm is tested on the Rhodes network. Several network partitioning scenarios are examined (Figure 36 - Figure 39). More specifically, feeder R-260 has been divided into 2, 3, and 4 areas and R-220 into 1 and 2 areas for the purposes of the multi-area state estimation. We are considering five different combinations of area divisions, as shown in Table 3 to Table 8. Case 0 corresponds to the centralized (integrated) state estimator. The local state estimators are executed independently, in a sequential way, on a single CPU machine and the estimated border states and measurements are transmitted to the coordination estimator, which computes the system-wide solution.

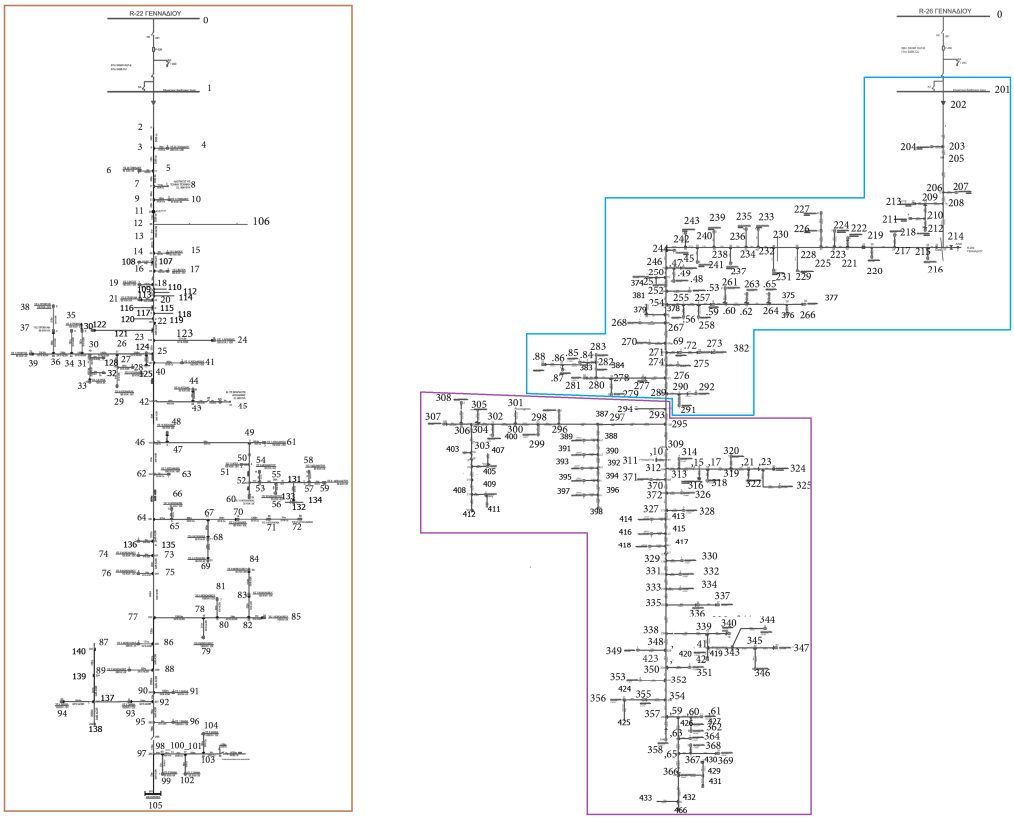

Figure 36 - Case 1: Division into 3 areas (R-220 (1) & R-260 (2))

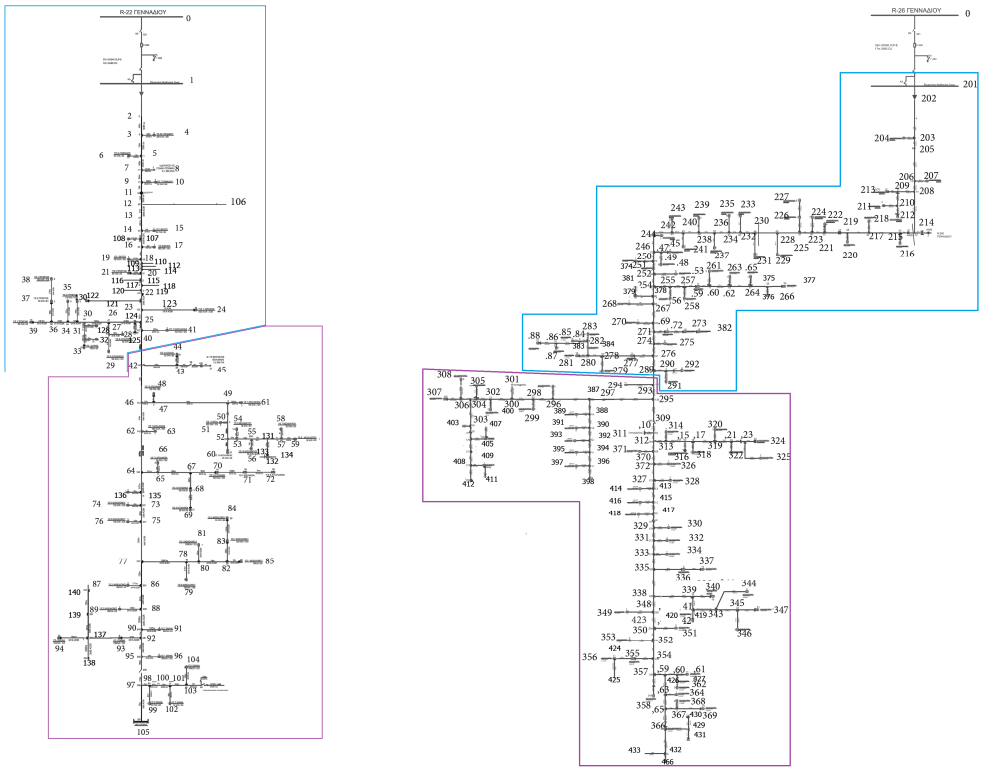

Figure 37 - Case 2: Division into 4 areas (R-220 (2) & R-260 (2))

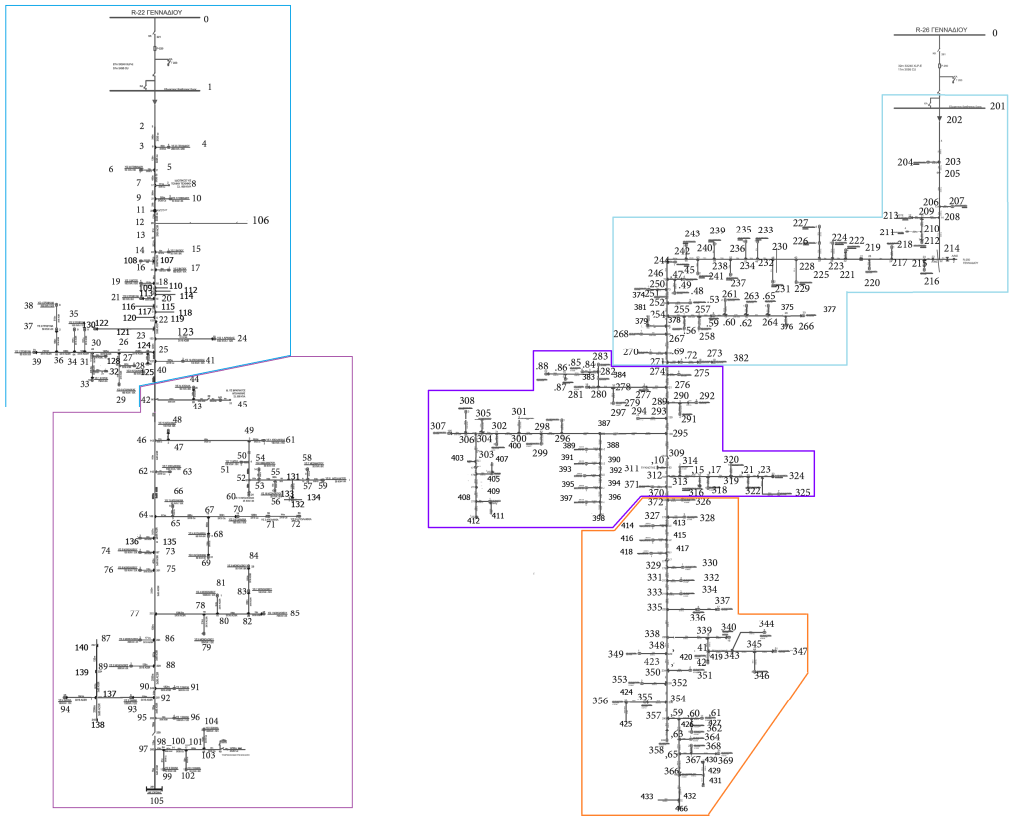

Figure 38 - Case 3: Division into 5 areas (R-220 (2) & R-260 (3))

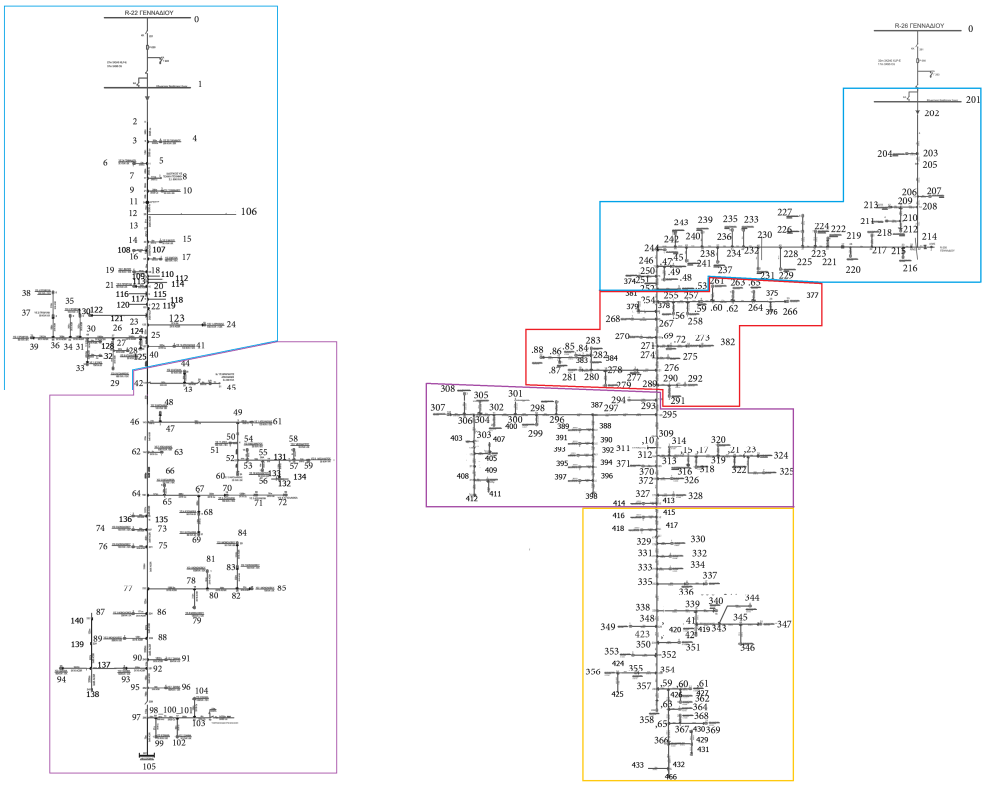

Figure 39 - Case 4: Division into 6 areas (R-220 (2) & R-260 (4))

Each subsystem comprises pairs of P/Q power flow measurements at one end of internal lines and pairs of P/Q power injection measurements related to the internal buses, while each tie-line has one P/Q power flow measurement at one of its terminal buses. A number of boundary buses are injection measured. For each area a local phase angle reference bus is considered and a voltage magnitude measurement is assigned assumed. Based on the area number for each bus (field IA of bus data structure in Appendix A), each slave processor retrieves its own area's network and measurement data and the root processor retrieves the boundary buses and measurements.

Table 3 - Measurement configuration for each test case

	Case 0	Case 1	Case 2	Case 3	Case 4
Internal P/Q flows	1	1	1	1	1
Boundary P/Q flows	1	1	1	1	1
Internal P/Q injections	372	370	368	366	364
Boundary P/Q injections	1	3	5	7	9

Tabular results with the total execution time, regarding each configuration and case, are shown in Table 4 to Table 7.

Table 4 - CPU time for Case 0

	Area 1 R-220	Area 2 R-260
Buses range	1-140	201-433
Number of buses	140	233
Time for local calculations (msec)	180	500
Time for coordination calculations (msec)	200	200
Total time (msec)	380	700

Table 5 - CPU time for Case 1

	Area 1 R-220	Area 2 R-260	Area 3 R-260
Buses range	1-140	201-292, 373-386	293-372, 387-433
Number of buses	140	106	127
Time for local calculations (msec)	180	120	140
Time for coordination calculations (msec)	120	120	120
Total time (msec)	300	240	260

Table 6 - CPU time for Case 2

	Area 1 R-220	Area 2 R-220	Area 3 R-260	Area 4 R-260
Buses range	1-41, 106-130	42-105, 131-140	201-292, 373-386	293-372, 387-433
Number of buses	66	74	106	127
Time for local calculations (msec)	50	60	120	140
Time for coordination calculations (msec)	80	80	80	80
Total time (msec)	130	140	200	220

Table 7 - CPU time for Case 3

	Area 1 R-220	Area 2 R-220	Area 3 R-260	Area 4 R-260	Area 5 R-260
Buses range	1-41, 106-130	42-105, 131-140	201-273, 373-382	274-308, 370-371, 383-412	309-372, 413-433
Number of buses	66	74	85	67	83
Time for local calculations (msec)	50	60	70	50	70
Time for coordination calculations (msec)	70	70	70	70	70
Total time (msec)	120	130	140	130	140

Table 8 - CPU for Case 4

	Area 1 R-220	Area 2 R-220	Area 3 R-260	Area 4 R-260	Area 5 R-260	Area 6 R-260
Buses range	1-41, 106-130	42-105, 131-140	201-253, 373-374	254-292, 375-386	293-328, 387-414	329-372, 415-433
Number of buses	66	74	55	51	64	63
Time for local calculations (msec)	50	60	40	80	70	80
Time for coordination calculations (msec)	50	50	50	50	50	50
Total time (msec)	100	110	90	130	120	130

Table 9 compares the maximum total computation times of case 0, which is associated with the centralized state estimation simulation, and the distributed estimation of cases 1 to 4. Both the centralized and the distributed algorithm needed 5 iterations to converge. The maximum total computation time corresponds to the slowest converging area in each case.

Table 9 - Comparison of maximum CPU times for the test cases

	Maximum CPU time (msec)
Case 0	700
Case 1	300
Case 2	220
Case 3	140
Case 4	130

Note that for the centralized algorithm, neither data transmission nor coordination phases are considered. Regarding the communication timings, the time needed to send to and receive from the root solver the necessary border (boundary) data is a small percentage of the total time, which renders this communication cost almost negligible when compared with the actual computation time. As expected, the total CPU time for the distributed implementation is smaller than the one corresponding to the time required to solve the centralized problem. Furthermore, as the number of areas increases, the advantage of the distributed implementation over the centralized becomes more pronounced.

4.4 Meter placement studies

In order to investigate the reduction of voltage standard deviations, due to the placement of additional measurements at potential points of the test network, four cases are examined. Voltage magnitude measurements at heavily loaded MV buses or active/reactive power flow measurements at large transmission lines are considered as candidates. The test cases are described inTable 10.

Table 10 - Description of test cases for meter placement

Case	Type and location of additional measurements
1	Voltage magnitude at buses 4, 29, 45, 94, 116 of feeder R220
2	Voltage magnitude at buses 213, 224, 227, 316, 324 of feeder R260
3	P/Q power flows at lines 5-7, 22-23, 82-83 of feeder R220
4	P/Q power flows at lines 210-212, 221-223, 252-254 of feeder R260

The state uncertainties, given by (20), are calculated and plotted against bus number in Figure 40 to Figure 43. Each diagram corresponds to one case and is separated in two subplots: magnitude and angle of state variables.

It is obvious that uncertainties in both voltage magnitude and angle are remarkably higher in MV load buses than DG or MV zero injection buses. Maximum uncertainties are related to unmeasured MV load buses, being approximately 12% and 2% for voltage magnitude and angle, respectively. Moreover, buses of feeder R220 show lower voltage angle uncertainties, while buses of feeder R260 have relatively lower voltage magnitude uncertainties. Feeder R260 is more complex, with more DG buses. The uncertainty of voltage magnitudes is relatively lows, whereas the uncertainty of voltage angles is significantly higher than feeder's R220. Thus, it needs more additional voltage magnitude measurements comparing to feeder R220.

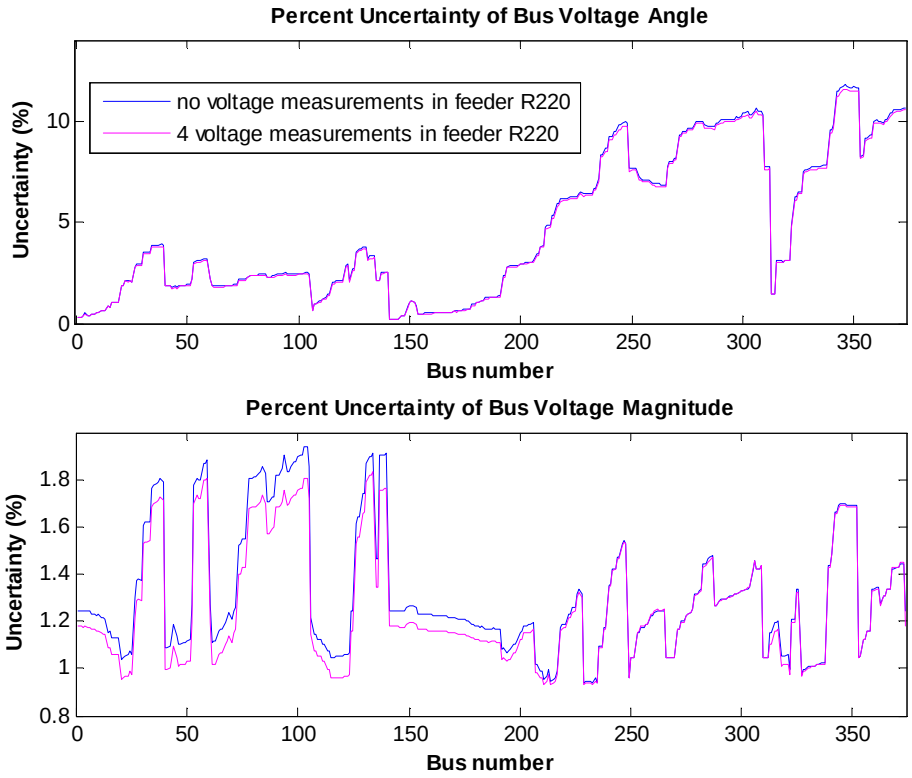

Figure 40 - Uncertainty of magnitude and angle of estimated bus voltages (Case 1).

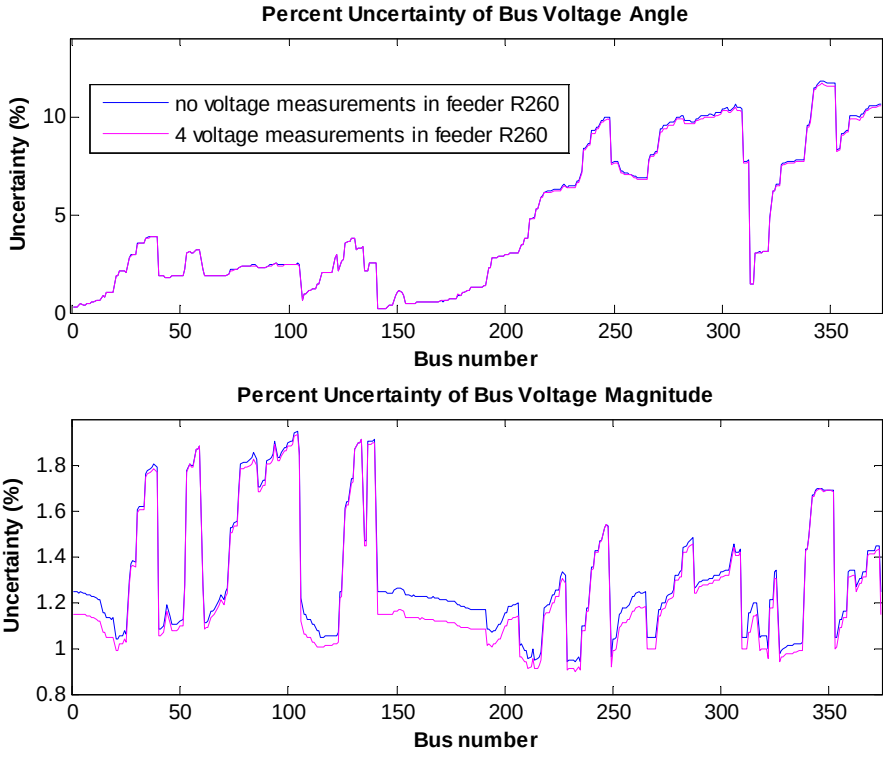

Figure 41 - Uncertainty of magnitude and angle of estimated bus voltages (Case 2).

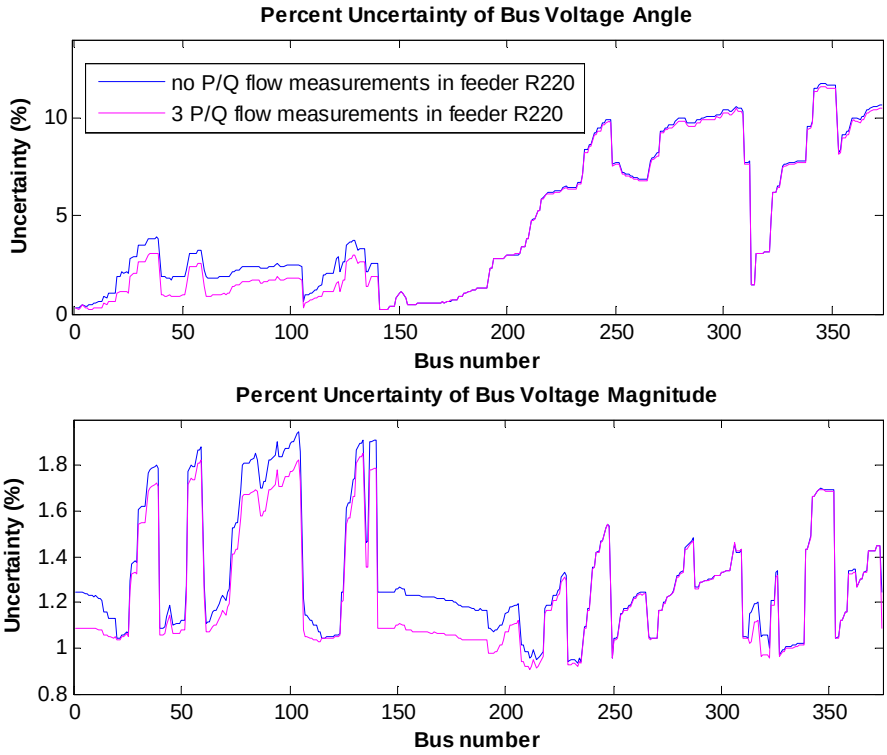

Figure 42 - Uncertainty of magnitude and angle of estimated bus voltages (Case 3).

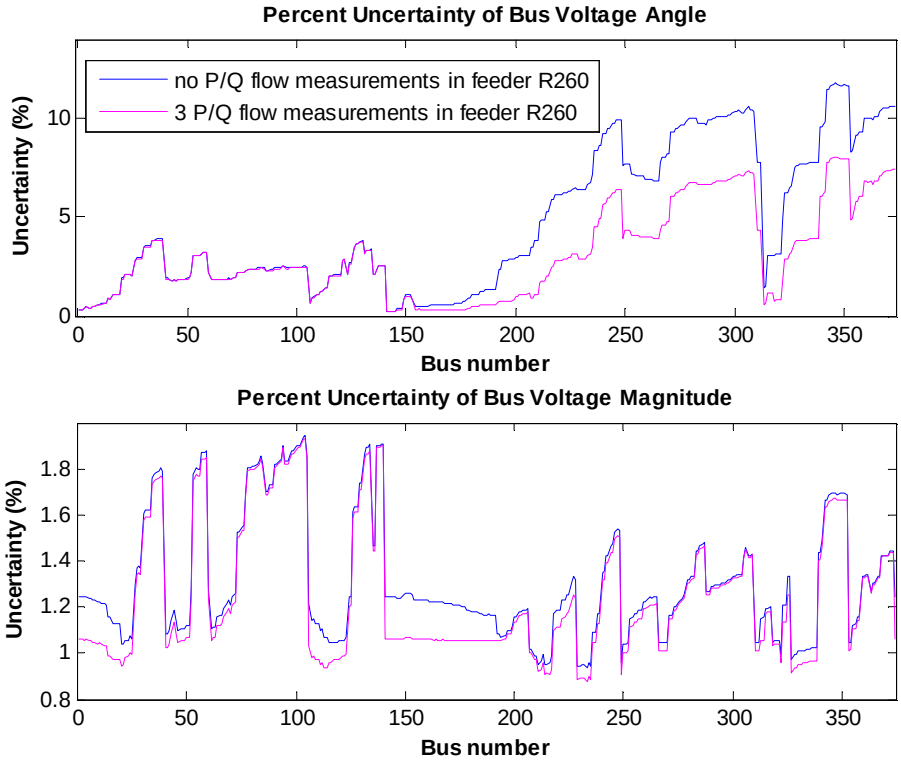

Figure 43 - Uncertainty of magnitude and angle of estimated bus voltages (Case 4).

Referring to Figure 40 and Figure 41, the addition of 4 voltage measurements either in feeder R220 or R260, improves the uncertainty of voltage magnitudes of the corresponding buses, that is, buses 1 to 140 for feeder R220 and buses 141 to 373 for feeder R260. On the contrary, uncertainty of voltage angle barely improves. Additionally, there is a group of buses, 1 to 20 and 140 to 190, whose voltage magnitude uncertainty is improved significantly in both cases. Referring to Figure 42 and Figure 43, the addition of 3 measurements of P/Q power flows either in feeder R220 or R260, improves the uncertainty of voltage angles of the corresponding buses, that is, buses 1 to 140 for feeder R220 and buses 141 to 373 for feeder R260. Moreover, the uncertainty of voltage magnitudes improves, but slightly less.

Conclusively, placement of meters for P/Q line power flows is more advantageous, since fewer metering associated locations provide better results, concerning uncertainties of bus voltage magnitudes and angles, than meters of bus voltage magnitudes. The results show an improvement in the voltage estimation in the region close to the location of the added measurements. The improvement is local, the voltage uncertainty at other regions remains almost the same.

4.5 Topology identification simulations

Several topology configurations are simulated as summarized in Table 11 to Table 13, where the true, assumed, and estimated switch statuses are shown. Cases 1–7 investigate a multiple configuration change (connection / disconnection of load at buses 110 and 320 and in / off service of DG at buses 121, 140 and 380). Five fictitious buses, numbered as 3000 to 3004, are introduced in the network and five switching devices, namely $s_{110-3003}$, $s_{121-3001}$, $s_{140-3002}$, $s_{320-3004}$ and $s_{380-3000}$, are considered for switching operations. The CB status is reported as 1 for closed and 0 for open switching device. Absence of bad analog measurements is assumed for cases 1–7. For case 8, a gross error of 40σ is added to the true value of active (P_{3003}) load pseudo measurement at bus 3003. For case 9, a gross error of 12σ and 18σ is added to the true value of active (P_{3003}) and reactive (Q_{3003}) load pseudo measurement at bus 3003. For case 10, a gross error of 10σ and 6σ is added to P_{3003} and Q_{3003}, respectively. Cases 11–13 consider the connection / outage of line 111–113 of feeder R220, where the fictitious bus 3005 and the switching device $s_{111-3005}$ are added in the network, respectively.

Table 11 - True, assumed and estimated status of switching devices for cases 1 to 3

Case	Switching device	True status	Assumed status	Estimated status
1	$s_{110-3003}$	1	1	1.0000000
	$s_{121-3001}$	1	1	1.0000000
	$s_{140-3002}$	1	1	0.9999999
	$s_{320-3004}$	1	1	1.0000000
	$s_{380-3000}$	1	1	1.0000000
2	$s_{110-3003}$	0	0	0.0042700
	$s_{121-3001}$	0	0	0.0042700
	$s_{140-3002}$	0	0	0.0042700
	$s_{320-3004}$	0	0	0.0042700
	$s_{380-3000}$	0	0	0.0042700
3	$s_{110-3003}$	1	1	1.0000000
	$s_{121-3001}$	1	0	1.0000000
	$s_{140-3002}$	1	1	1.0000000
	$s_{320-3004}$	1	1	1.0000000
	$s_{380-3000}$	1	1	0.9999810

Table 12 - True, assumed and estimated status of switching devices for cases 4 to 8

Case	Switching device	True status	Assumed status	Estimated status
4	$S_{110-3003}$	1	1	0.9999987
	$S_{121-3001}$	1	0	0.9999980
	$S_{140-3002}$	1	1	1.0000000
	$S_{320-3004}$	1	1	1.0000000
	$S_{380-3000}$	1	0	0.9999980
5	$S_{110-3003}$	1	0	1.0000000
	$S_{121-3001}$	1	1	1.0000000
	$S_{140-3002}$	1	1	1.0000000
	$S_{320-3004}$	0	0	0.0004170
	$S_{380-3000}$	1	1	0.9999690
6	$S_{110-3003}$	1	0	1.0000000
	$S_{121-3001}$	0	1	0.0000184
	$S_{140-3002}$	1	1	1.0000000
	$S_{320-3004}$	0	0	0.0004376
	$S_{380-3000}$	1	1	0.9999870
7	$S_{110-3003}$	1	0	1.0000000
	$S_{121-3001}$	1	0	0.9999184
	$S_{140-3002}$	0	1	0.0000132
	$S_{320-3004}$	0	0	0.0004376
	$S_{380-3000}$	1	1	0.9999870
8	$S_{110-3003}$	1	1	1.0000000
	$S_{121-3001}$	1	1	1.0000000
	$S_{140-3002}$	0	0	0.0000005
	$S_{320-3004}$	0	0	0.0001740
	$S_{380-3000}$	1	1	1.0000000

Table 13 - True, assumed and estimated status of switching devices for cases 9 to 13

Case	Switching device	True status	Assumed status	Estimated status
9	$s_{110-3003}$	1	0	1.0000000
	$s_{121-3001}$	1	1	1.0000000
	$s_{140-3002}$	0	0	0.0000005
	$s_{320-3004}$	0	0	0.0001740
	$s_{380-3000}$	1	1	1.0000000
10	$s_{110-3003}$	1	0	1.0000000
	$s_{121-3001}$	1	1	1.0000000
	$s_{140-3002}$	1	0	0.9999976
	$s_{320-3004}$	0	0	0.0000089
	$s_{380-3000}$	1	1	1.0000000
11	$s_{111-3005}$	1	1	1.0000000
12	$s_{111-3005}$	1	0	0.9997080
13	$s_{111-3005}$	0	1	0.0000500

The three largest normalized residuals for each bad data identification cycle are reported in Tables 14–18, where the last column gives the status of the switching devices at the beginning of each state estimation cycle. Normalized residuals $\left|\hat{r}^N_{\max}\right| > 3$ are shown in bold. It is worth to be noted that the estimated status of the switch 7–21, after the first state estimation cycle, is $\hat{s}_{110-3003} = 0.54$ for case 9 and $\hat{s}_{110-3003} = 0.58$ for case 10, indicating uncertain status. However, at the end of the estimation/bad data detection cycle, after all bad analog and status data have been identified, the correct status is found. In case 13, line 111–113 is assumed out of operation (the initial status of switching devices 111–3005 is reported as open), thus splitting the network into two disconnected energized islands and the Jacobian matrix becomes singular. In order to compute the state estimate, one pseudo measurement of type (27) is introduced as follows:

$$0 = (1 - s_{111-3005})\delta_{112}$$

where bus 112 is chosen to be the angle reference bus at the second island.

As can be observed from Tables 14–18, the algorithm successfully determines the correct topology configuration, whether or not a correct or incorrect topology configuration is initially assumed, using real and pseudo analog measurements, with or without gross errors, and operational constraints for the switching devices.

Table 14 - Normalized residual test for Cases 1 to 5

Case	SE run	Meas.	$\left\|\hat{r}_{N,i}\right\|_{max}$	Assumed status				
				$s^{assumed}_{110-3003}$	$s^{assumed}_{121-3001}$	$s^{assumed}_{140-3002}$	$s^{assumed}_{320-3004}$	$s^{assumed}_{380-3000}$
1	1st	P_{357}	2.8346867	1	1	1	1	1
		Q_{416}	2.6021712					
		Q_{102}	2.5638857					
2	1st	Q_{54}	2.5300879	0	0	0	0	0
		Q_{232}	2.2691149					
		Q_{80}	2.1177385					
3	1st	$S_{121-3001}$	50.0000000	1	0	1	1	1
		Q_{125}	2.7612610					
		P_{36}	2.6551977					
	2nd	Q_{432}	2.6752228	1	1	1	1	1
		Q_{408}	2.0081600					
		Q_{412}	1.9969794					
4	1st	$S_{121-3001}$	**50.5200000**	1	0	1	1	0
		$S_{380-3000}$	50.0199999					
		Q_{430}	2.7612859					
	2nd	$S_{380-3000}$	**49.9999999**	1	1	1	1	0
		Q_{430}	2.5310128					
		Q_{410}	2.0531465					
	3rd	Q_{430}	2.0230509	1	1	1	1	1
		P_{430}	1.6513273					
		P_{382}	1.6373424					
5	1st	$S_{110-3003}$	**50.6570000**	0	1	1	1	1
		P_{112}	2.0042713					
		P_{18}	1.9203360					
	2nd	P_{114}	1.7654282	1	1	1	1	1
		Q_{32}	1.4301449					
		Q_{363}	1.3755285					

Table 15 - Normalized residual test for Cases 6 to 7

Case	SE run	Meas.	$\left\|\hat{r}_{N,i}\right\|_{max}$	Assumed status				
				$s^{assumed}_{110-3003}$	$s^{assumed}_{110-3003}$	$s^{assumed}_{110-3003}$	$s^{assumed}_{110-3003}$	$s^{assumed}_{110-3003}$
6	1st	$s_{110-3003}$	**54.0000186**	0	1	1	0	1
		$s_{121-3001}$	50.9860921					
		Q_{314}	2.6496588					
	2nd	$s_{121-3001}$	**49.9998989**	1	1	1	0	1
		Q_{314}	2.4992126					
		Q_{70}	2.1130723					
	3rd	Q_{314}	1.9357252	1	0	1	0	1
		P_{331}	1.7063631					
		Q_{285}	1.2495267					
7	1st	$s_{140-3002}$	**50.6950000**	0	0	1	0	1
		$s_{121-3001}$	50.1720000					
		$s_{110-3003}$	50.0990000					
	2nd	$s_{121-3001}$	**50.5340000**	0	0	0	0	1
		$s_{110-3003}$	49.9980000					
		Q_{310}	2.6954336					
	3rd	$s_{110-3003}$	**50.1640000**	0	1	0	0	1
		P_{28}	2.1786122					
		Q_{310}	2.0645192					
	4th	Q_{310}	1.8706431	1	1	0	0	1
		P_{311}	1.5382432					
		Q_{363}	1.3755285					

Table 16 - Normalized residual test for Cases 8 to 9

Case	SE run	Meas.	$\left\|\hat{r}_{N,i}\right\|_{max}$	Assumed status				
				$s^{assumed}_{110-3003}$	$s^{assumed}_{121-3001}$	$s^{assumed}_{140-3002}$	$s^{assumed}_{320-3004}$	$s^{assumed}_{380-3000}$
8	1st	$P_{110-3003}$	**49.9843900**	1	1	0	0	1
		Q_{320}	2.8796522					
		P_{32}	2.0192643					
	2nd	P_{332}	1.8653279	1	1	0	0	1
		P_{32}	1.8426943					
		Q_{318}	1.2856112					
9	1st	$S_{110-3003}$	**52.6869419**	0	1	0	0	1
		$P_{110-3003}$	17.8692114					
		$Q_{110-3003}$	12.1948572					
	2nd	$P_{110-3003}$	**16.9592432**	1	1	0	0	1
		$Q_{110-3003}$	14.4856997					
		P_{46}	2.2565125					
	3rd	$Q_{110-3003}$	**15.9242638**	1	1	0	0	1
		Q_{310}	2.8956487					
		P_{46}	2.3419148					
	4th	Q_{310}	2.6456932	1	1	0	0	1
		P_{46}	1.9569423					
		Q_{224}	1.6459691					

Table 17 - Normalized residual test for Case 10

Case	SE run	Meas.	$\left\|\hat{r}_{N,i}\right\|_{max}$	Assumed status				
				$s^{assumed}_{110-3003}$	$s^{assumed}_{121-3001}$	$s^{assumed}_{140-3002}$	$s^{assumed}_{320-3004}$	$s^{assumed}_{380-3000}$
10	1st	$S_{110-3003}$	**56.2830000**	0	1	0	0	1
		$S_{140-3002}$	52.9260000					
		$Q_{110-3003}$	27.9188492					
	2nd	$S_{140-3002}$	**49.9998000**	1	1	0	0	1
		$Q_{110-3003}$	22.6834517					
		$P_{110-3003}$	20.0065311					
	3rd	$Q_{110-3003}$	**12.5961924**	1	1	1	0	1
		$P_{110-3003}$	9.8720618					
		Q_{320}	1.9607600					
	4th	$P_{110-3003}$	**10.9825641**	1	1	1	0	1
		Q_{280}	1.9672683					
		Q_{320}	1.9019603					
	5th	Q_{320}	1.9272790	1	1	1	0	1
		P_{114}	1.9160936					
		Q_{280}	1.1145891					

Table 18 - Normalized residual test for Cases 11 to 13

Case	SE run	Meas.	$\left\|\hat{r}_{N,i}\right\|_{max}$	Assumed status
				$s^{assumed}_{111-3005}$
11	1st	Q_{375}	2.9352446	1
		Q_{406}	2.5721460	
		Q_{295}	2.1036809	
12	1st	$S_{111-3005}$	**49.9997216**	0
		Q_{405}	2.6886924	
		Q_{369}	2.5187516	
	2nd	Q_{405}	2.2361544	1
		Q_{359}	1.9738494	
		Q_{369}	1.8113372	
13	1st	$S_{111-3005}$	**51.0066494**	1
		P_{139}	2.8621559	
		P_{214}	2.6611891	
	2nd	Q_{408}	2.4431672	0
		Q_{329}	2.0173849	
		P_{139}	1.8476614	

5 Simulations with Évora distribution network

5.1 Study Case – Generation of Pseudo-Measurements

As mentioned before, the purpose of the present work is to estimate the MV network operation state using data of the real-time measurements available on the MV network, as well as pseudo-measurements for the MV/LV secondary substations not being telemetered. These pseudo-measurements will be generated using real-time measurements taken from smart meters located in LV network. Active and reactive injected power and voltage magnitude at in the lower voltage bus of the secondary substation are the pseudo-measurements values to be generated. In the context of this study, it is assumed that only one MV/LV secondary substation does not own telemetry equipment with the capacity of transmitting measurements in real-time (the one for which pseudo-measurements are generated).

In this section, the generation of pseudo-measurements was performed according to the methodology previously described.

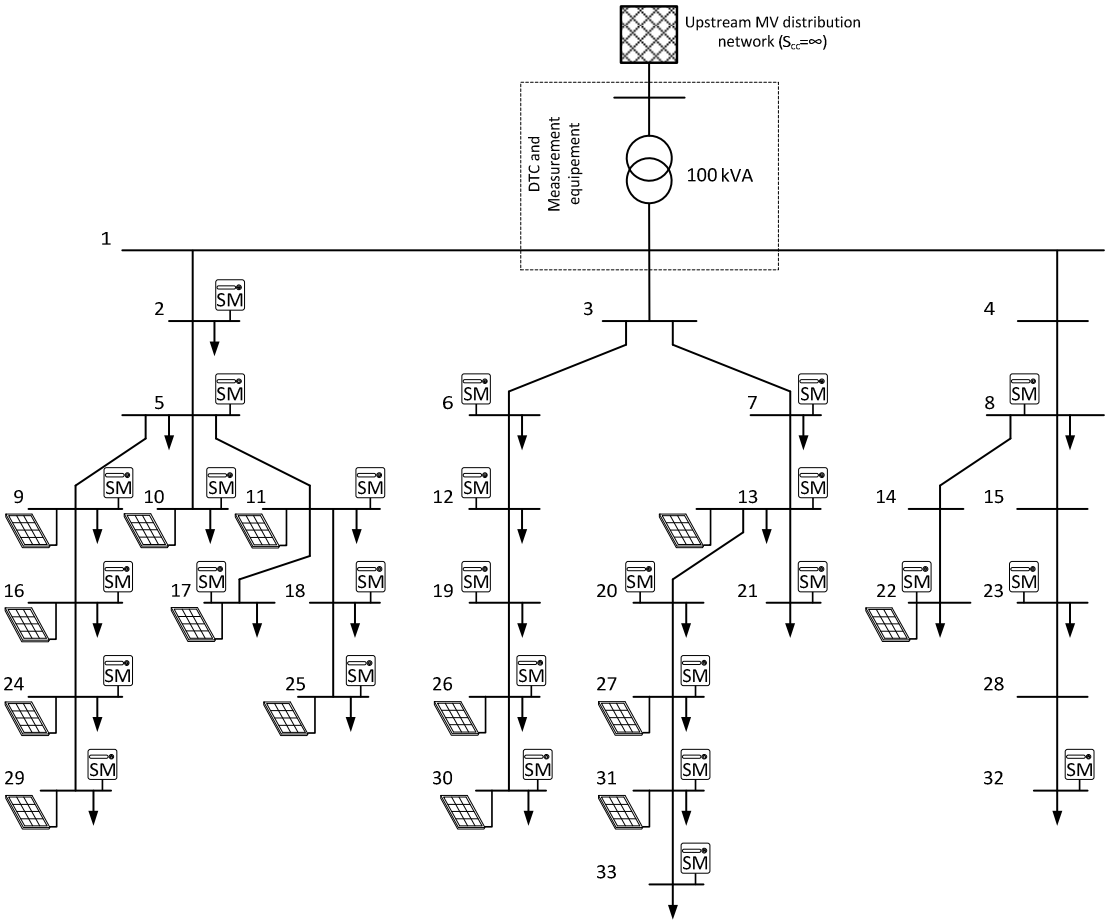

Figure 44 - Typical Portuguese LV network of 100 kVA considered

5.1.1 Low Voltage Network Characterization

The pseudo-measurements generation methodology was tested in a small typical Portuguese LV network (Figure 44) where the MV/LV secondary substation – which it is connected to, is equipped with one transformer with a rated power of 100 kVA. The grid contains 57 consumers with contracted powers that vary in a range between 3.45 to 6.9 kVA for single-phase consumers and 6.9 to 13.8 kVA for three-phase consumers (Table 19). Since a significant amount of single-phase loads is present, load distribution among phases is not completely balanced. Even so, the load is almost balanced at the MV/LV substation level. The network has a total of 33 nodes and a peak load of 62.6 kW for the winter period.

Table 19 - Consumers and microgeneration distribution

Client Number	Location Bus	Contracted Power (kVA)	Microgeneration Installed Capacity (kVA)	Client Number	Location Bus	Contracted Power (kVA)	Microgeneration Installed Capacity (kVA)
1	2	3.45	0	30	20	3.45	0
2	2	3.45	0	31	21	3.45	0
3	5	3.45	0	32	21	3.45	0
4	6	1.15	0	33	22	6.9	3.45
5	7	3.45	0	34	22	3.45	0
6	7	3.45	0	35	22	3.45	0
7	7	3.45	0	36	22	3.45	0
8	8	3.45	0	37	23	3.45	0
9	8	3.45	0	38	24	3.45	0
10	8	3.45	0	39	24	17.25	5.75
11	9	6.9	3.45	40	24	17.25	5.75
12	9	3.45	0	41	24	17.25	5.75
13	9	3.45	0	42	24	3.45	0
14	10	3.45	0	43	25	3.45	0
15	10	13.8	5.75	44	25	13.8	5.75
16	11	3.45	0	45	26	13.8	5.75
17	11	6.9	3.45	46	27	6.9	3.45
18	12	3.45	0	47	27	3.45	0
19	12	3.45	0	48	27	3.45	0
20	13	6.9	3.45	49	29	3.45	0
21	13	3.45	0	50	29	3.45	0
22	13	3.45	0	51	29	6.9	3.45
23	16	6.9	3.45	52	29	3.45	0
24	17	13.8	5.75	53	30	13.8	5.75
25	18	3.45	0	54	31	6.9	3.45
26	18	3.45	0	55	32	3.45	0
27	19	3.45	0	56	32	3.45	0
28	19	3.45	0	57	33	3.45	0
29	20	3.45	0				

In this study, the consumers' load was aggregated at the correspondent connection node and its distribution per phase was assumed to be completely balanced. Nevertheless, as this process is performing after using each individual consumer power value for a given time instant, the different consumers' load patterns are still reflected on the equivalent load. There are two main reasons for this simplification. Firstly, by assuming balanced loads, single-phase power flows can be run instead of three-phase power flows. Secondly, the assumption made does not compromise in any way the quality of the pseudo-measurements generated through the use of autoencoders.

Several microgeneration units (photovoltaic panels) were added and randomly distributed through the network clients, totalizing ≈74% of the secondary substation transformer capacity (ca. 74 kVA). The microgeneration units represent 50% of the contracted power of each consumer.

5.1.2 Modelling Load and Microgeneration Variability

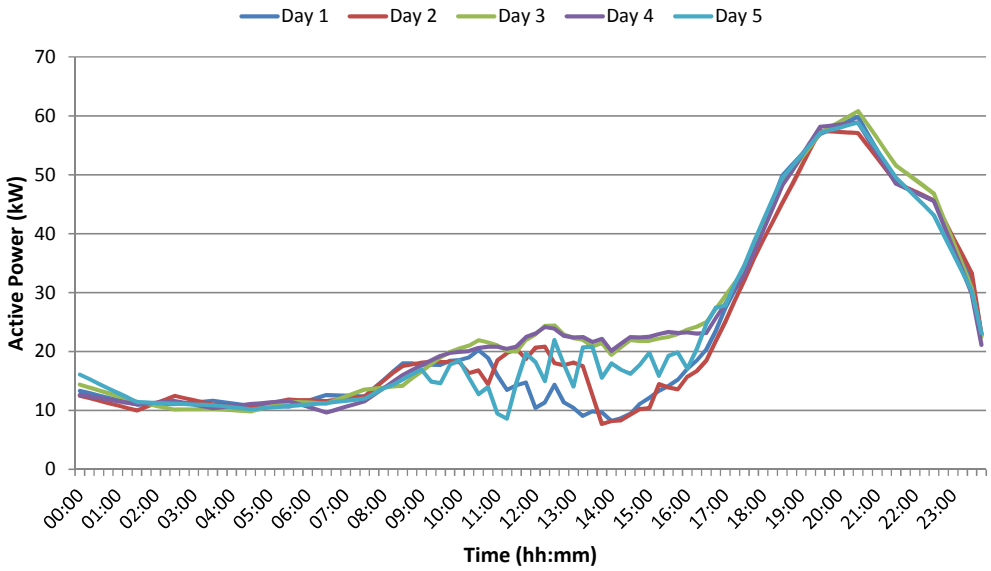

Figure 45 - Example of the active power measured at the substation level for the first 5 days

Regarding the data related to the load, the only available for this grid were average values of the active and reactive power for time steps of 15 minutes as well as the voltage magnitude value for the same time periods. All these data were obtained at the lower voltage bus of the secondary substation and correspond to an entire winter season (from 21st of December to 20th of March). In order to represent the behaviour of the individual loads dispersed among the grid for each time instant, a load allocation technique was required to be performed. The approach consisted on the distribution of the active and reactive power measured values at the substation level proportionally to the contracted

power of the existing clients in the grid (see Table 19). This load allocation task was done in such a way that both the values of voltage magnitude and injected power at the reference bus (bus 1 in Figure 44) are in accordance with measurements existing in the historical database. An example of the active power measured at the substation level for the first 5 days are presented in Figure 45.

For the microgeneration, in order to represent different days (e.g. sunny, cloudy, rainy, etc.), 5 different real profiles obtained from a real meteorological station [59] were randomly distributed by the existing units according to their probability of occurrence in a typical Portuguese winter. These 5 profiles are presented in Figure 46.

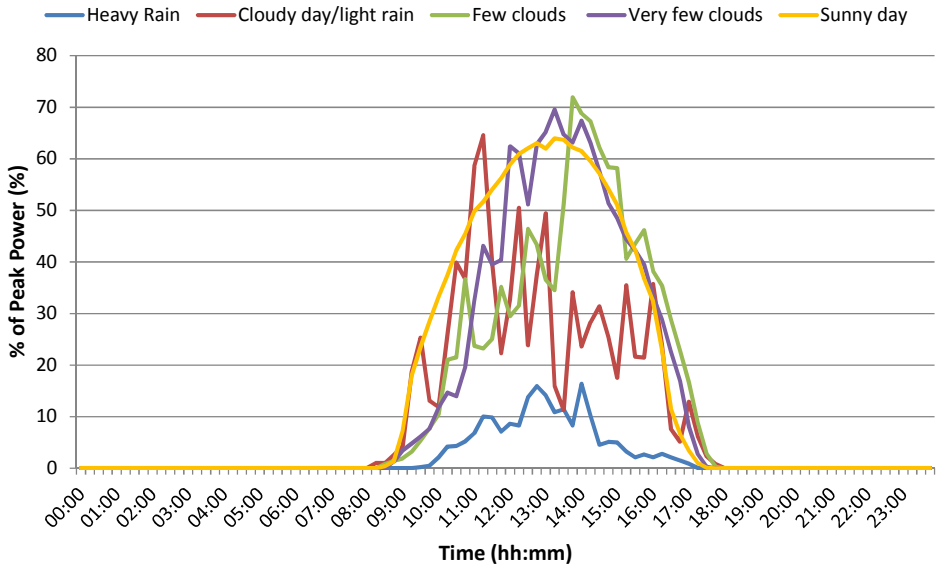

Figure 46 - Microgeneration production diagrams obtained from a real meteorological station

5.1.3 Description of Smart Grid Features

The MV/LV secondary substation houses a Distribution Transformer Controller (DTC) as well as the associated measurement equipment which is capable of saving information about active and reactive power flows in the transformer and the voltage magnitude at the low voltage side of it.

It was also considered that each consumer has a smart meter (SM) to monitor his consumption and communicate it to the DTC for billing purposes. The customer that own a microgeneration unit have an additional SM for measuring its power production. As it happens in some real smart grid test sites, not all SM are capable of transmitting data in real-time[1] due to communication infrastructure restrictions. Only some of the SM, which use, for instance, GPRS technology, have that capability. The selected SM that have this functionality, in each scenario analysed, are presented in section 5.1.5.1.5 and it was assumed that their active (P) and reactive (Q) power and voltage magnitude (|V|) measurements are synchronised. Phase angles were assumed not to be measured as the majority of the smart meters foreseen to be deployed in LV grids do not have this capability.

5.1.4 Autoencoder Parameterization

The choice of the most adequate parameters for an autoencoder, in such a way that estimation accuracy is increased, is not a trivial task. To do that, several tests with a different number of training epochs, hidden layer neurons and quantity of data for training purposes (in the historical database) were performed.

Regarding the amount of data for training purposes, were considered several sizes: 60 days (2 months), 30 days (1 month), 15 days (≈ 2 weeks), 7 days (1 week), 4 days and 1 day. For each one of these training data sets, the influence on having different values for the hidden layer reduction rate (HLRR – measured as the ratio between the number of neurons in the hidden layer and the number of neurons in the input/output layer) was tested. The values selected were: 0.02, 0.1, 0.2, 0.3, 0.4, 0.5 and 0.6. Then, for each combination of these values, the influence of varying the number of training epochs were tested for the following values: 100, 200, 300, 400, 500 and 600 epochs. It is important to refer that the last 30 days of the historical database was divided in two sets: 23 days were used as the test set of the cross-validation procedure and the remaining (7 days) to the evaluation set.

The generation of pseudo-measurements at the MV/LV substation selected (see Figure 44) requires, in a first instance, the definition of which the LV clients will own SM with the capability of transmitting measurements in real-time. In this sense, a study to determine what should be the best locations when considering different quantities of these devices was performed. In the context of this study, the best locations means those

[1] For the purpose of this work, the term “real-time” is used in the sense of measuring the variables in a short period of time, around 15 minutes.

with more influence on the performance of the pseudo-measurements generation method. This study was based on Information Theoretic concepts similarly to the presented in [60], but instead of use a Genetic algorithm, here it was employed an EPSO algorithm. Table 20 shows the best results obtained.

Table 20 - Set of SM with the capability of transmitting data in real-time with more influence in pseudo-measurements generation performance

Number of SM	Location of SM
1	1
2	1-30
3	1-30-28
4	1-30-28-32
5	1-30-28-32-25
6	1-30-28-32-25-24
7	1-30-28-32-25-24-23
8	1-30-28-32-24-23-27-2
9	1-30-28-32-24-23-2-25-31
10	1-30-28-32-23-2-25-26-27-7
11	1-30-28-32-23-2-25-7-24-3-31

It should be noted that the buses without load/microgeneration were not considered for the autoencoder training purposes, since no historical data was available for them. In this sense, as it is illustrated in Figure 44, the buses number 3, 4, 14, 15 and 28 were not considered. In order to find the most adequate autoencoder parameters, it was considered a scenario with 8 SM with the capability of transmitting data in real-time (located at the buses 2, 7, 23, 24, 25, 30, 31 and 32).

The autoencoder performance in terms of accuracy was then evaluated through the mean absolute error (MAE), for the evaluation set, for each one of the test settings exposed in the beginning of this section. The MAE was calculated as shown in (29), where y_i represents the real values (present in the historical dataset), f_i the pseudo-measurement generated by the autoencoder and n the number of samples (number of 15 minutes instants).

$$MAE = \frac{1}{n}\sum_{i=1}^{n}\left|f_i - y_i\right| \quad (29)$$

Table 21, Table 22 and Table 23 summarize the MAE (respectively in MW and Mvar for injected active power and injected reactive power and in p.u. for voltage magnitude) obtained during the tests performed.

It is important to stress that in order to facilitate the analyse of the results, they were grouped by the amount of data for training purposes. Furthermore, it was applied a colour *dégradé* for each variable (P, Q and |V|).

Table 21 - Injected active power MAE (MW) – darker values means a higher error

HLRR	Number of Training Epochs						Amount of data for training procedure
	100	200	300	400	500	600	
0.02	0.00495	0.00498	0.00477	0.00473	0.00472	0.00470	1 day
0.1	0.00222	0.00218	0.00200	0.00206	0.00199	0.00195	
0.2	0.00250	0.00203	0.00188	0.00182	0.00172	0.00178	
0.3	0.00285	0.00284	0.00264	0.00252	0.00264	0.00269	
0.4	0.00240	0.00194	0.00172	0.00170	0.00174	0.00176	
0.5	0.00307	0.00253	0.00244	0.00240	0.00233	0.00241	
0.6	0.00219	0.00194	0.00188	0.00191	0.00194	0.00196	
0.02	0.00269	0.00232	0.00200	0.00189	0.00184	0.00184	4 days
0.1	0.00328	0.00179	0.00155	0.00145	0.00142	0.00139	
0.2	0.00258	0.00193	0.00180	0.00183	0.00176	0.00166	
0.3	0.00241	0.00171	0.00168	0.00146	0.00132	0.00121	
0.4	0.00272	0.00188	0.00177	0.00185	0.00188	0.00184	
0.5	0.00189	0.00149	0.00146	0.00154	0.00162	0.00158	
0.6	0.00211	0.00236	0.00224	0.00213	0.00205	0.00210	
0.02	0.00242	0.00257	0.00281	0.00285	0.00301	0.00305	7 days
0.1	0.00146	0.00135	0.00123	0.00129	0.00130	0.00133	
0.2	0.00193	0.00158	0.00157	0.00144	0.00144	0.00142	
0.3	0.00283	0.00249	0.00252	0.00242	0.00236	0.00230	
0.4	0.00275	0.00248	0.00238	0.00225	0.00220	0.00222	
0.5	0.00202	0.00175	0.00160	0.00164	0.00167	0.00165	
0.6	0.00241	0.00217	0.00231	0.00233	0.00244	0.00254	
0.02	0.00529	0.00451	0.00410	0.00394	0.00381	0.00374	15 days
0.1	0.00192	0.00169	0.00160	0.00167	0.00172	0.00173	
0.2	0.00271	0.00248	0.00242	0.00220	0.00190	0.00170	
0.3	0.00124	0.00122	0.00125	0.00118	0.00120	0.00117	
0.4	0.00245	0.00192	0.00185	0.00181	0.00162	0.00156	
0.5	0.00172	0.00136	0.00127	0.00118	0.00118	0.00122	
0.6	0.00142	0.00133	0.00127	0.00119	0.00125	0.00136	
0.02	0.00473	0.00446	0.00414	0.00385	0.00367	0.00359	30 days
0.1	0.00245	0.00151	0.00160	0.00172	0.00177	0.00175	
0.2	0.00179	0.00163	0.00160	0.00153	0.00147	0.00140	
0.3	0.00138	0.00132	0.00142	0.00143	0.00130	0.00115	
0.4	0.00203	0.00148	0.00156	0.00142	0.00145	0.00153	
0.5	0.00286	0.00230	0.00196	0.00172	0.00164	0.00167	
0.6	0.00190	0.00163	0.00176	0.00170	0.00171	0.00178	
0.02	0.00242	0.00211	0.00287	0.00268	0.00258	0.00252	60 days
0.1	0.00276	0.00216	0.00199	0.00194	0.00184	0.00178	
0.2	0.00203	0.00146	0.00134	0.00130	0.00128	0.00129	
0.3	0.00150	0.00133	0.00122	0.00120	0.00123	0.00123	
0.4	0.00172	0.00146	0.00137	0.00127	0.00120	0.00113	
0.5	0.00132	0.00125	0.00131	0.00132	0.00135	0.00124	
0.6	0.00134	0.00114	0.00120	0.00122	0.00117	0.00117	

Table 22 - Injected reactive power MAE (Mvar) – darker values means a higher error

HLRR	Number of Training Epochs						Amount of data for training procedure
	100	200	300	400	500	600	
0.02	0.00136	0.00123	0.00118	0.00121	0.00118	0.00119	1 day
0.1	0.00108	0.00086	0.00078	0.00082	0.00085	0.00088	
0.2	0.00185	0.00178	0.00151	0.00135	0.00120	0.00108	
0.3	0.00147	0.00147	0.00136	0.00131	0.00131	0.00126	
0.4	0.00112	0.00101	0.00095	0.00087	0.00082	0.00080	
0.5	0.00114	0.00106	0.00098	0.00099	0.00097	0.00098	
0.6	0.00095	0.00088	0.00083	0.00078	0.00078	0.00078	
0.02	0.00087	0.00081	0.00074	0.00069	0.00070	0.00067	4 days
0.1	0.00077	0.00065	0.00064	0.00067	0.00065	0.00067	
0.2	0.00075	0.00069	0.00067	0.00067	0.00066	0.00068	
0.3	0.00067	0.00065	0.00066	0.00071	0.00069	0.00066	
0.4	0.00092	0.00067	0.00058	0.00056	0.00055	0.00056	
0.5	0.00065	0.00060	0.00056	0.00056	0.00058	0.00061	
0.6	0.00066	0.00056	0.00051	0.00052	0.00051	0.00051	
0.02	0.00108	0.00115	0.00122	0.00124	0.00124	0.00118	7 days
0.1	0.00135	0.00121	0.00111	0.00110	0.00107	0.00107	
0.2	0.00057	0.00054	0.00055	0.00054	0.00053	0.00054	
0.3	0.00080	0.00059	0.00061	0.00059	0.00058	0.00056	
0.4	0.00061	0.00054	0.00053	0.00053	0.00052	0.00050	
0.5	0.00074	0.00071	0.00066	0.00066	0.00061	0.00061	
0.6	0.00063	0.00055	0.00057	0.00060	0.00065	0.00069	
0.02	0.00094	0.00086	0.00080	0.00077	0.00079	0.00078	15 days
0.1	0.00087	0.00082	0.00082	0.00080	0.00080	0.00074	
0.2	0.00062	0.00062	0.00061	0.00061	0.00066	0.00067	
0.3	0.00071	0.00054	0.00048	0.00048	0.00047	0.00048	
0.4	0.00069	0.00053	0.00051	0.00050	0.00049	0.00048	
0.5	0.00052	0.00051	0.00046	0.00046	0.00047	0.00047	
0.6	0.00060	0.00054	0.00049	0.00048	0.00051	0.00054	
0.02	0.00097	0.00091	0.00086	0.00081	0.00080	0.00080	30 days
0.1	0.00072	0.00057	0.00054	0.00052	0.00051	0.00049	
0.2	0.00115	0.00105	0.00095	0.00092	0.00088	0.00088	
0.3	0.00112	0.00091	0.00087	0.00083	0.00077	0.00072	
0.4	0.00047	0.00044	0.00042	0.00041	0.00043	0.00045	
0.5	0.00075	0.00058	0.00048	0.00048	0.00047	0.00049	
0.6	0.00086	0.00073	0.00071	0.00071	0.00075	0.00080	
0.02	0.00078	0.00083	0.00065	0.00062	0.00060	0.00060	60 days
0.1	0.00091	0.00080	0.00075	0.00074	0.00073	0.00072	
0.2	0.00061	0.00061	0.00063	0.00061	0.00058	0.00058	
0.3	0.00075	0.00065	0.00059	0.00055	0.00054	0.00053	
0.4	0.00055	0.00053	0.00050	0.00047	0.00046	0.00043	
0.5	0.00064	0.00054	0.00057	0.00057	0.00059	0.00060	
0.6	0.00058	0.00045	0.00047	0.00045	0.00047	0.00048	

Table 23 - Voltage Magnitude (p.u.) – darker values means a higher error

HLRR	Number of Training Epochs						Amount of data for training procedure
	100	200	300	400	500	600	
0.02	0.00800	0.00788	0.00781	0.00783	0.00784	0.00783	1 day
0.1	0.00437	0.00304	0.00265	0.00229	0.00217	0.00206	
0.2	0.00199	0.00145	0.00135	0.00121	0.00122	0.00116	
0.3	0.00169	0.00169	0.00168	0.00169	0.00160	0.00152	
0.4	0.00184	0.00152	0.00136	0.00129	0.00124	0.00117	
0.5	0.00176	0.00135	0.00122	0.00122	0.00102	0.00104	
0.6	0.00152	0.00133	0.00122	0.00116	0.00115	0.00115	
0.02	0.00844	0.00837	0.00836	0.00835	0.00837	0.00838	4 days
0.1	0.00382	0.00296	0.00278	0.00252	0.00241	0.00227	
0.2	0.00296	0.00232	0.00215	0.00208	0.00198	0.00188	
0.3	0.00359	0.00292	0.00251	0.00235	0.00231	0.00230	
0.4	0.00258	0.00187	0.00152	0.00140	0.00136	0.00140	
0.5	0.00139	0.00155	0.00158	0.00161	0.00160	0.00159	
0.6	0.00198	0.00154	0.00137	0.00130	0.00123	0.00120	
0.02	0.00614	0.00483	0.00419	0.00388	0.00336	0.00293	7 days
0.1	0.00297	0.00246	0.00226	0.00215	0.00206	0.00199	
0.2	0.00288	0.00240	0.00219	0.00217	0.00210	0.00198	
0.3	0.00145	0.00150	0.00140	0.00140	0.00140	0.00135	
0.4	0.00192	0.00134	0.00110	0.00098	0.00082	0.00085	
0.5	0.00169	0.00205	0.00202	0.00207	0.00204	0.00205	
0.6	0.00314	0.00282	0.00242	0.00225	0.00213	0.00208	
0.02	0.00818	0.00795	0.00800	0.00799	0.00795	0.00790	15 days
0.1	0.00338	0.00252	0.00237	0.00240	0.00230	0.00233	
0.2	0.00212	0.00166	0.00137	0.00147	0.00157	0.00156	
0.3	0.00362	0.00304	0.00275	0.00255	0.00236	0.00232	
0.4	0.00156	0.00125	0.00108	0.00092	0.00085	0.00084	
0.5	0.00131	0.00108	0.00097	0.00087	0.00086	0.00086	
0.6	0.00186	0.00180	0.00175	0.00162	0.00154	0.00150	
0.02	0.00827	0.00824	0.00792	0.00804	0.00804	0.00794	30 days
0.1	0.00423	0.00332	0.00305	0.00295	0.00264	0.00256	
0.2	0.00279	0.00203	0.00181	0.00170	0.00169	0.00157	
0.3	0.00168	0.00137	0.00151	0.00159	0.00153	0.00141	
0.4	0.00169	0.00111	0.00095	0.00101	0.00097	0.00091	
0.5	0.00176	0.00153	0.00125	0.00123	0.00119	0.00119	
0.6	0.00196	0.00138	0.00139	0.00131	0.00128	0.00130	
0.02	0.00925	0.00879	0.00902	0.00909	0.00905	0.00905	60 days
0.1	0.00300	0.00349	0.00342	0.00326	0.00322	0.00316	
0.2	0.00453	0.00386	0.00355	0.00360	0.00358	0.00353	
0.3	0.00384	0.00325	0.00290	0.00237	0.00204	0.00202	
0.4	0.00230	0.00163	0.00178	0.00185	0.00200	0.00204	
0.5	0.00279	0.00255	0.00257	0.00246	0.00224	0.00215	
0.6	0.00201	0.00185	0.00174	0.00169	0.00167	0.00164	

From the results it is possible to conclude that the number of training epochs is the parameter with less influence on accuracy when generating pseudo-measurements. However, in general, with the increase of the number of training epochs, the MAE decreases.

For the hidden layer neurons, it is also possible to observe that a smaller hidden layer reduction rate is usually associated with a higher MAE. In other words, MAE generally decreases when hidden layer reduction rate is increased. Table 24 presents the correspondence between the hidden layer reduction rates considered and the hidden layer neurons, for the scenario described before.

Table 24 - Hidden layer reduction rates and its hidden layer neurons correspondence, for the described scenario

Hidden layer reduction rate	Nr. of hidden layer neurons
0.02	1
0.1	3
0.2	5
0.3	8
0.4	11
0.5	14
0.6	16

Regarding the quantity of data for training purposes, the conclusions are identical to those obtained for the other parameters in study: analysing all variables (P, Q and |V|) as a whole, it is observed that a train dataset higher than 15 days inclusive (for the studies performed) it is associated to a smaller MAE.

After this preliminary analysis, it was intended to intersect all the variables in order to obtain the optimal parameters to set the autoencoder without compromise the results accuracy. It should be noted that it was given priority to P and Q variables, once their relative errors were higher than observed to |V|. Therefore, and at the same time, it was intended to make the following:

- Decrease the number of training epochs: becomes training process faster.
- Decrease the number of hidden layer neurons (hidden layer reduction rate): becomes training process faster, as well as the autoencoder running (pseudo-measurements generation, in this case).
- Decrease the amount of data for training the autoencoder (quantity of data for training purposes): besides a fewer amount of data needed to have the autoencoder properly trained, the training process is performed more quickly.

Although the training process was performed offline, how much faster the training process was performed, more quickly the autoencoder will be operational.

Thus, it was defined the parameterization:

- Number of training epochs: **300**
- Hidden layer reduction rate: **0.4**
- Amount of data for training purposes: **30 days**

This set of parameters was identified as the most adequate to set an autoencoder in the present work and will be used for the generation of pseudo-measurements for each scenario presented in the next section.

5.1.5 Scenarios for real-time Measurements

For the purpose of generating pseudo-measurements for MV/LV secondary substation without real-time measurements and in order to evaluate the performance of the autoencoder, 5 scenarios were created. In each scenario, the number of SM with the capability of transmitting data in real-time was assumed to be different. It is important to mention again that for the purpose of this work, the term “real-time” is used in the sense of measuring the variables in a short period of time, around 15 minutes.

In scenario 1, was considered 1 SM with the capability of transmitting data in real-time, which, according to the aforementioned study, has more influence in pseudo-measurements generation performance.

Scenario 2 holds 4 SM with the capability of transmitting data in real-time according to the same foregoing study.

In scenario 3, were considered the same 8 SM used to determine the most adequate parameters to set an autoencoder, assumed before.

Scenario 4 includes 8 SM, with the same capabilities, located on the load buses farthest from the secondary substation.

In scenario 5, was assumed that all the buses with microgeneration have a SM with the capabilities referred before.

In summary, Table 25 presents the SM location for each created scenario.

Table 25 - Number of SM and its location for each created scenario

Scenario	Number of SM	Location of SM
1	1	30
2	4	24-25-30-32
3	8	2-7-23-24-25-30-31-32
4	8	17-21-22-25-29-30-32-33
5	14	9-10-11-13-16-17-22-24-25-26-27-29-30-31

It is important to state that whenever the quantity and type of measurements (number of SM) present in the input dataset is changed, a new process of training must be performed, i.e., it is necessary to perform an autoencoder training for each created scenario.

5.1.6 Pseudo-Measurements Generation

The results obtained for the pseudo-measurements generation are presented below. In order to be easy to compare the results obtained for each scenario, it was decided to present the absolute error of the evaluation set (last 7 days from the historical database) by means of boxplots (Figure 47 to Figure 49). Boxplot provides a very enlightening representation about data distribution (the absolute error, in this case). In addition, it was also presented the MAE of the pseudo-measurements generated (Table 26) as well as several graphical representations of the real values and the pseudo-measurements for the entire evaluation set, for each scenario (Figure 50 to Figure 52).

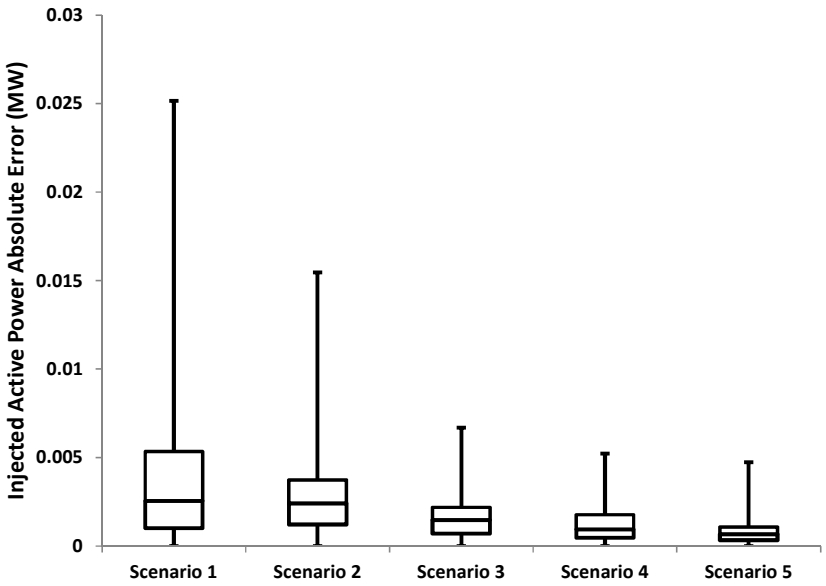

Figure 47 - Absolute error of the injected active power for each scenario (MW)

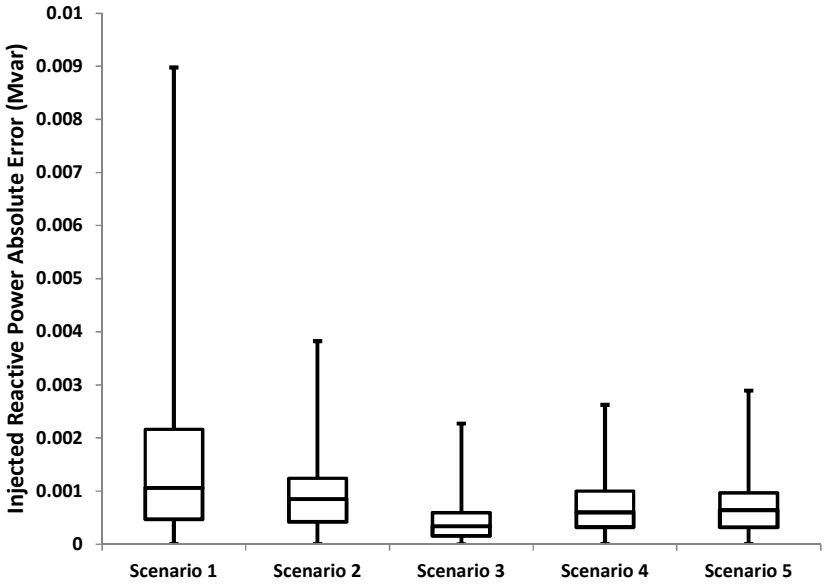

Figure 48 - Absolute error of the injected reactive power for each scenario (Mvar)

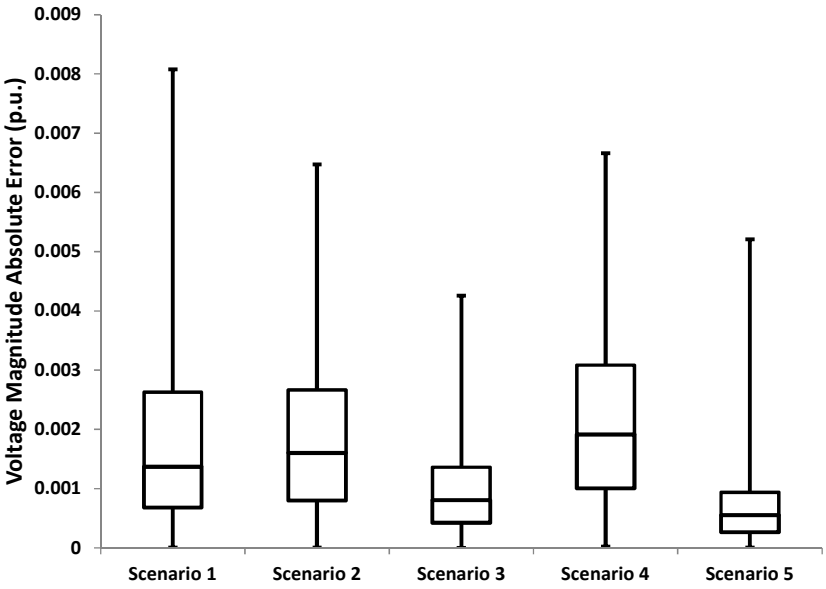

Figure 49 - Absolute error of the voltage magnitude for each scenario (p.u.)

Table 26 - Pseudo-measurements MAE for each scenario

Pseudo-Measurement	Scenario 1	Scenario 2	Scenario 3	Scenario 4	Scenario 5
P (MW)	0.00350	0.00278	0.00156	0.00119	0.00076
Q (Mvar)	0.00148	0.00089	0.00042	0.00069	0.00068
|V| (p.u.)	0.00179	0.00183	0.00095	0.00210	0.00069

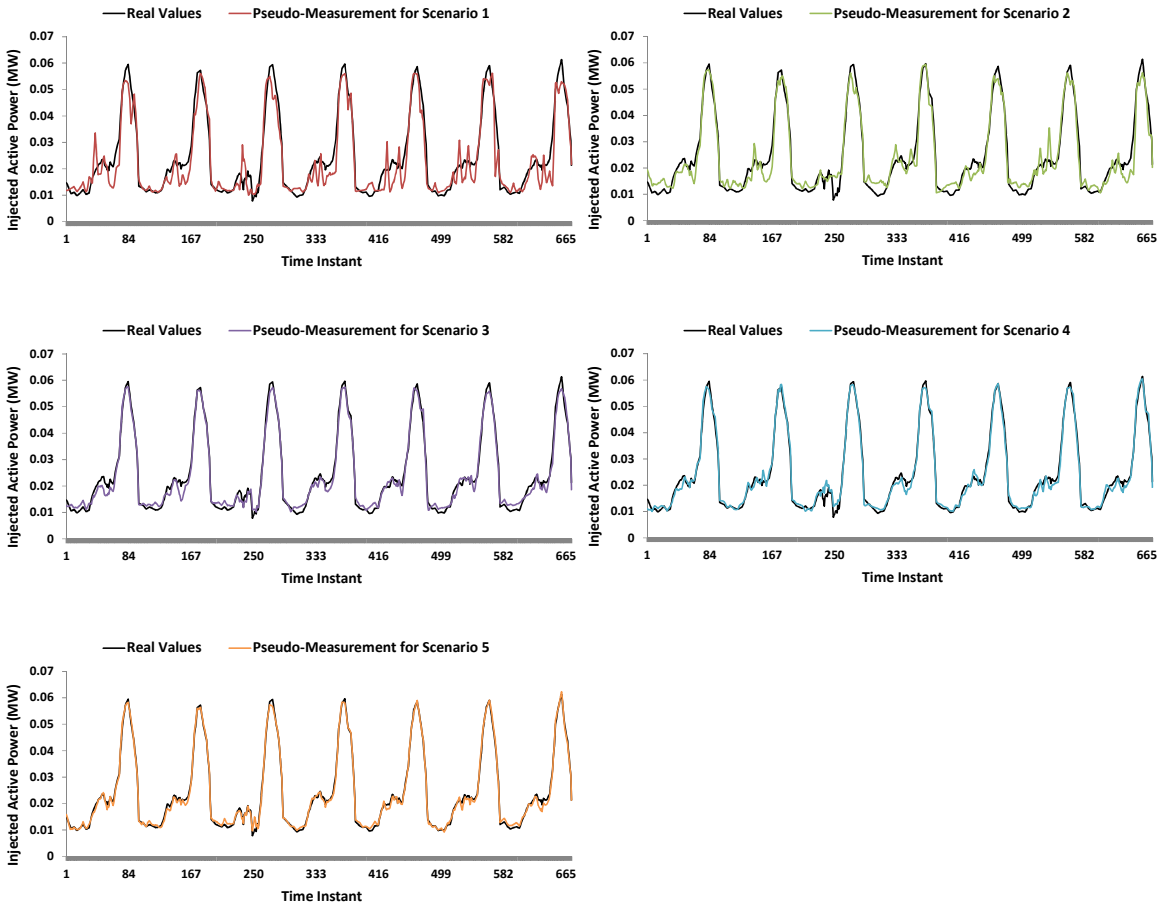

Figure 50 - Pseudo-measurements and real values of injected active power for the entire evaluation set, for each scenario (MW)

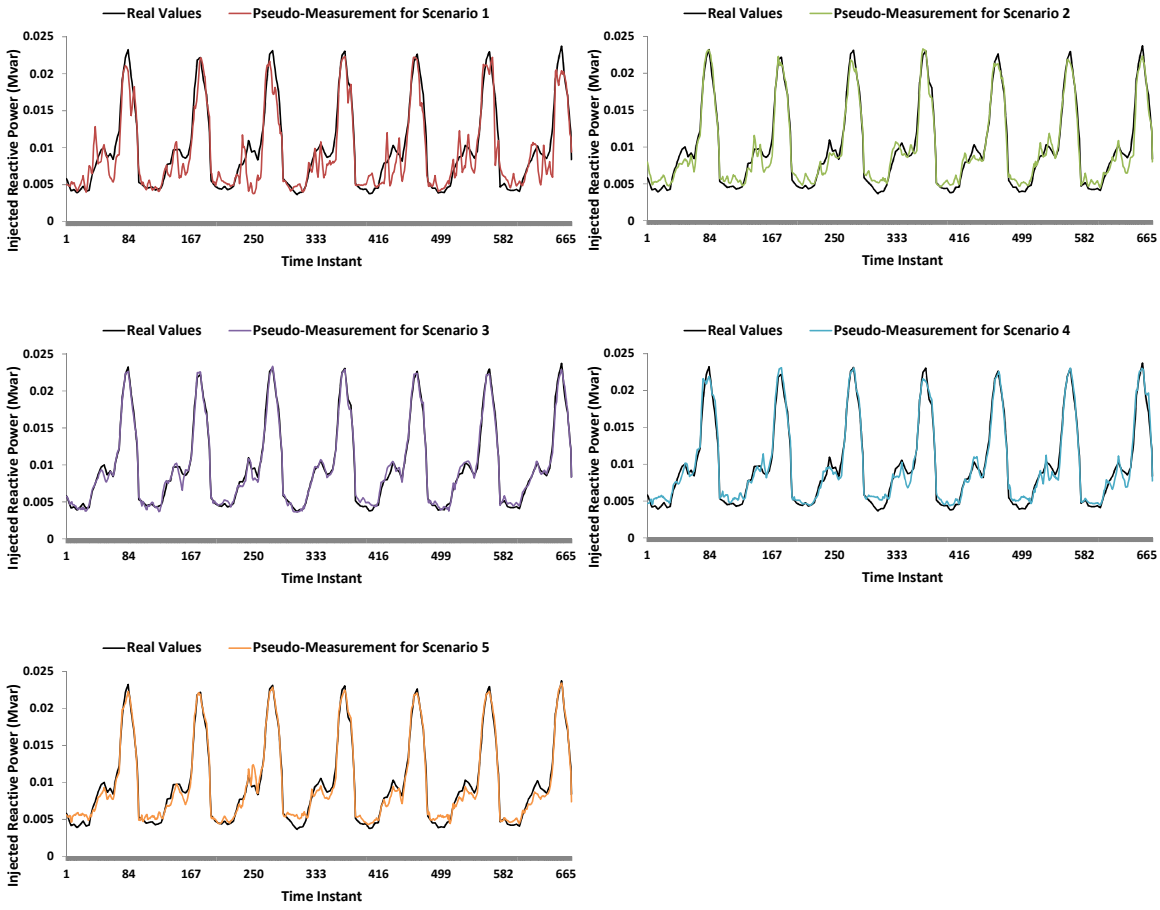

Figure 51 - Pseudo-measurements and real values of injected reactive power for the entire evaluation set, for each scenario (Mvar)

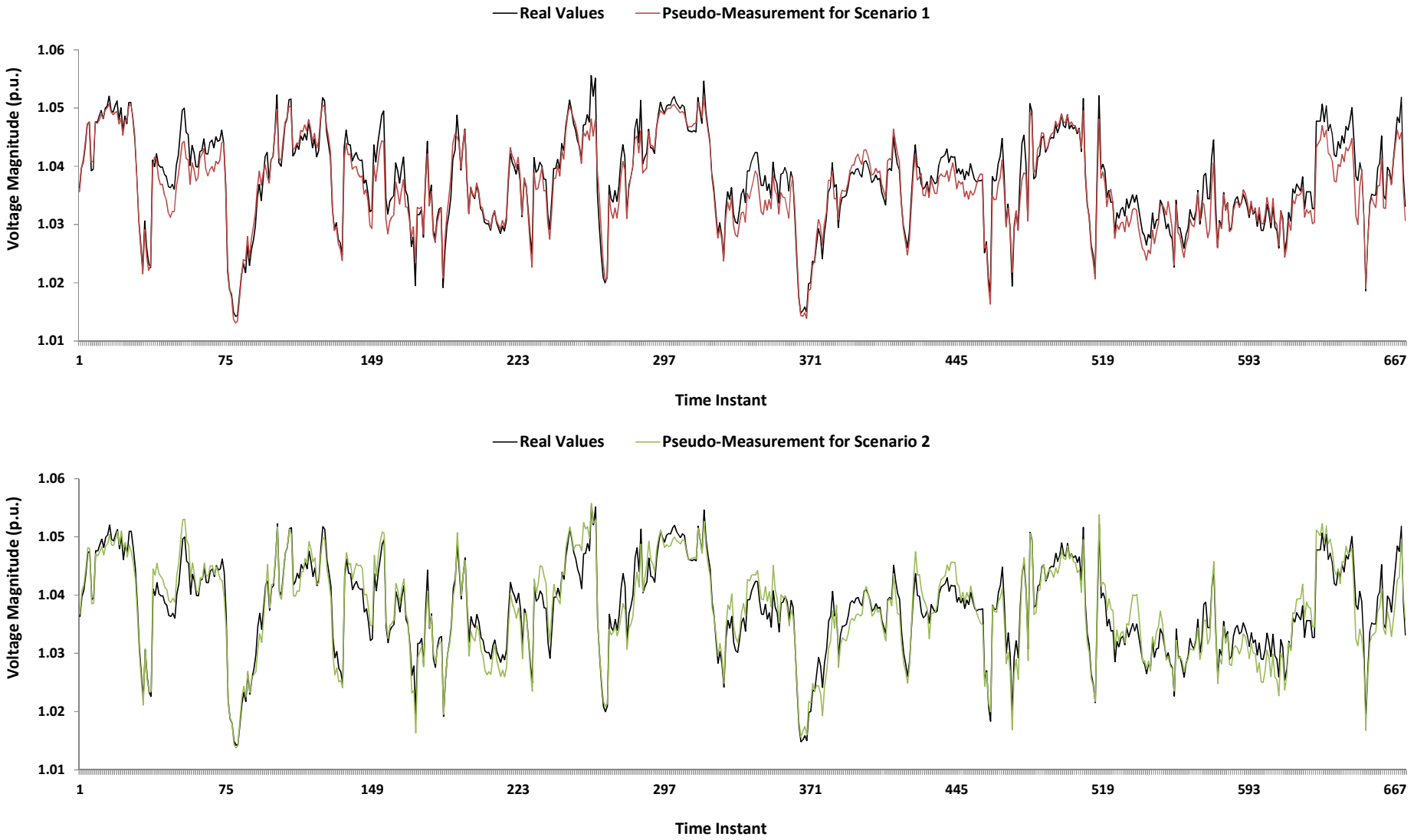
Real Values
Pseudo-Measurement for Scenario 1
Voltage Magnitude (p.u.)
1.06
1.05
1.04
1.03
1.02
1.01
1
75
149
223
297
371
445
519
593
667
Time Instant
Real Values
Pseudo-Measurement for Scenario 2
Voltage Magnitude (p.u.)
1.06
1.05
1.04
1.03
1.02
1.01
1
75
149
223
297
371
445
519
593
667
Time Instant

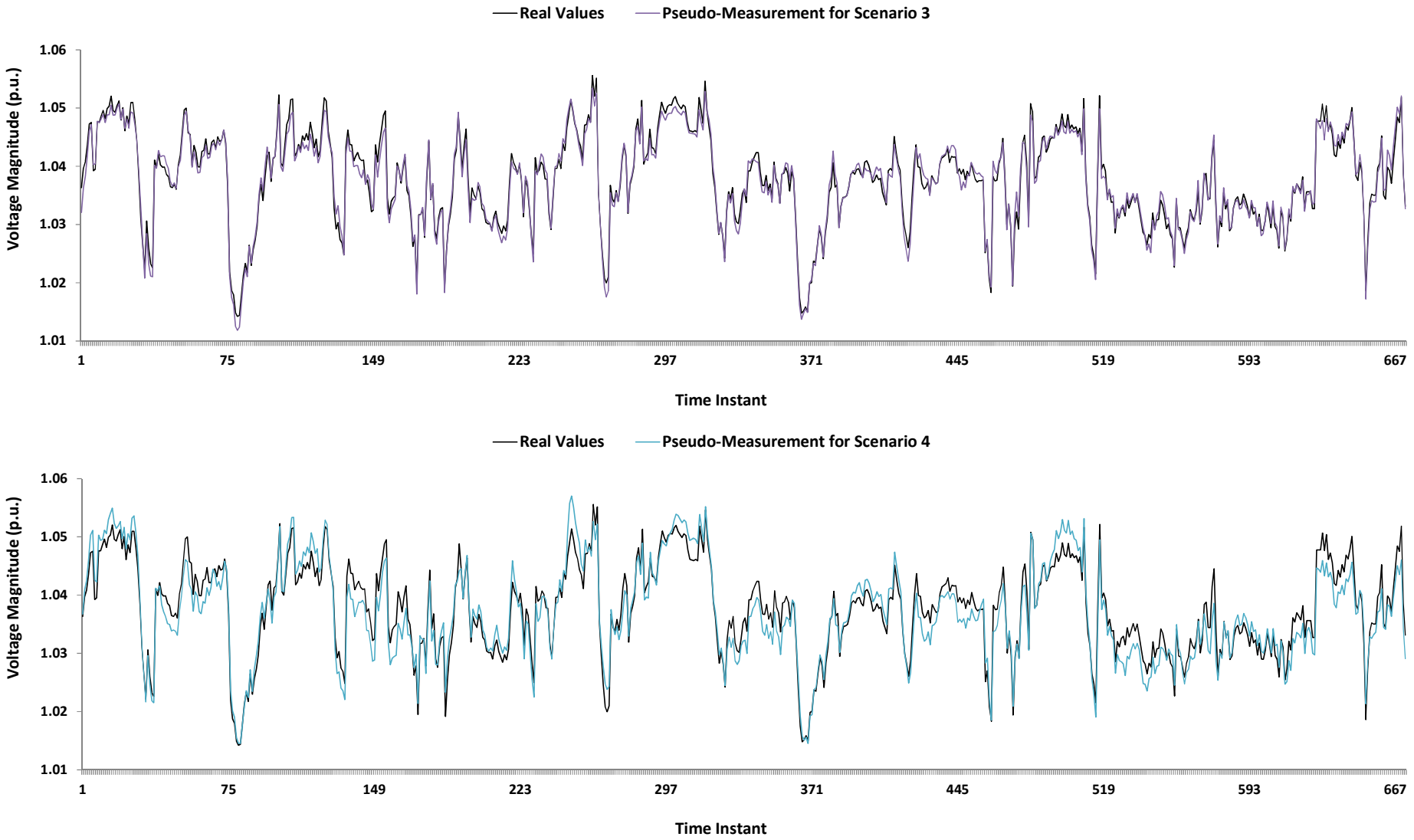
Real Values
Pseudo-Measurement for Scenario 3
Voltage Magnitude (p.u.)
1.06
1.05
1.04
1.03
1.02
1.01
1
75
149
223
297
371
445
519
593
667
Time Instant
Real Values
Pseudo-Measurement for Scenario 4
Voltage Magnitude (p.u.)
1.06
1.05
1.04
1.03
1.02
1.01
1
75
149
223
297
371
445
519
593
667
Time Instant

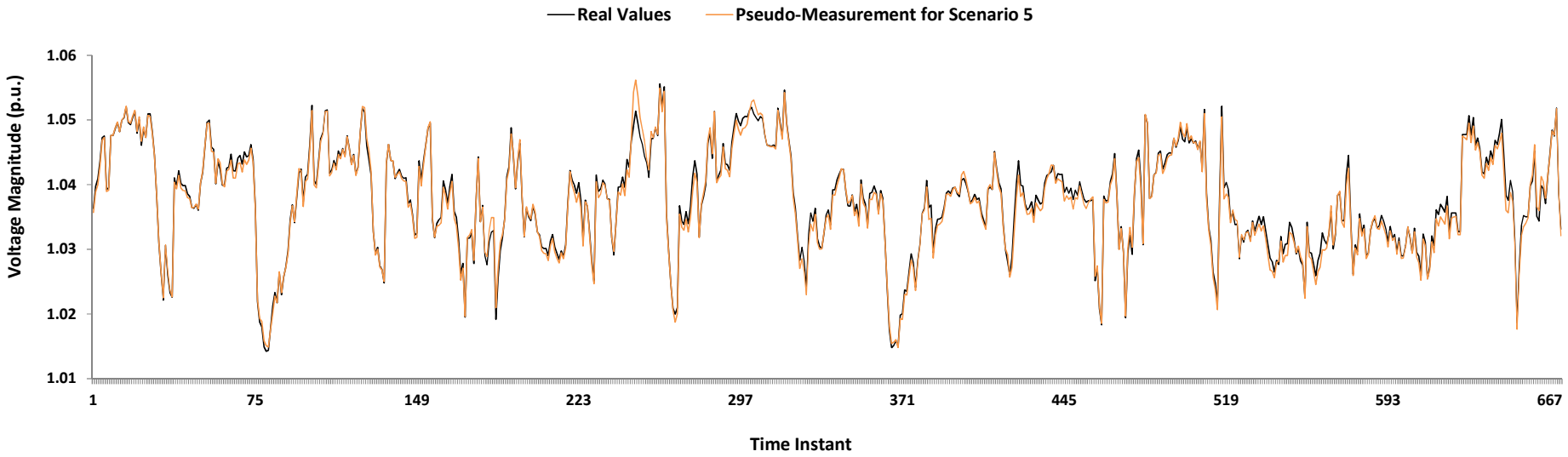

Figure 52 - Pseudo-measurements and real values of voltage magnitude for the entire evaluation set, for each scenario (p.u.)

Analysing the results previously exposed, it is possible to realise that, in a general way, the scenarios 3 and 5 are those that present, in this work, the pseudo-measurements with the lowest absolute error. However, the scenario 3 requires a smaller number of SM with the capability of transmitting data in real-time, what means a better trade-off between the number of real-time measurements required and the accuracy of the pseudo-measurement generated.

Although the scenario 4 is identical to scenario 3 (with respect to the number of SM with the capability of transmitting data in real-time), its pseudo-measurements are, in general, worse. This is because the SM of the scenario 4 do not belong to the set of SM with more influence on the performance of the pseudo-measurements generation method.

Still observing the obtained results, it is clear that the scenarios 1 and 2 yield, in general, the pseudo-measurements with the highest absolute error, which is normal because these are the scenarios with less real-time measurements. Nevertheless, their pseudo-measurements are quite acceptable, what allow to conclude that an autoencoder properly trained yields accurate results with just a few real-time measurements.

Another parameter to take into account to assess the autoencoder performance is the running time. Table 27 presents the running time for one time instant of running (a 15 minutes interval), for each scenario, as well as the time required to perform the training process for each autoencoder. It can be seen that the training and running times are higher when more real-time measurements are passed to the autoencoder during the training procedure (due to a higher number of hidden layer neurons).

Table 27 - Training and running times for each created scenario

Scenario	Training time (s)	Running time (s)
1	1.394	0.444
2	2.454	0.549
3	4.991	0.703
4	5.003	0.700
5	10.324	0.930

The times presented were obtained for autoencoders coded in Python programming language and run in a computer with an Intel Core i7-2600 CPU at 3.40 GHz and 8.00 GB of RAM memory.

It is important to refer that running times are highly influenced by several parameters, such as the convergence criterion of the EPSO or the number of neurons in the autoencoder hidden layer, as mentioned before. In fact, a clear trade-off exists

between these parameters and the autoencoder accuracy. Thus, it is possible to reduce running times to the detriment of results accuracy or vice-versa.

The running times presented should not be seen as absolute values since the algorithms can be coded in more efficient programming languages, leading to lower computation times.

5.2 Study Case – State Estimation

As originally stated, the aim of this work is to estimate the MV network operation state using data of the real-time measurements available on the MV network and, in case of unavailability of such measurements, make use of pseudo-measurements in order to guarantee the system observability.

5.2.1 Medium Voltage Network Characterization

Figure 53 presents the single line diagram of the 15 kV MV network used as test case, which operation state is intended to be estimated. Highlighted with an orange circle is the only one MV/LV secondary substation without the capability of transmitting data in real-time considered in the scope of this work (substation number 0426). The network corresponds to one complete feeder taken from Évora substation (Casinha-Sul). A total of 28 MV/LV secondary substations exist in this network (plus 2 more secondary substations that are normally disconnected from this feeder). The primary substation (Évora subestation) is equipped with two transformers, each one with a rated power of 31.5 MVA and the peak load verified in the selected feeder for the winter season (time period under analysis) was 2.5 MW.

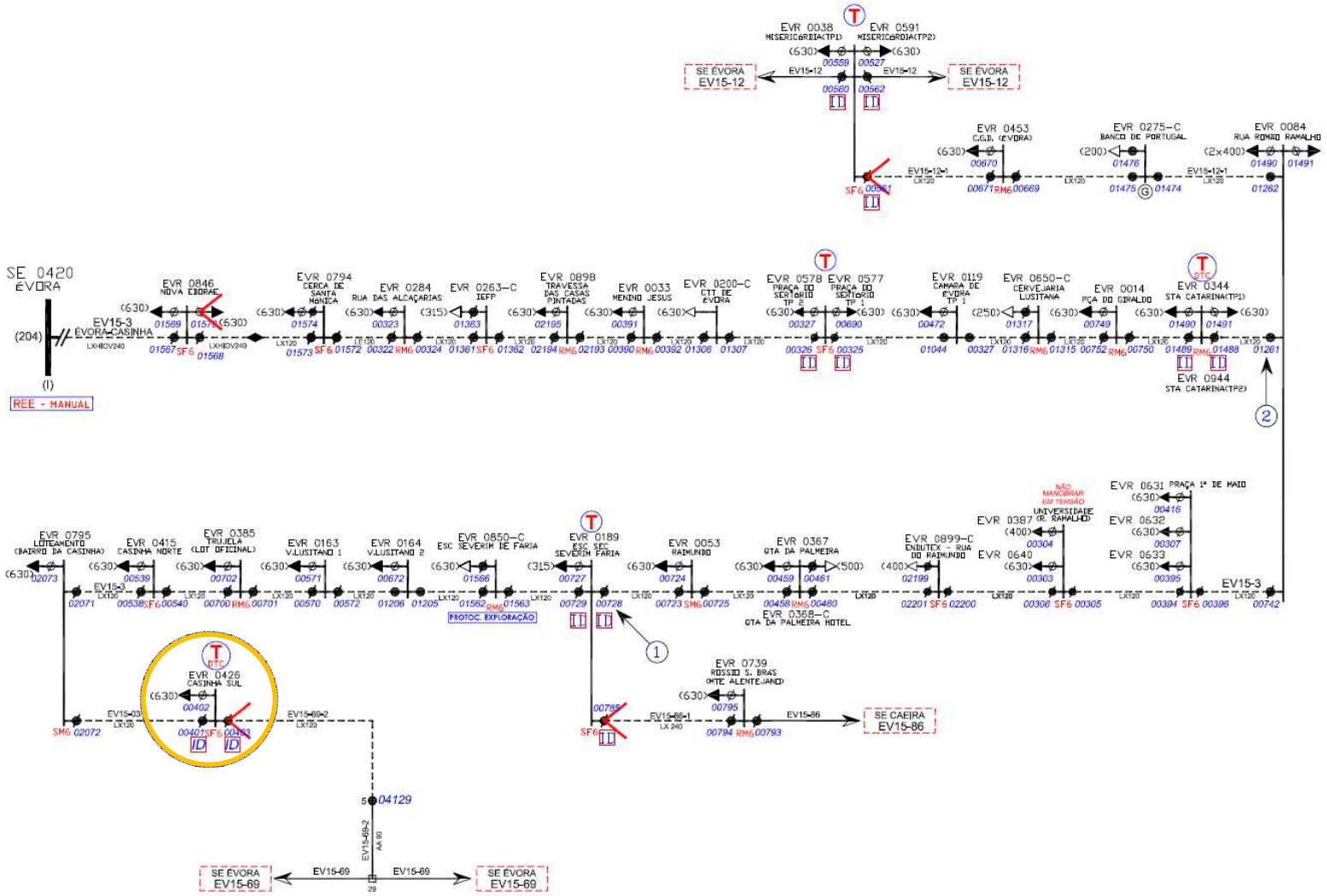

Figure 53 - Portuguese MV network used as test case. The orange circle identifies the only one MV/LV secondary substation without the capability of transmitting data in real-time considered – substation number 0426 (Casinha-Sul)

5.2.2 Load and Existing Telemetry Equipment

In order to evaluate the performance of the algorithm, it was necessary to create a set of true data for the time period under analysis. This was achieved by running several power flows using for load values real data from Évora Pilot Site. The real load data used correspond to average measurements of the active and reactive power for a time period of 15 minutes.

With respect to the measurement equipment, it was assumed that the lower voltage side of the primary HV/MV substation has one RTU equipment with the capability of monitoring in real-time the following variables: active and reactive power flows in the transformer and in the MV feeders and voltage magnitude at the high and medium voltage side of the transformer. Concerning to the MV/LV substations (MV loads), it was assumed that each one has a DTC as well as the associated measurement equipment with the capability of monitoring the same variables as in the primary substation.

In terms of data accuracy, the precision of referred equipment are usually categorized in classes, according to the confidence level specified by the manufactures. In this work some typical values were assumed. Voltage measurements were considered with ± 1% accuracy and P and Q measurements with ± 2%, all of them with a confidence level of 95%. The equipment accuracy was then modelled in accordance with the referred values by adding Gaussian noise to the results of the mentioned power flow simulations.

5.2.3 State Estimation

In order to fulfil the purpose of this work, a classical state estimator based on Weighted Least Squares (WLS) algorithm was used. The algorithm was run for one week in time steps of 15 minutes. The week considered was exactly the same as in the study performed in the previous section. Once more, for the secondary substation considered without real-time measurements, it were used the pseudo-measurements generated with the methodology presented in the previous section. Although the pseudo-measurements had been generated for the lower voltage bus of the referred substation (LV side), for a matter of simplicity, it was assumed that they can be used as pseudo-measurements for the MV side. This assumption was made after checking the following aspects in the studied network: the existing MV/LV transformers have low power losses and their transformation ratio is 1:1. The first aspect implies that both active and reactive power remains practically unchanged when looking to both sides of the transformer and the second implies that voltage has exactly the same value (in p.u.) at the low voltage and at the high voltage side of the MV/LV substation. Since the two referred aspects have been completely verified for the network under study, the quality of the results is not affected.

Within the state estimation algorithm, the following measurements were assumed to be available in real time: active and reactive power flows in the transformer of each secondary MV substation and in the MV feeder (from SE 0420 to EVR 0846 in Figure 53)

and voltage magnitude values at the medium voltage side of each secondary MV substation. The WLS weights were adjusted individually in accordance with uncertainty associated to the different measurements given by the telemetry equipment. In order to have a benchmark case for comparison, the state estimation algorithm was also run without pseudo-measurements for the substation without real-time measurements aforementioned. It is important to denote that the redundancy level was at minimum value, and if some measurement value is unavailable the system will be non observable.

The obtained results for the estimation of the MV network operation state are displayed below. Firstly, it is presented the absolute error of the voltage magnitude obtained for all the secondary MV substations, with and without using the pseudo-measurements values generated (Figure 54 to Figure 59). Next, it will be shown a voltage magnitude absolute error comparison, for the secondary substation without real-time measurements considered, between the estimated values obtained with and without using the referred pseudo-measurements (Figure 60). Moreover, it is exposed a table of the MAE of the voltage magnitude for the same conditions (Table 28), as well as several graphical representations of the voltage magnitude (real and estimated values) for the aforementioned conditions, all of them for the considered period (Figure 61 to Figure 66). Finally, it is shown, for all the secondary MV substations, a voltage magnitude comparison between the real values and the estimated ones using the pseudo-measurements generated in scenario 3 and without pseudo-measurements (Figure 67).

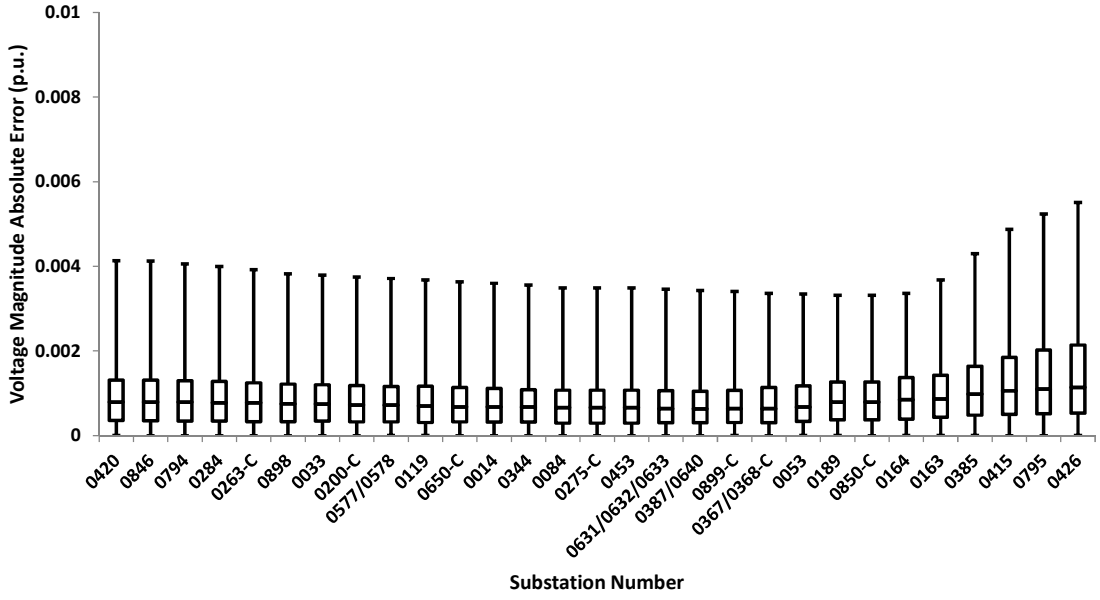

Figure 54 - Absolute error of the voltage magnitude obtained, for all MV/LV secondary substations, using the pseudo-measurements generated in scenario 1 (p.u.)

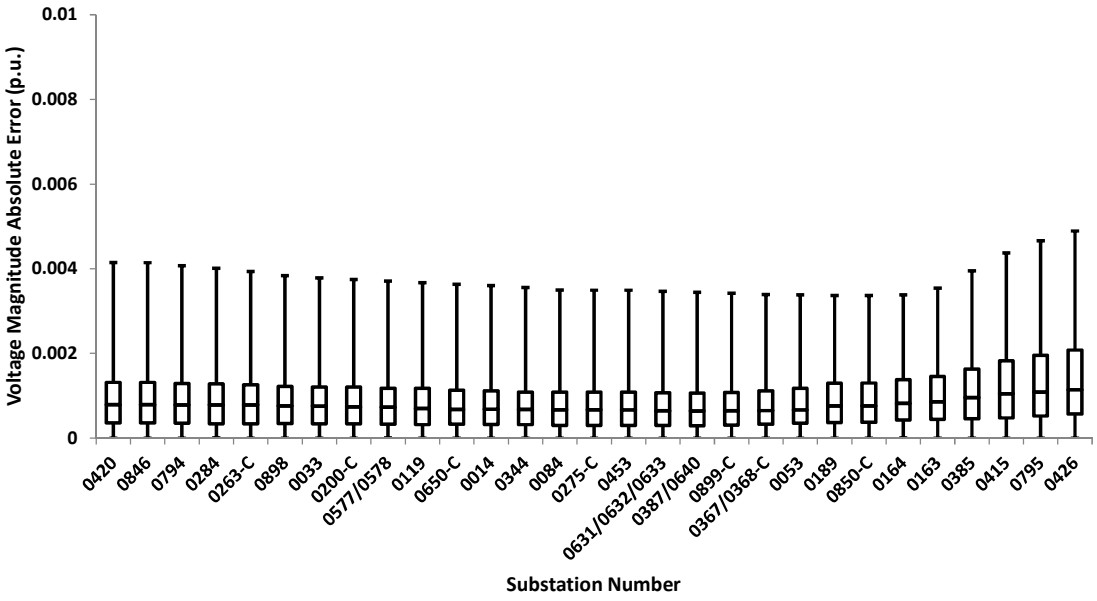

Figure 55 - Absolute error of the voltage magnitude obtained, for all MV/LV secondary substations, using the pseudo-measurements generated in scenario 2 (p.u.)

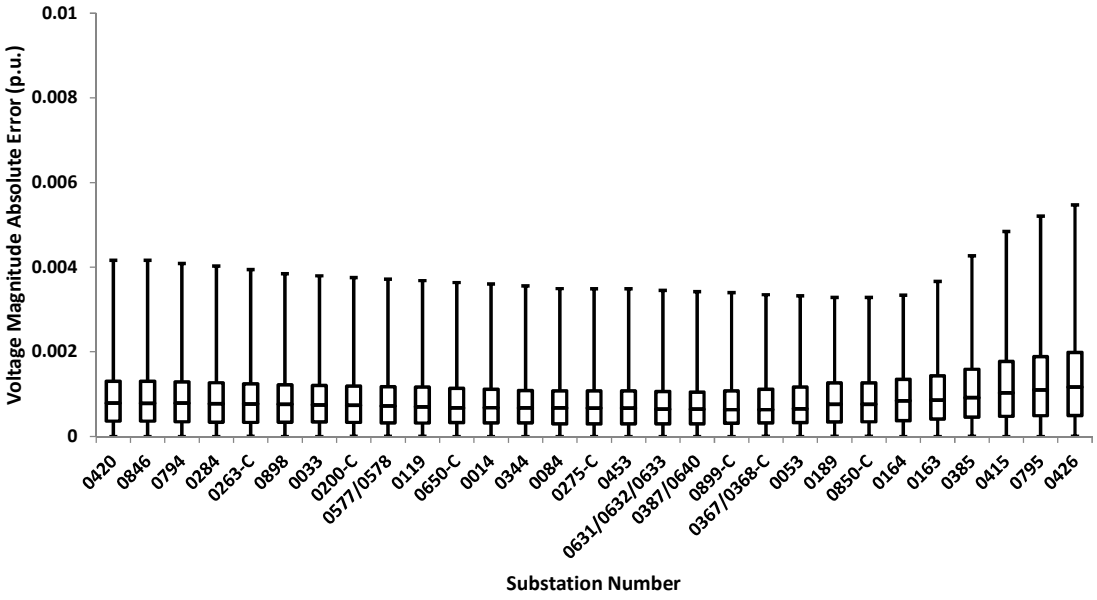

Figure 56 - Absolute error of the voltage magnitude obtained, for all MV/LV secondary substations, using the pseudo-measurements generated in scenario 3 (p.u.)

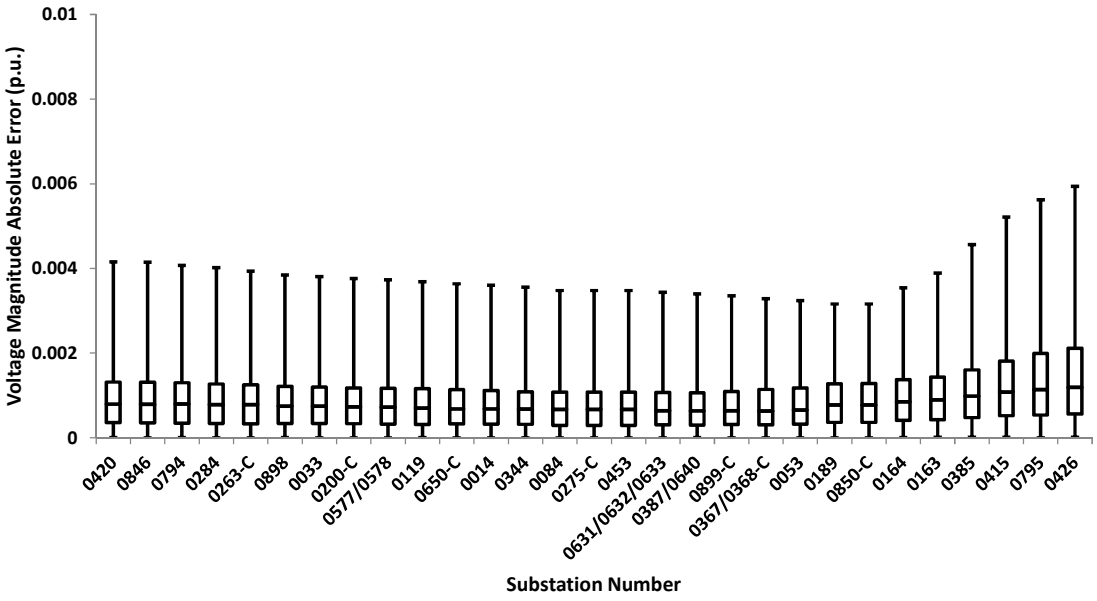

Figure 57 - Absolute error of the voltage magnitude obtained, for all MV/LV secondary substations, using the pseudo-measurements generated in scenario 4 (p.u.)

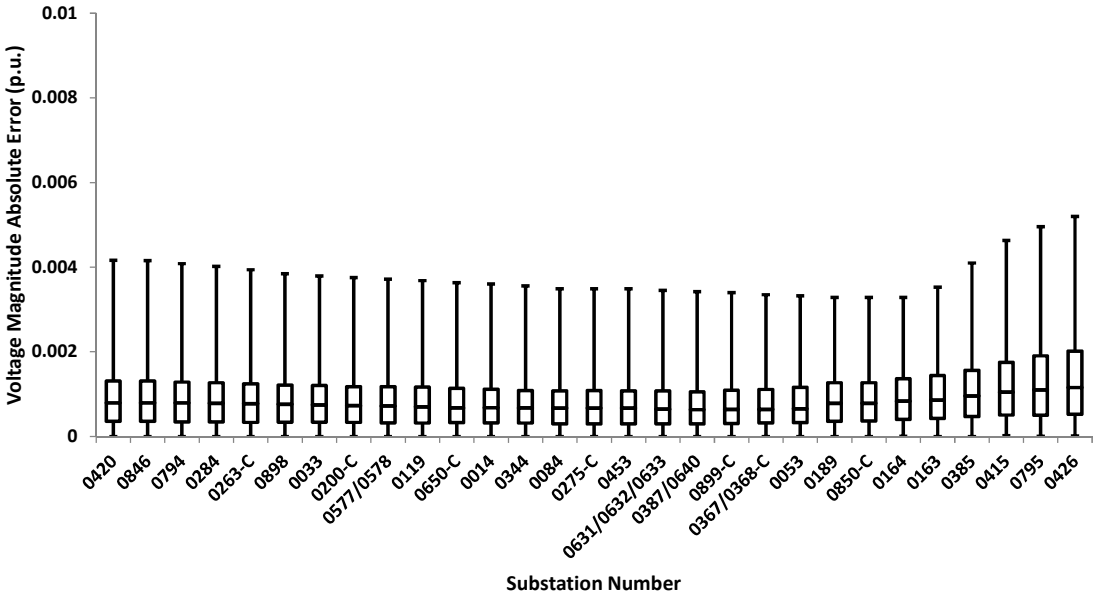

Figure 58 - Absolute error of the voltage magnitude obtained, for all MV/LV secondary substations, using the pseudo-measurements generated in scenario 5 (p.u.)

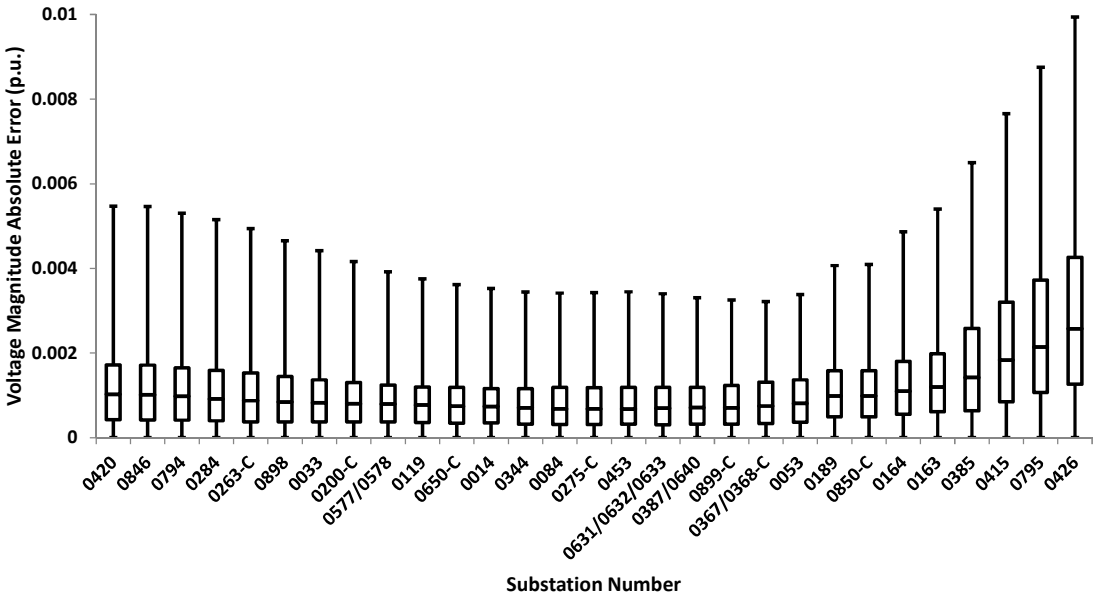

Figure 59 - Absolute error of the voltage magnitude obtained, for all MV/LV secondary substations, using no pseudo-measurements (p.u.)

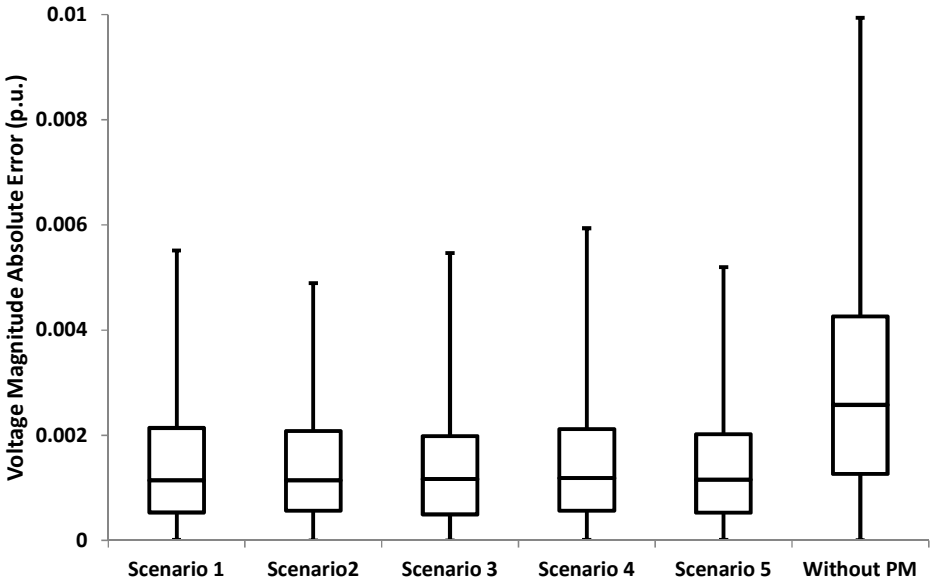

Figure 60 - Absolute error of the voltage magnitude obtained, for the MV/LV secondary substation without the capability of transmitting data in real-time considered, with and without using the pseudo-measurements generated in each scenario (p.u.)

Table 28 - Voltage magnitude MAE obtained with and without using the pseudo-measurements generated in each scenario (p.u.)

	Scenario 1	Scenario 2	Scenario 3	Scenario 4	Scenario 5	Without PM
Voltage Magnitude MAE (p.u.)	0.00140	0.00139	0.00135	0.00141	0.00135	0.00301

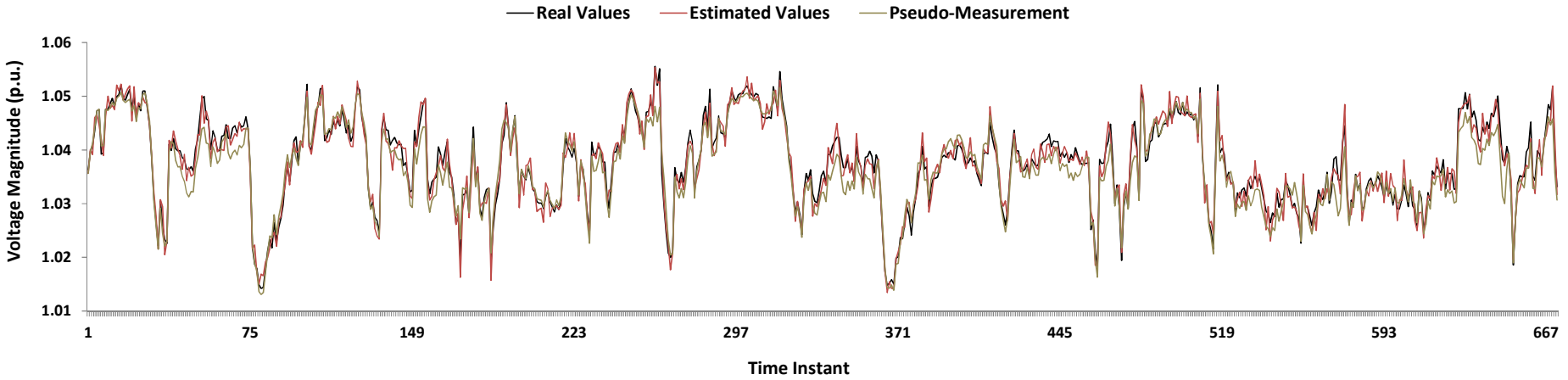

Figure 61 - Representation of the voltage magnitude for the considered period: real values and estimated ones using the pseudo-measurements generated in scenario 1. The pseudo-measurement of the voltage magnitude used is also shown (p.u.)

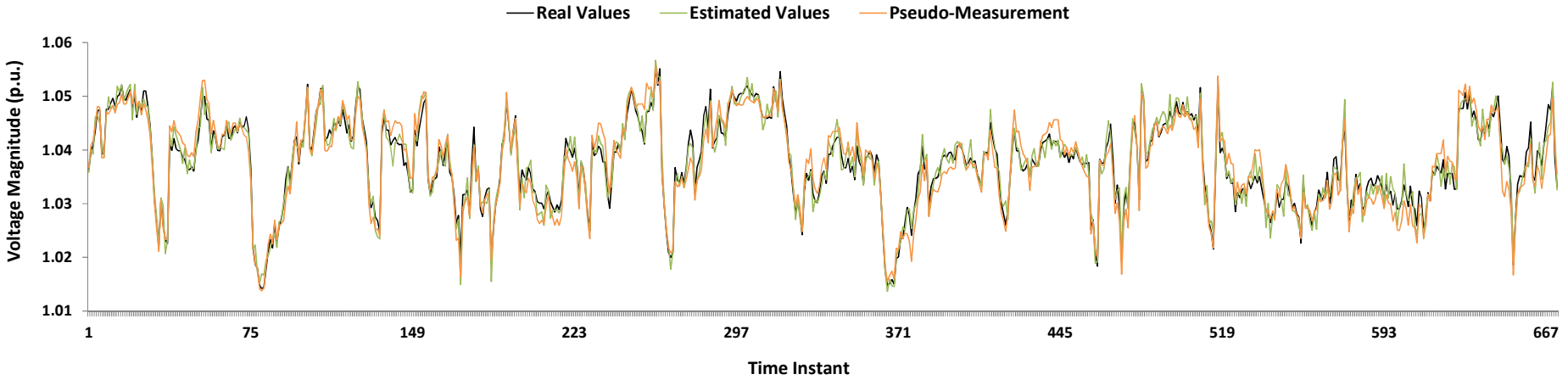

Figure 62 - Representation of the voltage magnitude for the considered period: real values and estimated ones using the pseudo-measurements generated in scenario 2. The pseudo-measurement of the voltage magnitude used is also shown (p.u.)

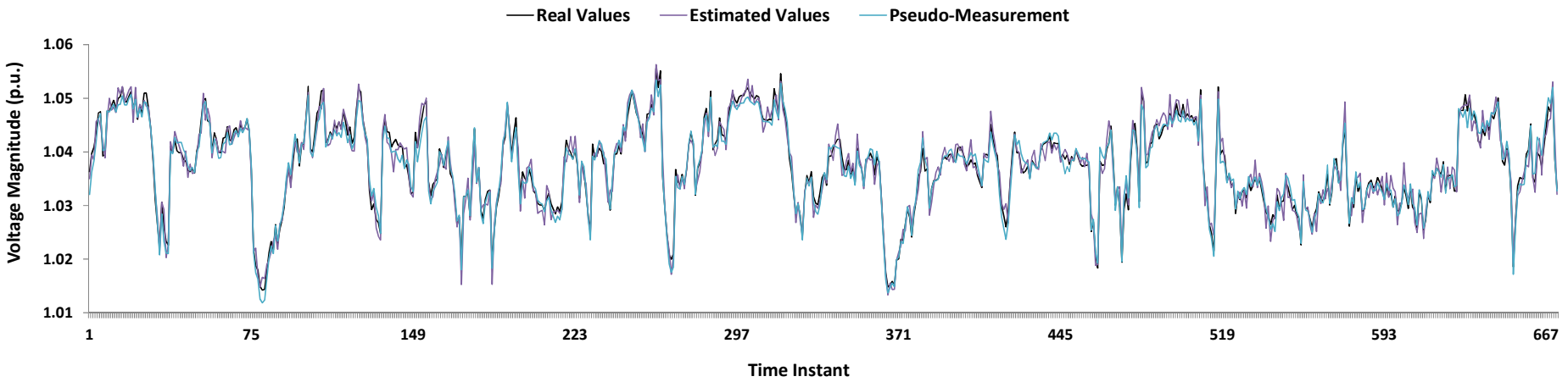

Figure 63 - Representation of the voltage magnitude for the considered period: real values and estimated ones using the pseudo-measurements generated in scenario 3. The pseudo-measurement of the voltage magnitude used is also shown (p.u.)

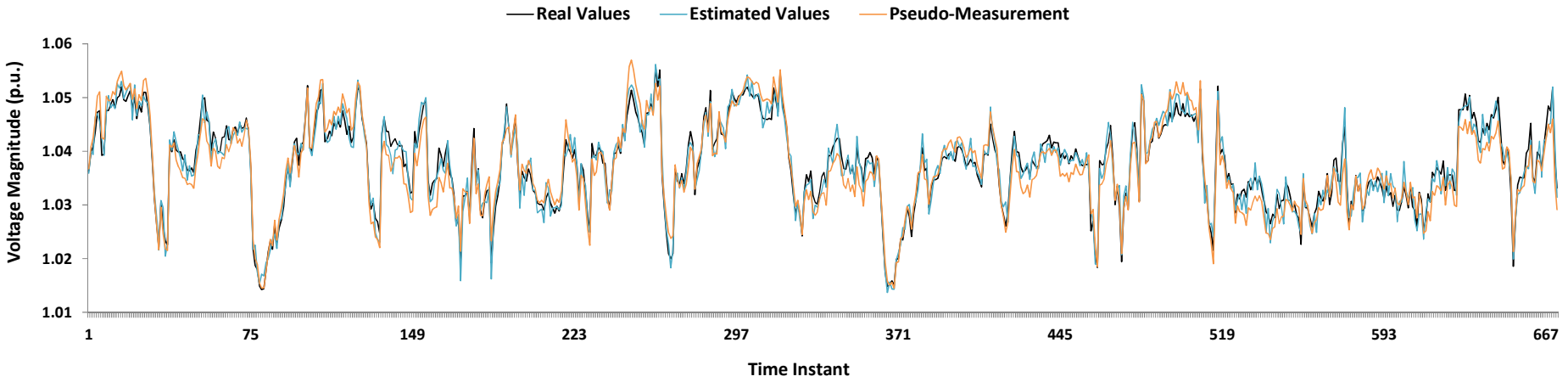

Figure 64 - Representation of the voltage magnitude for the considered period: real values and estimated ones using the pseudo-measurements generated in scenario 4. The pseudo-measurement of the voltage magnitude used is also shown (p.u.)

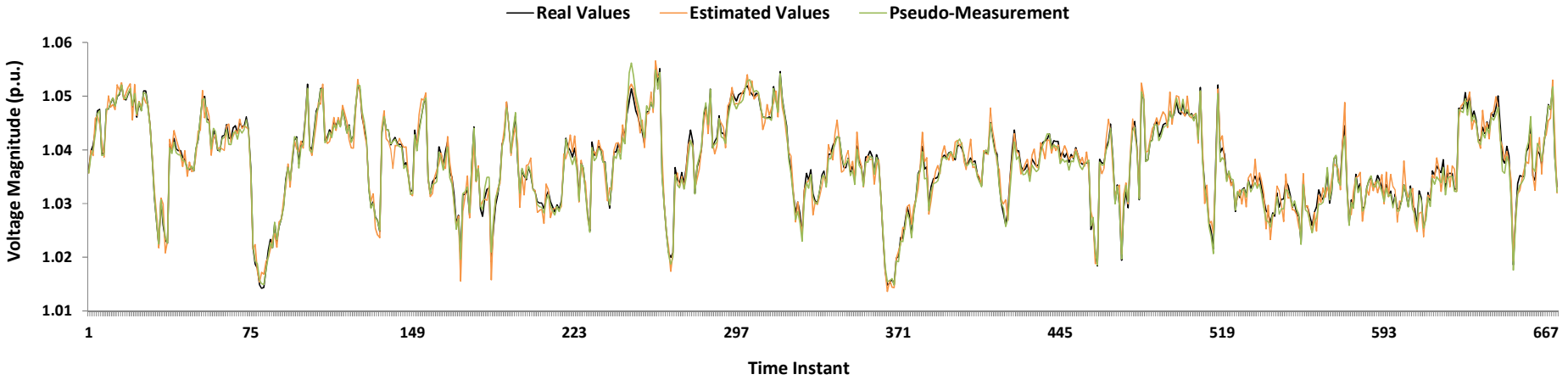

Figure 65 - Representation of the voltage magnitude for the considered period: real values and estimated ones using the pseudo-measurements generated in scenario 5. The pseudo-measurement of the voltage magnitude used is also shown (p.u.)

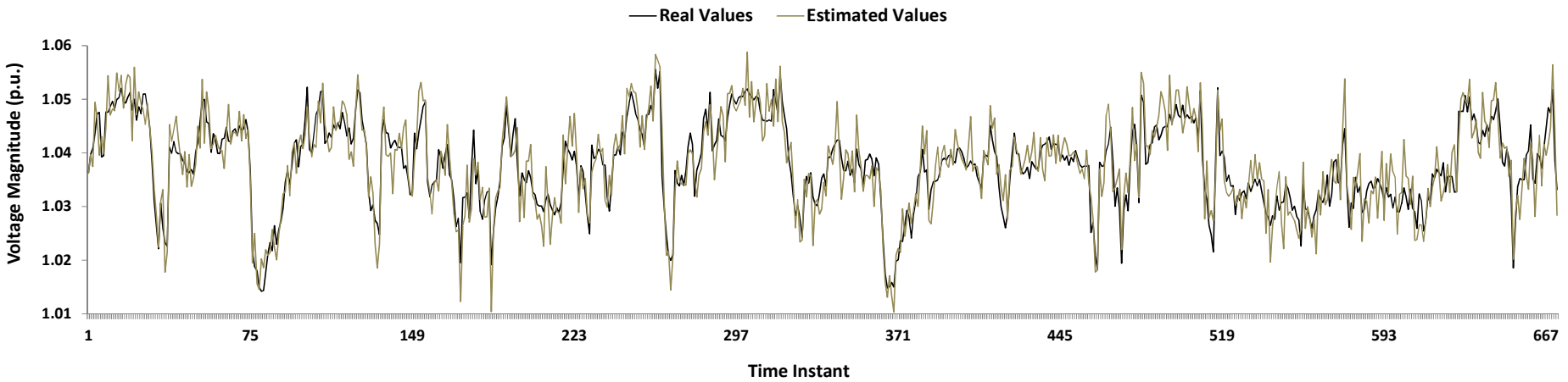

Figure 66 - Representation of the voltage magnitude for the considered period: real values and estimated ones using no pseudo-measurements (p.u.)

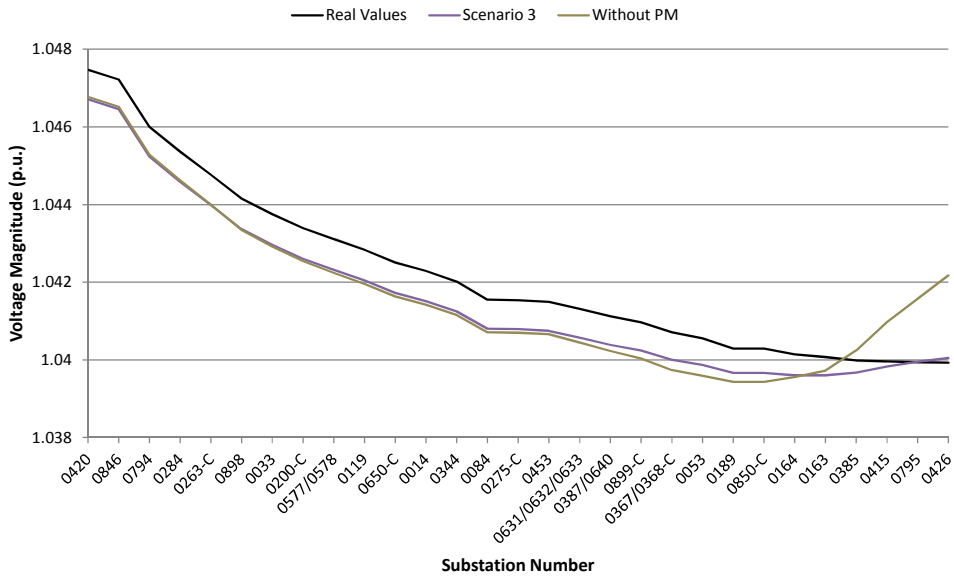

Figure 67 - Representation of the voltage magnitude for all MV/LV secondary substations: real values and estimated ones with and without using the pseudo-measurements generated in scenario 3 (p.u.)

After running the state estimator algorithm, the influence of the generated pseudo-measurements is then evaluated. Observing the exposed results, it is clear that the MV network operation state estimated using no pseudo-measurements is the one with the highest absolute error (Figure 59).

Looking now for the results obtained using the pseudo-measurements generated and although the referred pseudo-measurements are significantly different, it is possible to conclude that the WLS algorithm have converged in all cases to nearly the real values (Figure 54 to Figure 58, Figure 60 and Figure 61 to Figure 66). Although these results reflect the robustness of the state estimation algorithm, it should be noted that only a MV/LV secondary substation without real-time measurements was considered, thus the number of real-time measurements available were large. As it can be seen by observing Figure 54 to Figure 59, the highest errors on the voltage magnitude estimation are in buses belonging to substations close located to the 0426 one. Nevertheless, the contribution given by the pseudo-measurements can be seen when comparing the results to the case where their use were not considered. In these circumstances, as it can be concluded looking to Figure 54 to Figure 59, the error is higher when no pseudo-measurement is used in the state estimation.

Although the results are quite similar for all the pseudo-measurements scenarios, the estimation error diminish when pseudo-measurements generated with the scenarios 3 and 5 are used (Figure 60 and Table 28). However, it is important to remember that scenario 3 presents a better trade-off between the number of real-time measurements

required for pseudo-measurements generation and the accuracy of the pseudo-measurements generated.

Finally, in Figure 67 it can be seen, once again, that the state estimation obtained using pseudo-measurements (generated in scenario 3, in this particular case) is more accurate than when no pseudo-measurements are used. Logically, this is more noticeable for the MV/LV secondary substation where the pseudo-measurements were considered (0426). In this figure, the radial topology of the studied MV network is clearly shown by the voltage drop along the network.

5.3 KPI calculations

The variations of the index RPE per network substation are shown in Figure 68 to Figure 74. In Figure 68 is presented one day (first one) of the considered week for each pseudo-measurements created scenario. In each one of these scenarios is included 96 RPE values for each substation (one per 15 minutes state estimation running). Similarly, Figure 69 to Figure 74 present the distribution of the voltage magnitude RPE for the entire considered week (672 RPE values for each substation).

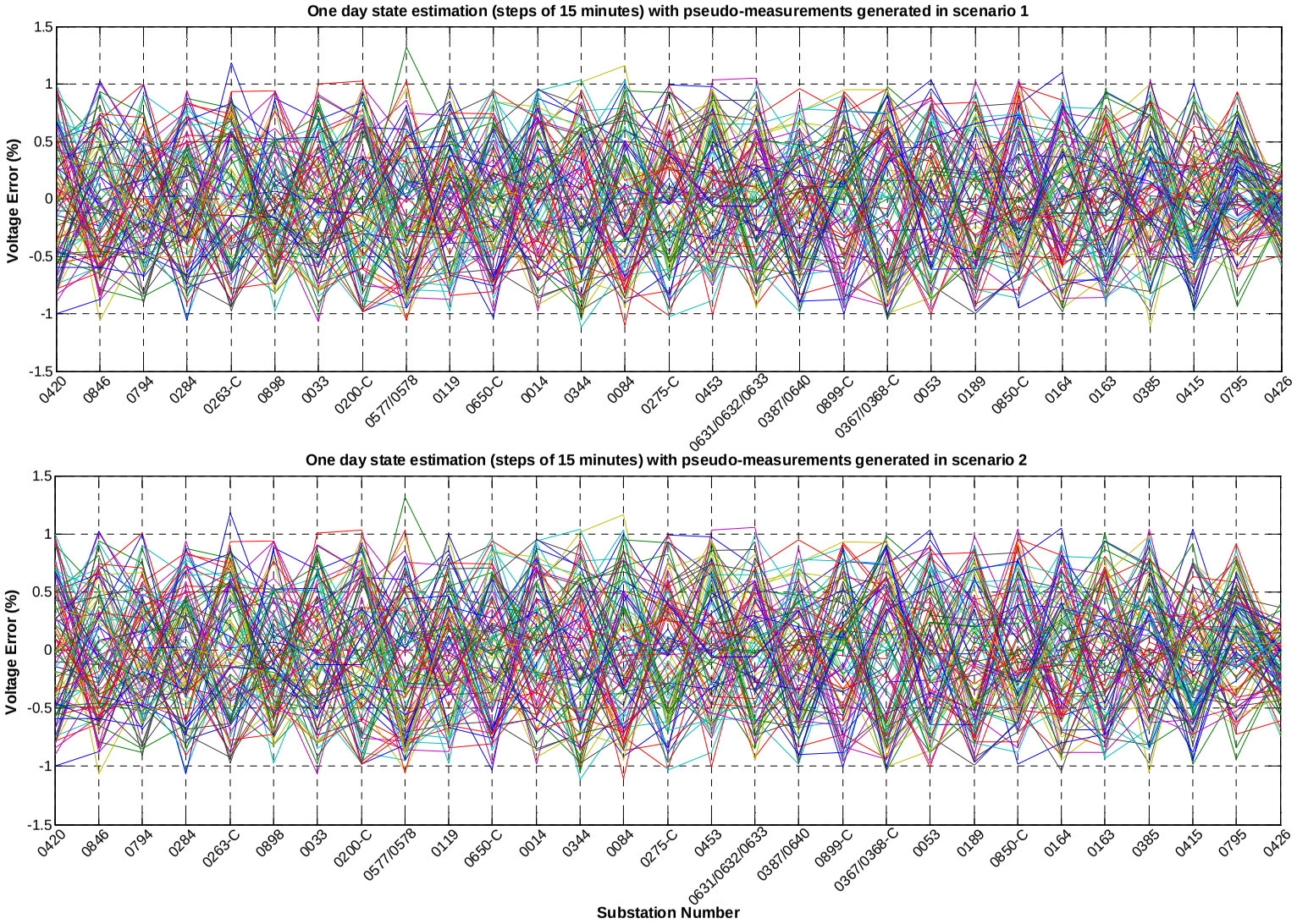
One day state estimation (steps of 15 minutes) with pseudo-measurements generated in scenario 1
Voltage Error (%)
1.5
1
0.5
0
-0.5
-1
-1.5
0420
0846
0794
0284
0263-C
0898
0033
0200-C
0577/0578
0119
0650-C
0014
0344
0084
0275-C
0453
0631/0632/0633
0387/0640
0899-C
0367/0368-C
0053
0189
0850-C
0164
0163
0385
0415
0795
0426
One day state estimation (steps of 15 minutes) with pseudo-measurements generated in scenario 2
Voltage Error (%)
Substation Number

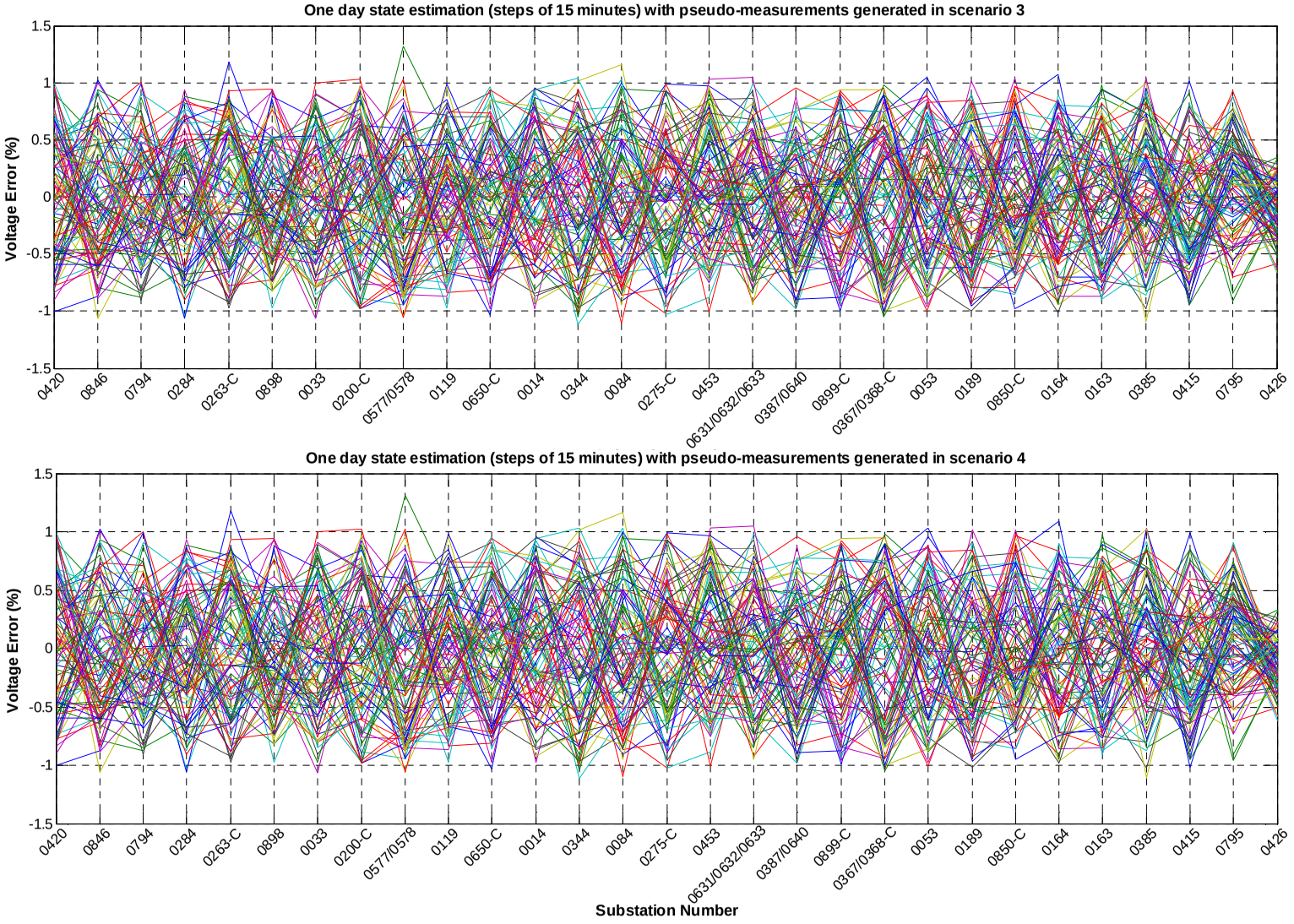
One day state estimation (steps of 15 minutes) with pseudo-measurements generated in scenario 3
Voltage Error (%)
1.5
1
0.5
0
-0.5
-1
-1.5
0420
0846
0794
0284
0263-C
0898
0033
0200-C
0577/0578
0119
0650-C
0014
0344
0084
0275-C
0453
0631/0632/0633
0387/0640
0899-C
0367/0368-C
0053
0189
0850-C
0164
0163
0385
0415
0795
0426
One day state estimation (steps of 15 minutes) with pseudo-measurements generated in scenario 4
Voltage Error (%)
Substation Number

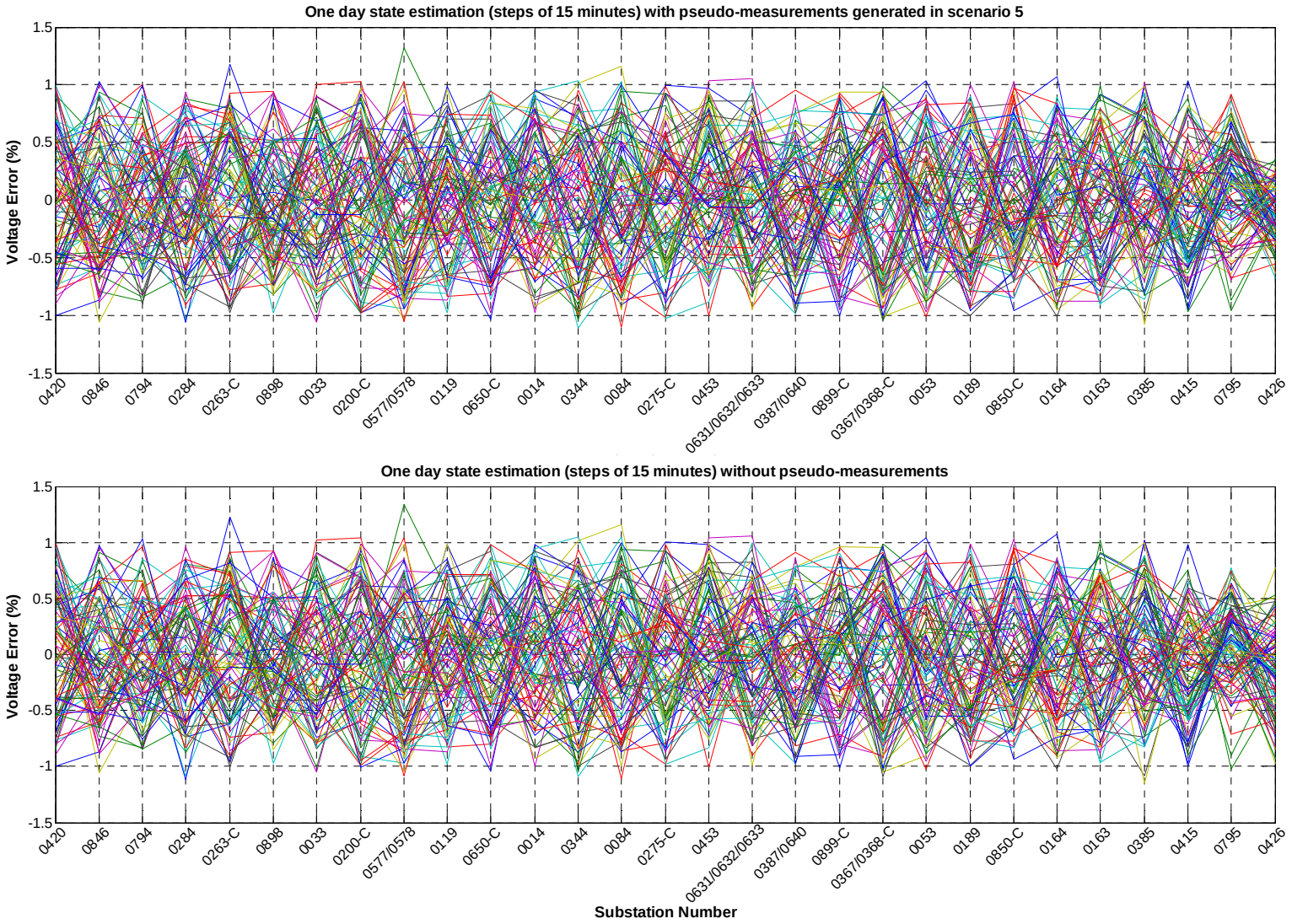

Figure 68 - Voltage magnitude relative percentage errors (RPE) per network substation (with and without using pseudo-measurements)

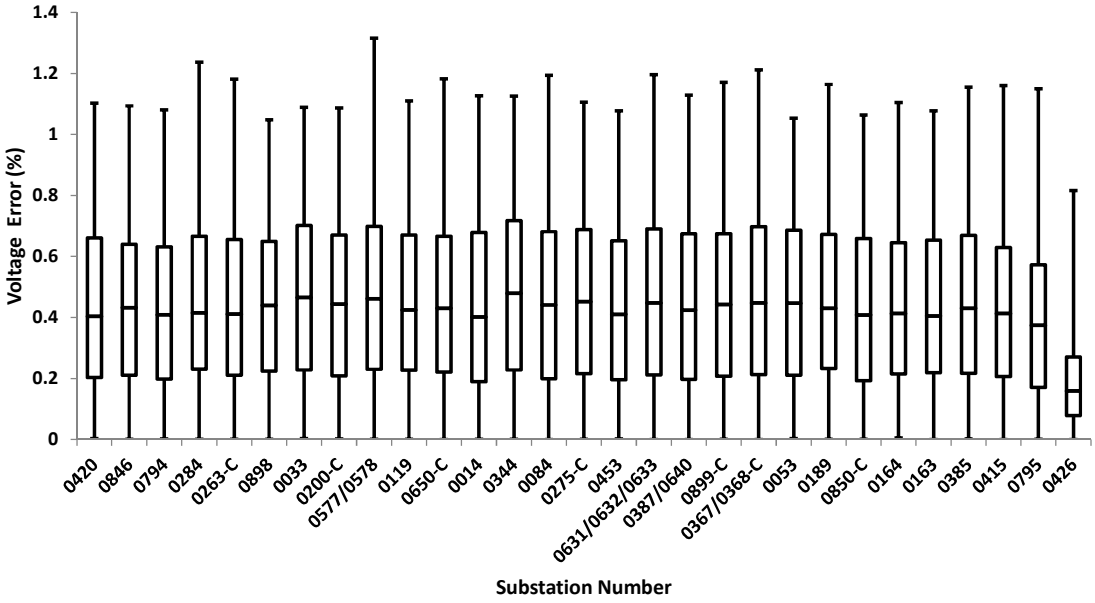

Figure 69 - Distribution of the voltage magnitude relative percentage errors (RPE) per network substation (with using pseudo-measurements generated in scenario 1) for the entire considered week

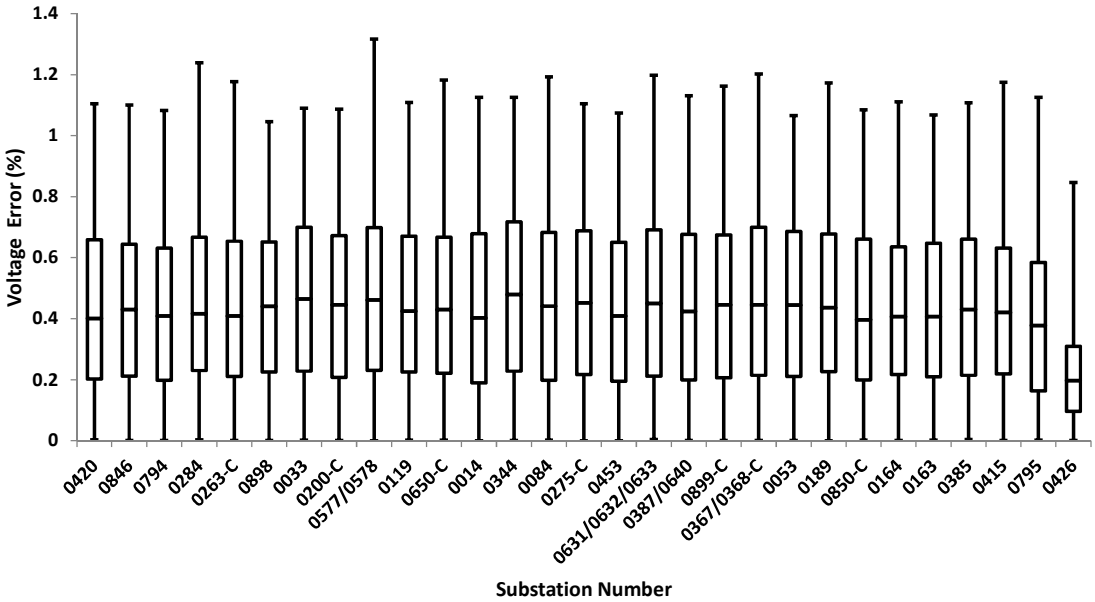

Figure 70 - Distribution of the voltage magnitude relative percentage errors (RPE) per network substation (with using pseudo-measurements generated in scenario 2) for the entire considered week

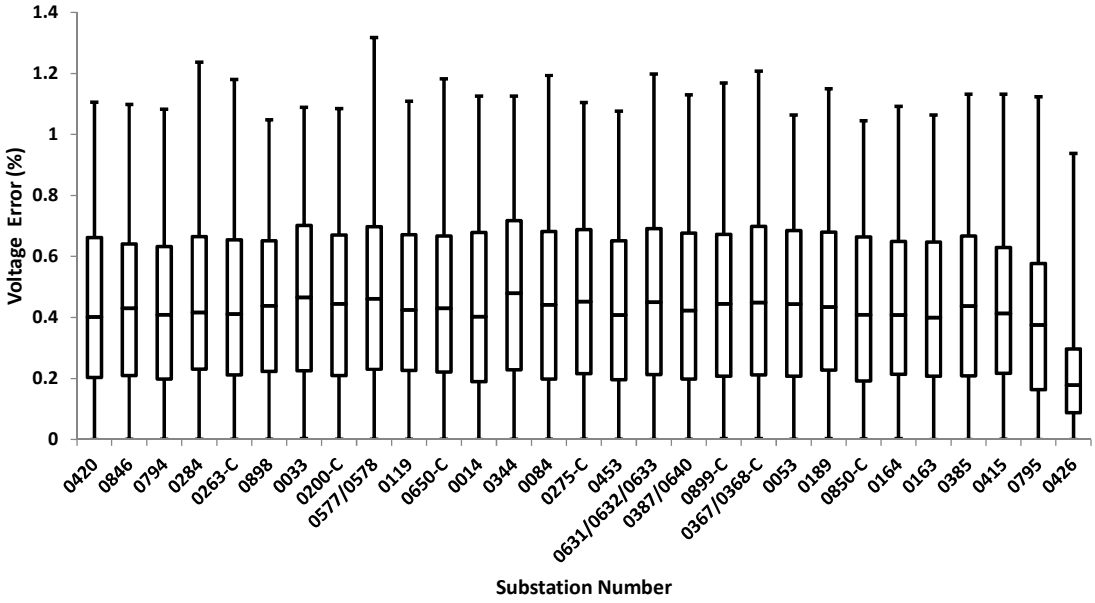

Figure 71 - Distribution of the voltage magnitude relative percentage errors (RPE) per network substation (with using pseudo-measurements generated in scenario 3) for the entire considered week

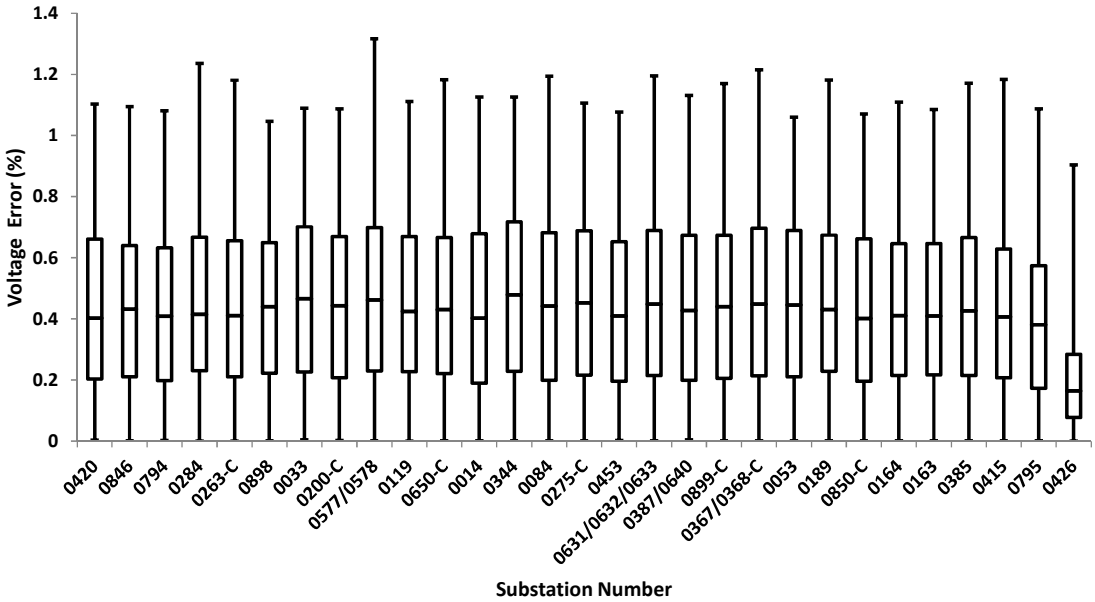

Figure 72 - Distribution of the voltage magnitude relative percentage errors (RPE) per network substation (with using pseudo-measurements generated in scenario 4) for the entire considered week

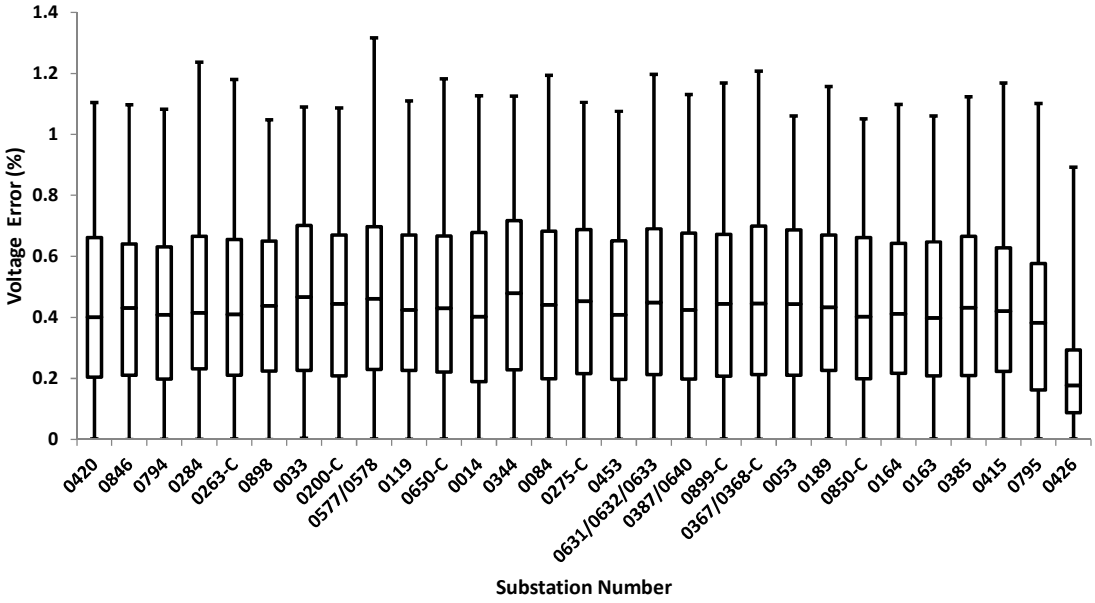

Figure 73 - Distribution of the voltage magnitude relative percentage errors (RPE) per network substation (with using pseudo-measurements generated in scenario 5) for the entire considered week

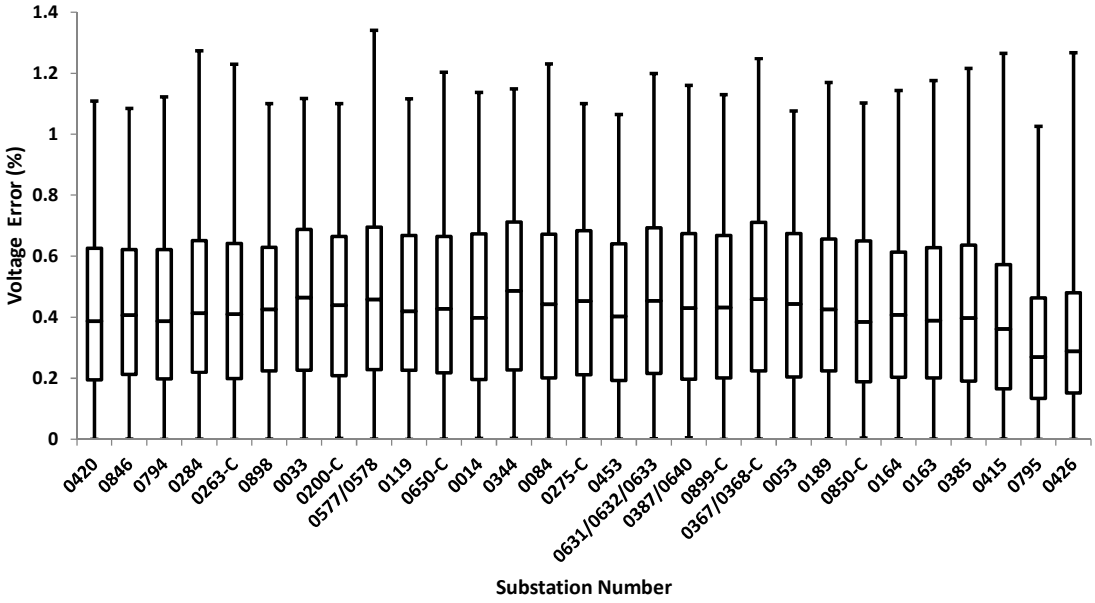

Figure 74 - Distribution of the voltage magnitude relative percentage errors (RPE) per network substation (without using pseudo-measurements) for the entire considered week

APPENDIX A. Architecture of the prototype software

The software prototype is based on MATPOWER [55], which is an open-source package of MATLAB m-files for solving steady-state power system analysis problems. This package has been modified and extended for the purposes of this project. The algorithms have been tested and tuned with several test systems. All floating-point computations are performed in double precision. Tolerance values of 0.001 p.u. were used for load-flow and state estimation convergence. Active and reactive power injection mismatches (for load flow) and voltage magnitude and angles (for state estimation) are checked for convergence. The codes run on an Intel Core i3 PC, clocking at 2.13 GHz with 2 GB of RAM, under the 64-bit Windows 7 operating system.

All the input data is provided in ASCII files with name "case_xxxx", where "xxxx" is the number of buses (4 digits), and extension ".raw", ".mes", and ".cbr". The file **"case_xxxx.raw"** contains the load flow data information [56], the file **"case_xxxx.mes"** includes the state estimation data information, and the file **"case_xxxx.cbr"** contains the circuit breaker (CB) information. The input data for the case to be simulated are converted into a set of data matrices packaged as the fields of a MATLAB struct denoted by the variable **mpc**. The main simulation routines, **"run_pf"** for load flow and **"run_se"** for state estimation, accept a MATPOWER case struct as an input. The output information for power flow and state estimation are provided in the ASCII files **"case_xxxx.pf"** and **"case_xxxx.se"** respectively, which are automatically generated and saved. The format of each ASCII file is described in the following subsections.

Description of the PTI load flow data format (ASCII file .raw)

```
Case Identification Data
========================

First record: IC,SBASE

   IC - 0 for base case, 1 for change data to be added
   SBASE - System MVA base

Records 2 and 3 - two lines of heading, up to 60 characters per line

Bus Data
========
Bus data records, terminated by a record with a bus number of zero.

I,IDE,PL,QL,GL,BL,IA,VM,VA,'NAME',BASKL,ZONE

I     - Bus number (1 to 29997)
IDE   - Bus type
      1 - Load bus (no generation)
      2 - Generator or plant bus
      3 - Swing bus
      4 - Isolated bus
```

```
PL    - Load MW
QL    - Load MVAR
GL    - Shunt conductance, MW at 1.0 per unit voltage
BL    - Shunt susceptance, MVAR at 1.0 per unit voltage. (- = reactor)
IA    - Area number, 1-100
VM    - Voltage magnitude, per unit
VA    - Voltage angle, degrees
NAME  - Bus name, 8 characters, must be enclosed in quotes
BASKV - Base voltage, KV
ZONE  - Loss zone, 1-999
```

Generator Data
==========

Generator data records, terminated by a generator with an index of zero.

I,ID,PG,QG,QT,QB,VS,IREG,MBASE,ZR,ZX,RT,XT,GTAP,STAT,RMPCT,PT,PB

```
I     - Bus number
ID    - Machine identifier (0-9, A-Z)
PG    - MW output
QG    - MVAR output
QT    - Max MVAR
QB    - Min MVAR
VS    - Voltage setpoint
IREG  - Remote controlled bus index (must be type 1), zero to control
        own voltage, and must be zero for gen at swing bus
MBASE - Total MVA base of this machine (or machines), defaults to system
        MVA base.
ZR,ZX - Machine impedance, pu on MBASE
RT,XT - Step up transformer impedance, p.u. on MBASE
GTAP  - Step up transformer off nominal turns ratio
STAT  - Machine status, 1 in service, 0 out of service
RMPCT - Percent of total VARS required to hold voltage at bus IREG to
        come from bus I - for remote buses controlled by several
        generators
PT    - Max MW
PB    - Min MW
```

Branch Data
==========

Branch records, ending with a record with from bus of zero

I,J,CKT,R,X,B,RATEA,RATEB,RATEC,RATIO,ANGLE,GI,BI,GJ,BJ,ST

```
I     - From bus number
J     - To bus number
CKT   - Circuit identifier (two character) not clear if integer or alpha
R     - Resistance, per unit
X     - Reactance, per unit
B     - Total line charging, per unit
RATEA - MVA rating A
RATEB,
RATEC - Higher MVA ratings
RATIO - Transformer off nominal turns ratio
ANGLE - Transformer phase shift angle
GI,BI - Line shunt complex admittance for shunt at from end (I) bus, pu.
```

GJ,BJ - Line shunt complex admittance for shunt at to end (J) bus, pu.
ST - Initial branch status, 1-in service, 0-out of service

Transformer Adjustment Data
==========

Ends with record with from bus of zero

I,J,CKT,ICONT,RMA,RMI,VMA,VMI,STEP,TABLE

I - From bus number
J - To bus number
CKT - Circuit number
ICONT - Number of bus to control. If different from I or J, sign of ICONT determines control. Positive sign, close to impedance (untapped) bus of transformer. Negative sign, opposite.
RMA - Upper limit of turns ratio or phase shift
RMI - Lower limit of turns ratio or phase shift
VMA - Upper limit of controlled volts, MW or MVAR
VMI - Lower limit of controlled volts, MW or MVAR
STEP - Turns ratio step increment
TABLE - Zero, or number of a transformer impedance correction table 1-5

Area Interchange Data
==========

Ends with I of zero

I,ISW,PDES,PTOL,'ARNAM'

I - Area number (1-100)
ISW - Area interchange slack bus number
PDES - Desired net interchange, MW + = out.
PTOL - Area interchange tolerance, MW
ARNAM - Area name, 8 characters, enclosed in single quotes.

Switch Shunt Data
==========

Ends with I = 0.

I,MODSW,VSWHI,VSWLO,SWREM,BINIT,N1,B1,N2,B2...N8,B8

I - Bus number
MODSW - Mode 0 - fixed 1 - discrete 2 - continuous
VSWHI - Desired voltage upper limit, per unit
VSWLO - Desired voltage lower limit, per unit
SWREM - Number of remote bus to control. 0 to control own bus.
VDES - Desired voltage setpoint, per unit
BINIT - Initial switched shunt admittance, MVAR at 1.0 per unit volts
N1 - Number of steps for block 1, first 0 is end of blocks
B1 - Admittance increment of block 1 in MVAR at 1.0 per unit volts.
N2, B2, etc, as N1, B1

Description of the switching device data format (ASCII file .cbr)

Switching Device Data
==========

Switching device records, ending with a record with from bus of zero.

I,J,ST

I - From bus number
J - To bus number
ST - Initial switching device status, 1-in service, 0-out of service

Description of the state estimation data format (ASCII file .ses)

Case Identification Data
==========

Record 1 - one line of heading, up to 60 characters

Voltage Measurement Data
==========

Voltage measurement data records, terminated by a record with a bus number of zero.

I,SNM,FS,ST,RTU

I - Bus number (1 to 29997)
SNM - Error multiplier
FS - The full scale of the meter
ST - Measurement status, 1-in service, 0-out of service
RTU - Index of the RTU where this measurement is assigned

Active Flow Measurement Data
==========

Active flow measurement data records, terminated by a record with from bus of zero.

I,J,CKT,SNM,FS,ST,RTU

I - From bus number
J - To bus number
CKT - Circuit identifier (integer)
SNM - Error multiplier
FS - The full scale of the meter
ST - Measurement status, 1-in service, 0-out of service
RTU - Index of the RTU where this measurement is assigned

Reactive Flow Measurement Data
==========

Similar data structure as that of the active flow measurement data.

Active Injection Measurement Data
==========

```
Active injection measurement data records, terminated by a record with a
bus number of zero.

I,SNM,FS,ST,RTU

I     - Bus number (1 to 29997)
SNM   - Error multiplier
FS    - The full scale of the meter
ST    - Measurement status, 1-in service, 0-out of service
RTU   - Index of the RTU where this measurement is assigned

Similar data records are assumed for reactive flow and injection
measurements.
```

Reactive Injection Measurement Data
==========

```
Similar data structure as that of the active injection measurement data.
```

The error multiplier variable may have one of the following values:

- $SNM = 0$: Load flow (exact) value is used (no error is added)
- $|SNM| < 1$: Predefined measurement value ($= SNM * 100$) is used
- $|SNM| = 1$: Gaussian random error is added at load flow value
- $|SNM| > 1$: Gross error ($= SNM * \sigma$) is added at load flow value, where σ is the measurement standard deviation.

All measurement values or errors are in per unit. Multiplier SNM is always positive for voltage measurements.

APPENDIX B. Rhodes distribution network

The Rhodes distribution system (Figure 75) has 47 MV distribution lines at 15 kV and 20 kV voltage levels and a HV network at 150 kV and 66 kV. There is a number of PVs and 4 Wind Farms. In SuSTAINABLE project, the two 20 kV distribution feeders R-220 (Figure 77) and R-260 (Figure 78), originating from the substation of Gennadiou (Figure 76), will be simulated.

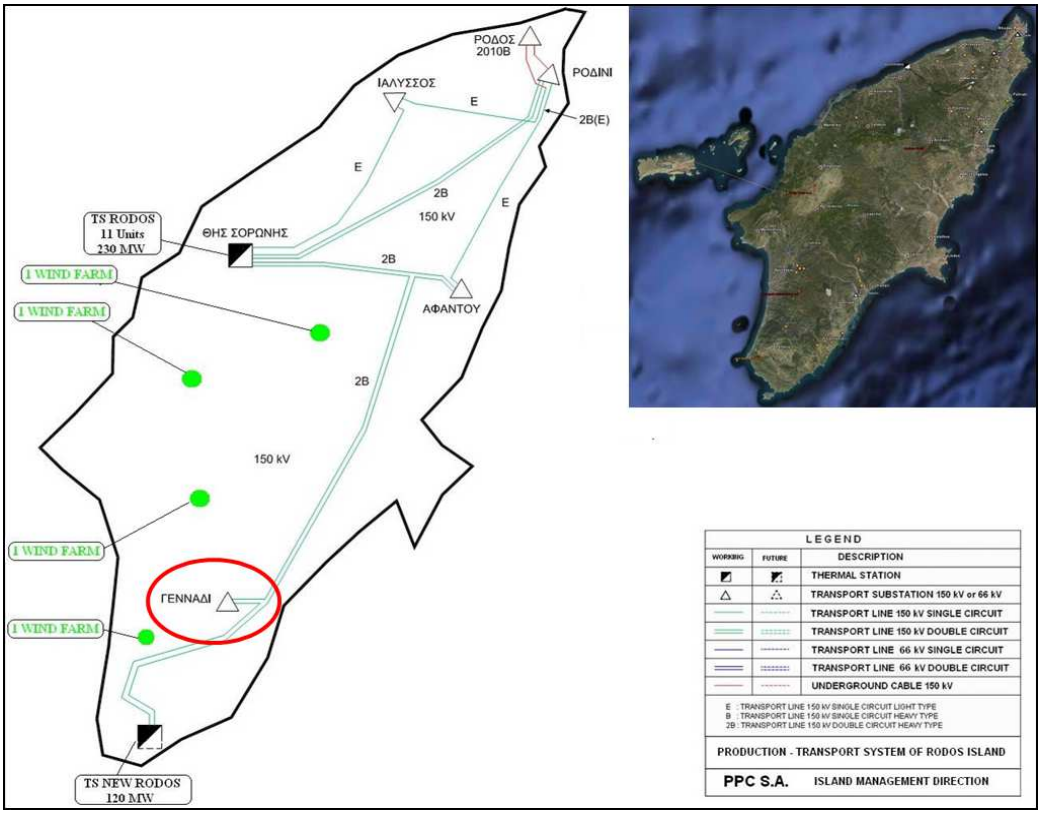

Figure 75 - Production and Transmission System of Rhodes

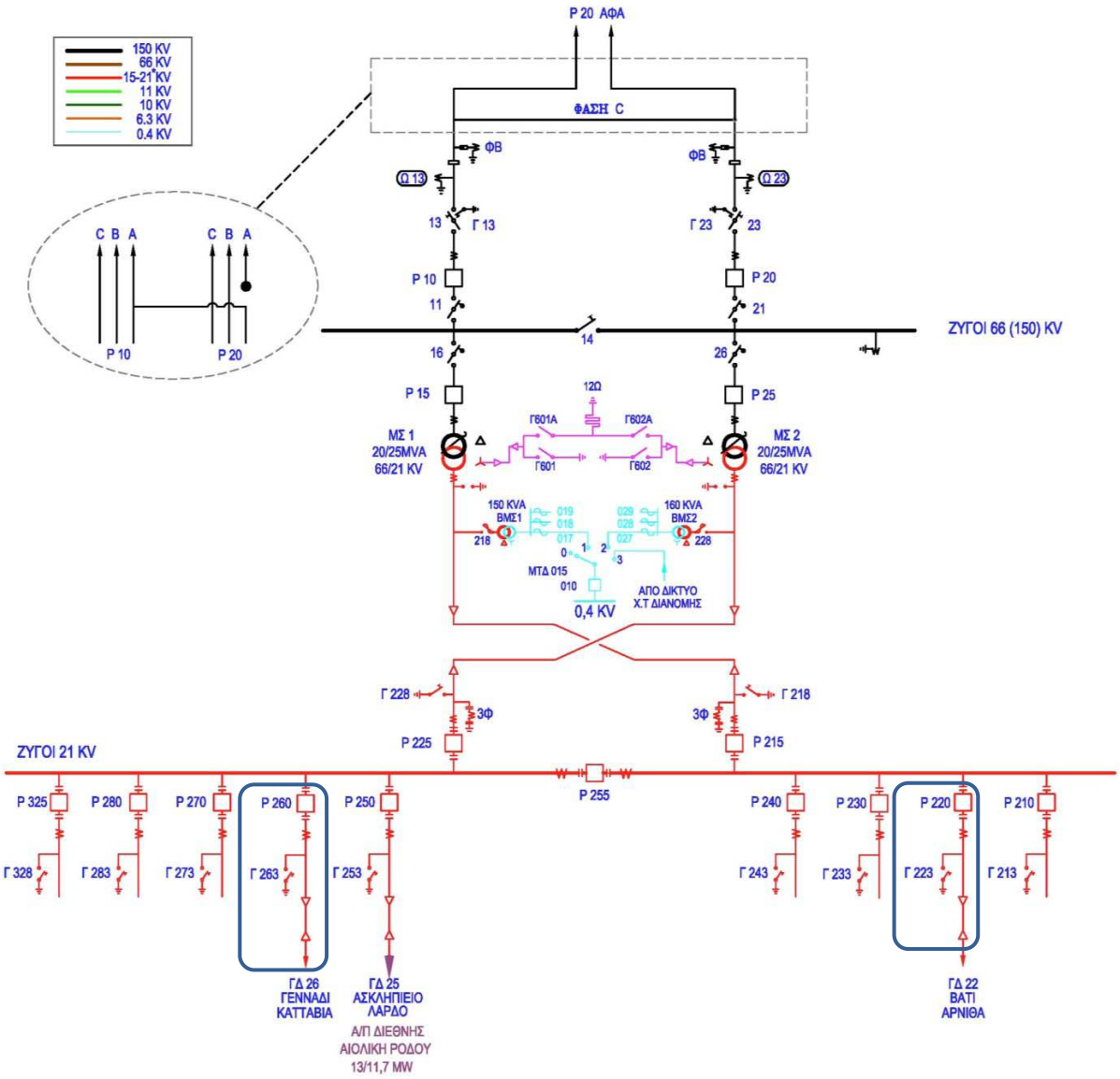

Figure 76 - Substation Gennadiou

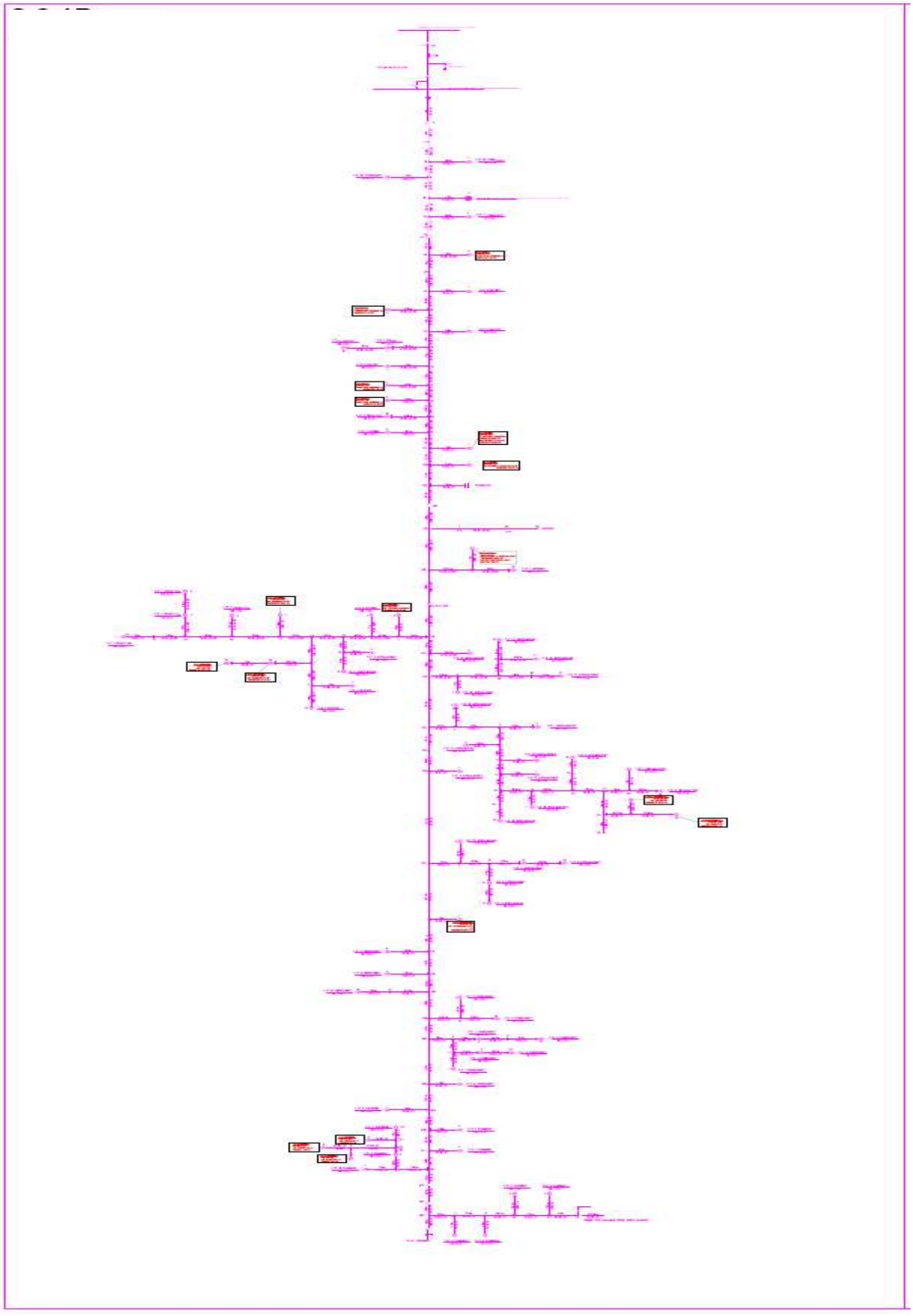

Figure 77 - Feeder R-220

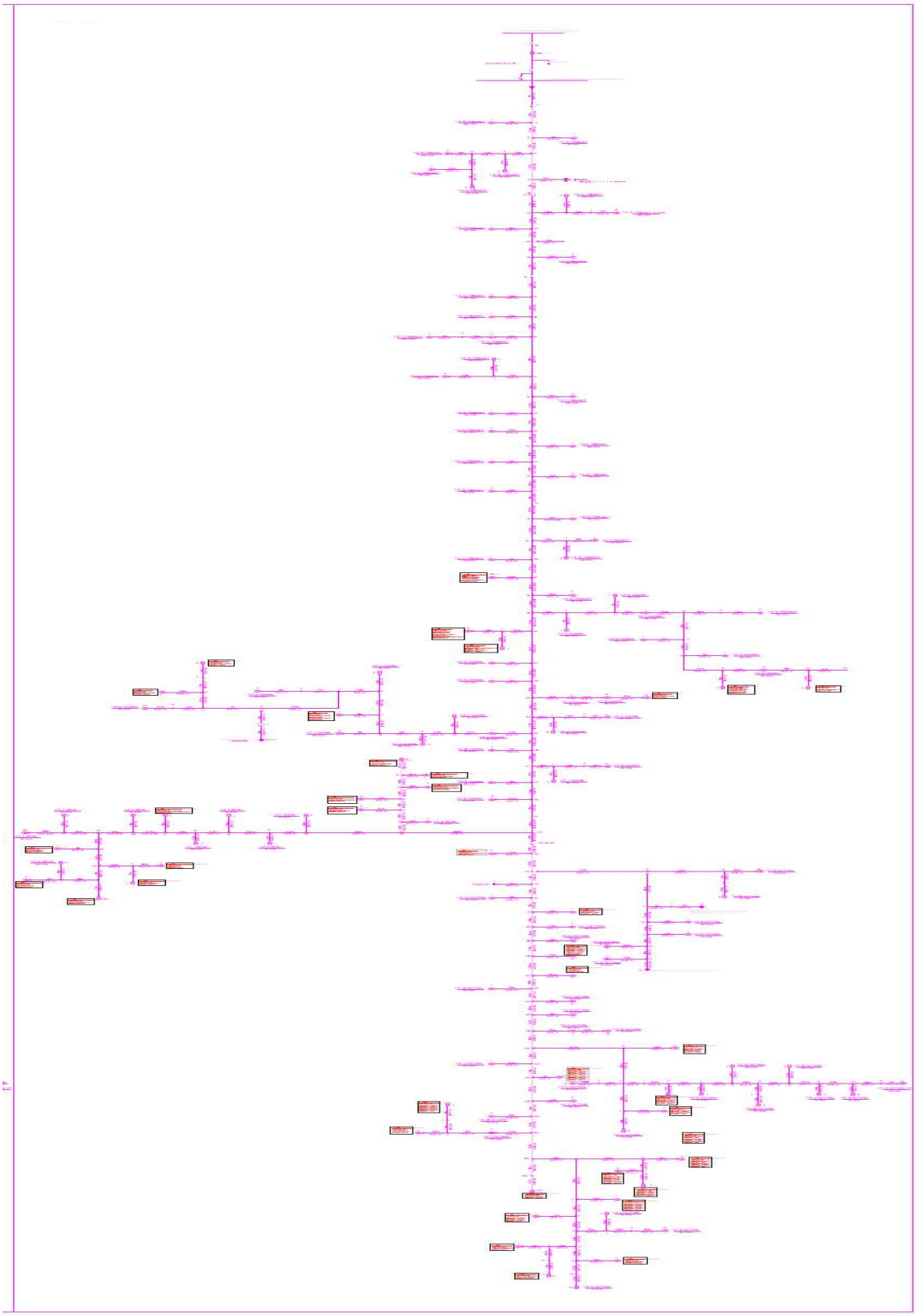

Figure 78 - Feeder R-260

Node 29997, to which this MV distribution network is connected, is represented by an infinite bus and considered as the global reference (slack) bus. A set of 53 and 84 MV/LV transformers are supplied through the two radial feeders R220 and R260 respectively. The simulated subnetwork includes **374** nodes – **19** DG nodes (2 WF and 17 PV nodes), **53** PQ nodes, and **68** ZI nodes at feeder R220 and **35** DG nodes (all PV nodes), **84** PQ nodes, **114** ZI nodes at feeder R260 – and **373** overhead lines. The per unit network parameters are calculated using a base power of **5 MVA** and a base voltage of **21 kV**.

Table 29, Table 30, Table 31 and Table 32 show the apparent power at the PQ nodes of feeder R220 and R260 respectively. A positive (negative) value means that a MV/LV transformer (standard induction generator) is connected at this node. A zero value means that neither generation nor load is connected at this node (zero injection node). A capacitor bank of 2.0 and 1.5 MVAr is connected at node 15 and 231 respectively.

Table 29 - Nominal apparent power at load and generation nodes of feeder R220

Bus	Type	kVA	Bus	Type	kVA
121	WF	-1000	**41**	PQ	100
122	WF	-1000	**44**	PQ	50
106	PV	-100	**45**	PQ	800
108	PV	-100	**48**	PQ	100
112	PV	-100	**51**	PQ	100
114	PV	-100	**54**	PQ	50
118	PV	-100	**56**	PQ	50
120	PV	-100	**58**	PQ	50
123	PV	-100	**59**	PQ	50
125	PV	-100	**60**	PQ	25
127	PV	-100	**61**	PQ	150
128	PV	-100	**63**	PQ	160
130	PV	-100	**66**	PQ	50
133	PV	-100	**68**	PQ	50
134	PV	-100	**69**	PQ	50
136	PV	-100	**70**	PQ	150
138	PV	-100	**71**	PQ	150
139	PV	-100	**72**	PQ	150
140	PV	-100	**74**	PQ	100
4	PQ	250	**76**	PQ	100
6	PQ	50	**79**	PQ	100
8	PQ	600	**81**	PQ	100
10	PQ	50	**83**	PQ	100
15	PQ	N/A	**84**	PQ	50
17	PQ	160	**85**	PQ	75
19	PQ	160	**87**	PQ	25
21	PQ	50	**89**	PQ	50
24	PQ	100	**91**	PQ	50
28	PQ	50	**93**	PQ	100
29	PQ	160	**94**	PQ	160
32	PQ	100	**96**	PQ	100
33	PQ	75	**99**	PQ	50
35	PQ	100	**102**	PQ	50
37	PQ	50	**104**	PQ	100
38	PQ	100	**110**	PQ	100
39	PQ	50	**116**	PQ	100

Table 30 - Zero injection nodes of feeder R220

Bus	Type	kVA	Bus	Type	kVA
1	PQ	0	**64**	PQ	0
2	PQ	0	**65**	PQ	0
3	PQ	0	**67**	PQ	0
5	PQ	0	**73**	PQ	0
7	PQ	0	**75**	PQ	0
9	PQ	0	**77**	PQ	0
11	PQ	0	**78**	PQ	0
12	PQ	0	**80**	PQ	0
13	PQ	0	**82**	PQ	0
14	PQ	0	**86**	PQ	0
16	PQ	0	**88**	PQ	0
18	PQ	0	**90**	PQ	0
20	PQ	0	**92**	PQ	0
22	PQ	0	**95**	PQ	0
23	PQ	0	**97**	PQ	0
25	PQ	0	**98**	PQ	0
26	PQ	0	**100**	PQ	0
27	PQ	0	**101**	PQ	0
30	PQ	0	**103**	PQ	0
31	PQ	0	**105**	PQ	0
34	PQ	0	**107**	PQ	0
36	PQ	0	**109**	PQ	0
40	PQ	0	**111**	PQ	0
42	PQ	0	**113**	PQ	0
43	PQ	0	**115**	PQ	0
46	PQ	0	**117**	PQ	0
47	PQ	0	**119**	PQ	0
49	PQ	0	**124**	PQ	0
50	PQ	0	**126**	PQ	0
52	PQ	0	**129**	PQ	0
53	PQ	0	**131**	PQ	0
55	PQ	0	**132**	PQ	0
57	PQ	0	**135**	PQ	0
62	PQ	0	**137**	PQ	0

Table 31 - Nominal apparent power at load and generation nodes of feeder R260

Bus	Type	kVA	Bus	Type	kVA
287	PV	-100	**216**	PQ	50
311	PV	-100	**218**	PQ	100
326	PV	-100	**220**	PQ	160
340	PV	-100	**222**	PQ	160
361	PV	-50	**224**	PQ	250
362	PV	-100	**226**	PQ	100
374	PV	-250	**227**	PQ	250
376	PV	-250	**229**	PQ	100
377	PV	-100	**231**	PQ	N/A
380	PV	-400	**233**	PQ	100
381	PV	-250	**235**	PQ	50
382	PV	-100	**237**	PQ	100
384	PV	-250	**239**	PQ	100
386	PV	-100	**241**	PQ	100
391	PV	-100	**243**	PQ	50
393	PV	-100	**245**	PQ	50
395	PV	-100	**248**	PQ	50
397	PV	-100	**249**	PQ	100
398	PV	-100	**251**	PQ	50
400	PV	-100	**253**	PQ	50
403	PV	-100	**256**	PQ	100
406	PV	-100	**258**	PQ	100
407	PV	-100	**259**	PQ	100
410	PV	-100	**261**	PQ	100
412	PV	-100	**263**	PQ	100
414	PV	-250	**265**	PQ	100
416	PV	-100	**266**	PQ	100
420	PV	-100	**268**	PQ	50
422	PV	-160	**270**	PQ	50
423	PV	-100	**272**	PQ	50
425	PV	-100	**273**	PQ	100
427	PV	-100	**275**	PQ	50
430	PV	-100	**277**	PQ	50
431	PV	-160	**279**	PQ	50
433	PV	-160	**281**	PQ	100
204	PQ	160	**283**	PQ	50
207	PQ	50	**285**	PQ	100
211	PQ	100	**288**	PQ	100
212	PQ	100	**291**	PQ	160
213	PQ	250	**292**	PQ	100

Table 32 - Nominal apparent power at load and generation nodes of feeder R260

Bus	Type	kVA	Bus	Type	kVA
294	PQ	50	**337**	PQ	50
297	PQ	25	**342**	PQ	50
299	PQ	50	**344**	PQ	160
301	PQ	50	**346**	PQ	50
303	PQ	100	**347**	PQ	100
305	PQ	25	**349**	PQ	50
307	PQ	50	**351**	PQ	50
308	PQ	50	**353**	PQ	50
314	PQ	50	**355**	PQ	50
316	PQ	400	**356**	PQ	160
318	PQ	50	**358**	PQ	160
320	PQ	50	**364**	PQ	50
322	PQ	50	**366**	PQ	50
324	PQ	734	**368**	PQ	50
325	PQ	50	**369**	PQ	160
328	PQ	100	**371**	PQ	50
330	PQ	50	**389**	PQ	100
332	PQ	50	**411**	PQ	100
334	PQ	50	**418**	PQ	100
336	PQ	100			

Table 33 - Zero injection nodes of feeder R260

201	PQ	0	**232**	PQ	0
202	PQ	0	**234**	PQ	0
203	PQ	0	**236**	PQ	0
205	PQ	0	**238**	PQ	0
206	PQ	0	**240**	PQ	0
208	PQ	0	**242**	PQ	0
209	PQ	0	**244**	PQ	0
210	PQ	0	**246**	PQ	0
214	PQ	0	**247**	PQ	0
215	PQ	0	**250**	PQ	0
217	PQ	0	**252**	PQ	0
219	PQ	0	**254**	PQ	0
221	PQ	0	**255**	PQ	0
223	PQ	0	**257**	PQ	0
225	PQ	0	**260**	PQ	0
228	PQ	0	**262**	PQ	0
230	PQ	0	**264**	PQ	0

Table 34 - Zero injection nodes of feeder R260

Bus	Type	kVA	Bus	Type	kVA
267	PQ	0	**352**	PQ	0
269	PQ	0	**354**	PQ	0
271	PQ	0	**357**	PQ	0
274	PQ	0	**359**	PQ	0
276	PQ	0	**360**	PQ	0
278	PQ	0	**363**	PQ	0
280	PQ	0	**365**	PQ	0
282	PQ	0	**367**	PQ	0
284	PQ	0	**370**	PQ	0
286	PQ	0	**372**	PQ	0
289	PQ	0	**373**	PQ	0
290	PQ	0	**375**	PQ	0
293	PQ	0	**378**	PQ	0
295	PQ	0	**379**	PQ	0
296	PQ	0	**383**	PQ	0
298	PQ	0	**385**	PQ	0
300	PQ	0	**387**	PQ	0
302	PQ	0	**388**	PQ	0
304	PQ	0	**390**	PQ	0
306	PQ	0	**392**	PQ	0
309	PQ	0	**394**	PQ	0
310	PQ	0	**396**	PQ	0
312	PQ	0	**399**	PQ	0
313	PQ	0	**401**	PQ	0
315	PQ	0	**402**	PQ	0
317	PQ	0	**404**	PQ	0
319	PQ	0	**405**	PQ	0
321	PQ	0	**408**	PQ	0
323	PQ	0	**409**	PQ	0
327	PQ	0	**413**	PQ	0
329	PQ	0	**415**	PQ	0
331	PQ	0	**417**	PQ	0
333	PQ	0	**419**	PQ	0
335	PQ	0	**421**	PQ	0
338	PQ	0	**424**	PQ	0
339	PQ	0	**426**	PQ	0
341	PQ	0	**428**	PQ	0
343	PQ	0	**429**	PQ	0
345	PQ	0	**432**	PQ	0
348	PQ	0			

Table 35 shows the various types of single circuit overhead cables and their associated electrical parameters.

Table 35 - Types and electric parameters of overhead cables

	R (ohm/km)	X (ohm/km)	C (nF/km)	B (mho/km)
AAAC-35	1.071	0.393	9.364	0.000002941787
ACSR-16	1.268	0.422	9.248	0.000002905345
ACSR-35	0.576	0.397	9.896	0.000003108920
ACSR-95 (single)	0.215	0.334	10.890	0.000003421194
CU-16	1.274	0.417	8.802	0.000002765230
CU-35	0.596	0.393	9.383	0.000002947756
CU-95 (single)	0.220	0.358	10.268	0.000003225787
XLPE-240	0.150	0.108	530.000	0.000166504411

The electric parameters for the overhead lines of feeders R220 and R260 are given in Table 36 to Table 45.

Table 36 - Line data for feeder R220 (on 5 MVA base)

From	To	Type	Length (m)	R (ohm)	X (ohm)	B (mho)	R (pu)	X (pu)	B (pu)
16	**17**	AAAC-35	88.0	0.0942	0.0346	0.0000002589	0.00118	0.00043	0.0000207102
98	**100**	AAAC-35	587.0	0.6287	0.2307	0.0000017268	0.00786	0.00288	0.0001381463
18	**19**	ACSR-16	175.5	0.2225	0.0741	0.0000005099	0.00278	0.00093	0.0000407910
23	**123**	ACSR-16	757.0	0.9599	0.3195	0.0000021993	0.01200	0.00399	0.0001759477
25	**124**	ACSR-16	2282.0	2.8936	0.9630	0.0000066300	0.03617	0.01204	0.0005303998
26	**27**	ACSR-16	1611.0	2.0427	0.6798	0.0000046805	0.02553	0.00850	0.0003744408
26	**30**	ACSR-16	1965.0	2.4916	0.8292	0.0000057090	0.03115	0.01037	0.0004567202
27	**28**	ACSR-16	507.0	0.6429	0.2140	0.0000014730	0.00804	0.00267	0.0001178408
27	**29**	ACSR-16	97.0	0.1230	0.0409	0.0000002818	0.00154	0.00051	0.0000225455
30	**129**	ACSR-16	1151.0	1.4595	0.4857	0.0000033441	0.01824	0.00607	0.0002675242
31	**32**	ACSR-16	25.0	0.0317	0.0106	0.0000000726	0.00040	0.00013	0.0000058107
31	**33**	ACSR-16	106.0	0.1344	0.0447	0.0000003080	0.00168	0.00056	0.0000246373
34	**35**	ACSR-16	757.0	0.9599	0.3195	0.0000021993	0.01200	0.00399	0.0001759477
34	**36**	ACSR-16	308.0	0.3905	0.1300	0.0000008948	0.00488	0.00162	0.0000715877
36	**37**	ACSR-16	196.0	0.2485	0.0827	0.0000005694	0.00311	0.00103	0.0000455558
36	**39**	ACSR-16	216.5	0.2745	0.0914	0.0000006290	0.00343	0.00114	0.0000503206
37	**38**	ACSR-16	516.0	0.6543	0.2178	0.0000014992	0.00818	0.00272	0.0001199326
43	**44**	ACSR-16	2443.0	3.0977	1.0309	0.0000070978	0.03872	0.01289	0.0005678206
73	**74**	ACSR-16	263.0	0.3335	0.1110	0.0000007641	0.00417	0.00139	0.0000611285
75	**76**	ACSR-16	115.0	0.1458	0.0485	0.0000003341	0.00182	0.00061	0.0000267292
77	**78**	ACSR-16	1396.5	1.7708	0.5893	0.0000040573	0.02213	0.00737	0.0003245851
78	**79**	ACSR-16	314.0	0.3982	0.1325	0.0000009123	0.00498	0.00166	0.0000729823
78	**80**	ACSR-16	100.0	0.1268	0.0422	0.0000002905	0.00159	0.00053	0.0000232428
80	**81**	ACSR-16	58.5	0.0742	0.0247	0.0000001700	0.00093	0.00031	0.0000135970
80	**82**	ACSR-16	236.0	0.2992	0.0996	0.0000006857	0.00374	0.00124	0.0000548529
82	**83**	ACSR-16	332.0	0.4210	0.1401	0.0000009646	0.00526	0.00175	0.0000771660
82	**85**	ACSR-16	31.0	0.0393	0.0131	0.0000000901	0.00049	0.00016	0.0000072053
83	**84**	ACSR-16	1313.5	1.6655	0.5543	0.0000038162	0.02082	0.00693	0.0003052936
86	**87**	ACSR-16	171.0	0.2168	0.0722	0.0000004968	0.00271	0.00090	0.0000397451
88	**89**	ACSR-16	133.0	0.1686	0.0561	0.0000003864	0.00211	0.00070	0.0000309129
90	**91**	ACSR-16	182.0	0.2308	0.0768	0.0000005288	0.00288	0.00096	0.0000423018
92	**93**	ACSR-16	508.0	0.6441	0.2144	0.0000014759	0.00805	0.00268	0.0001180732
93	**137**	ACSR-16	1541.0	1.9540	0.6503	0.0000044771	0.02442	0.00813	0.0003581709
95	**96**	ACSR-16	122.0	0.1547	0.0515	0.0000003545	0.00193	0.00064	0.0000283562
123	**24**	ACSR-16	757.0	0.9599	0.3195	0.0000021993	0.01200	0.00399	0.0001759477
124	**26**	ACSR-16	363.0	0.4603	0.1532	0.0000010546	0.00575	0.00191	0.0000843712
129	**34**	ACSR-16	268.0	0.3398	0.1131	0.0000007786	0.00425	0.00141	0.0000622906
137	**94**	ACSR-16	100.0	0.1268	0.0422	0.0000002905	0.00159	0.00053	0.0000232428
12	**106**	ACSR-35	99.0	0.0570	0.0393	0.0000003078	0.00071	0.00049	0.0000246226

Table 37 - Line data for feeder R220 (on 5 MVA base)

From	To	Type	Length (m)	R (ohm)	X (ohm)	B (mho)	R (pu)	X (pu)	B (pu)
20	**21**	ACSR-35	956.0	0.5507	0.3795	0.0000029721	0.00688	0.00474	0.0002377702
30	**126**	ACSR-35	106.0	0.0611	0.0421	0.0000003295	0.00076	0.00053	0.0000263636
42	**43**	ACSR-35	2687.0	1.5477	1.0667	0.0000083537	0.01935	0.01333	0.0006682935
43	**45**	ACSR-35	117.0	0.0674	0.0464	0.0000003637	0.00084	0.00058	0.0000290995
107	**108**	ACSR-35	255.0	0.1469	0.1012	0.0000007928	0.00184	0.00127	0.0000634220
109	**110**	ACSR-35	40.0	0.0230	0.0159	0.0000001244	0.00029	0.00020	0.0000099485
111	**112**	ACSR-35	460.0	0.2650	0.1826	0.0000014301	0.00331	0.00228	0.0001144083
126	**31**	ACSR-35	406.0	0.2339	0.1612	0.0000012622	0.00292	0.00201	0.0001009777
12	**13**	ACSR-95	91.0	0.0196	0.0304	0.0000003113	0.00024	0.00038	0.0000249063
13	**14**	ACSR-95	2021.0	0.4345	0.6750	0.0000069142	0.00543	0.00844	0.0005531387
14	**107**	ACSR-95	390.0	0.0839	0.1303	0.0000013343	0.00105	0.00163	0.0001067413
16	**18**	ACSR-95	96.0	0.0206	0.0321	0.0000003284	0.00026	0.00040	0.0000262748
18	**109**	ACSR-95	116.0	0.0249	0.0387	0.0000003969	0.00031	0.00048	0.0000317487
20	**115**	ACSR-95	908.0	0.1952	0.3033	0.0000031064	0.00244	0.00379	0.0002485156
22	**23**	ACSR-95	101.0	0.0217	0.0337	0.0000003455	0.00027	0.00042	0.0000276433
22	**121**	ACSR-95	2000.0	0.4300	0.6680	0.0000068424	0.00538	0.00835	0.0005473911
23	**25**	ACSR-95	323.0	0.0694	0.1079	0.0000011050	0.00087	0.00135	0.0000884037
25	**40**	ACSR-95	1167.0	0.2509	0.3898	0.0000039925	0.00314	0.00487	0.0003194027
40	**42**	ACSR-95	388.0	0.0834	0.1296	0.0000013274	0.00104	0.00162	0.0001061939
42	**46**	ACSR-95	203.0	0.0436	0.0678	0.0000006945	0.00055	0.00085	0.0000555602
46	**62**	ACSR-95	813.0	0.1748	0.2715	0.0000027814	0.00218	0.00339	0.0002225145
62	**64**	ACSR-95	1578.0	0.3393	0.5271	0.0000053986	0.00424	0.00659	0.0004318916
64	**65**	ACSR-95	373.0	0.0802	0.1246	0.0000012761	0.00100	0.00156	0.0001020884
73	**75**	ACSR-95	403.0	0.0866	0.1346	0.0000013787	0.00108	0.00168	0.0001102993
75	**77**	ACSR-95	2255.0	0.4848	0.7532	0.0000077148	0.00606	0.00941	0.0006171835
77	**86**	ACSR-95	135.0	0.0290	0.0451	0.0000004619	0.00036	0.00056	0.0000369489
86	**88**	ACSR-95	607.0	0.1305	0.2027	0.0000020767	0.00163	0.00253	0.0001661332
88	**90**	ACSR-95	2095.0	0.4504	0.6997	0.0000071674	0.00563	0.00875	0.0005733922
90	**92**	ACSR-95	210.0	0.0452	0.0701	0.0000007185	0.00056	0.00088	0.0000574761
92	**95**	ACSR-95	150.0	0.0323	0.0501	0.0000005132	0.00040	0.00063	0.0000410543
95	**97**	ACSR-95	903.0	0.1941	0.3016	0.0000030893	0.00243	0.00377	0.0002471471
97	**98**	ACSR-95	878.0	0.1888	0.2933	0.0000030038	0.00236	0.00367	0.0002403047
97	**105**	ACSR-95	73.0	0.0157	0.0244	0.0000002497	0.00020	0.00030	0.0000199798
107	**16**	ACSR-95	657.0	0.1413	0.2194	0.0000022477	0.00177	0.00274	0.0001798180
109	**111**	ACSR-95	782.0	0.1681	0.2612	0.0000026754	0.00210	0.00326	0.0002140299
111	**113**	ACSR-95	1105.0	0.2376	0.3691	0.0000037804	0.00297	0.00461	0.0003024336
113	**20**	ACSR-95	3168.0	0.6811	1.0581	0.0000108383	0.00851	0.01323	0.0008670675
115	**117**	ACSR-95	517.5	0.1113	0.1728	0.0000017705	0.00139	0.00216	0.0001416374
117	**119**	ACSR-95	12.5	0.0027	0.0042	0.0000000428	0.00003	0.00005	0.0000034212
119	**22**	ACSR-95	445.0	0.0957	0.1486	0.0000015224	0.00120	0.00186	0.0001217945

Table 38 - Line data for feeder R220 (on 5 MVA base)

From	To	Type	Length (m)	R (ohm)	X (ohm)	B (mho)	R (pu)	X (pu)	B (pu)
121	**122**	ACSR-95	400.0	0.0860	0.1336	0.0000013685	0.00108	0.00167	0.0001094782
14	**15**	CU-16	82.0	0.1045	0.0342	0.0000002267	0.00131	0.00043	0.0000181399
40	**41**	CU-16	257.0	0.3274	0.1072	0.0000007107	0.00409	0.00134	0.0000568531
49	**50**	CU-16	347.0	0.4421	0.1447	0.0000009595	0.00553	0.00181	0.0000767628
50	**51**	CU-16	342.5	0.4363	0.1428	0.0000009471	0.00545	0.00179	0.0000757673
50	**52**	CU-16	1868.0	2.3798	0.7790	0.0000051654	0.02975	0.00974	0.0004132359
52	**53**	CU-16	3373.0	4.2972	1.4065	0.0000093271	0.05372	0.01758	0.0007461696
52	**60**	CU-16	121.0	0.1542	0.0505	0.0000003346	0.00193	0.00063	0.0000267674
53	**54**	CU-16	1470.0	1.8728	0.6130	0.0000040649	0.02341	0.00766	0.0003251910
53	**55**	CU-16	140.0	0.1784	0.0584	0.0000003871	0.00223	0.00073	0.0000309706
57	**58**	CU-16	9.0	0.0115	0.0038	0.0000000249	0.00014	0.00005	0.0000019910
57	**59**	CU-16	544.0	0.6931	0.2268	0.0000015043	0.00866	0.00284	0.0001203428
62	**63**	CU-16	91.0	0.1159	0.0379	0.0000002516	0.00145	0.00047	0.0000201309
65	**66**	CU-16	369.0	0.4701	0.1539	0.0000010204	0.00588	0.00192	0.0000816296
65	**67**	CU-16	685.0	0.8727	0.2856	0.0000018942	0.01091	0.00357	0.0001515346
67	**68**	CU-16	663.0	0.8447	0.2765	0.0000018333	0.01056	0.00346	0.0001466678
67	**70**	CU-16	303.0	0.3860	0.1264	0.0000008379	0.00483	0.00158	0.0000670292
68	**69**	CU-16	1192.0	1.5186	0.4971	0.0000032962	0.01898	0.00621	0.0002636923
70	**71**	CU-16	1258.0	1.6027	0.5246	0.0000034787	0.02003	0.00656	0.0002782927
71	**72**	CU-16	701.0	0.8931	0.2923	0.0000019384	0.01116	0.00365	0.0001550741
98	**99**	CU-16	21.0	0.0268	0.0088	0.0000000581	0.00033	0.00011	0.0000046456
101	**102**	CU-16	58.0	0.0739	0.0242	0.0000001604	0.00092	0.00030	0.0000128307
103	**104**	CU-16	153.0	0.1949	0.0638	0.0000004231	0.00244	0.00080	0.0000338464
3	**4**	CU-35	382.0	0.2277	0.1501	0.0000011260	0.00285	0.00188	0.0000900834
5	**6**	CU-35	15.0	0.0089	0.0059	0.0000000442	0.00011	0.00007	0.0000035373
7	**8**	CU-35	111.0	0.0662	0.0436	0.0000003272	0.00083	0.00055	0.0000261761
9	**10**	CU-35	280.0	0.1669	0.1100	0.0000008254	0.00209	0.00138	0.0000660297
46	**47**	CU-35	218.0	0.1299	0.0857	0.0000006426	0.00162	0.00107	0.0000514089
47	**48**	CU-35	91.0	0.0542	0.0358	0.0000002682	0.00068	0.00045	0.0000214597
47	**49**	CU-35	102.0	0.0608	0.0401	0.0000003007	0.00076	0.00050	0.0000240537
49	**61**	CU-35	226.5	0.1350	0.0890	0.0000006677	0.00169	0.00111	0.0000534133
55	**56**	CU-35	46.0	0.0274	0.0181	0.0000001356	0.00034	0.00023	0.0000108477
55	**131**	CU-35	1159.0	0.6908	0.4555	0.0000034164	0.00863	0.00569	0.0002733160
100	**101**	CU-35	150.0	0.0894	0.0590	0.0000004422	0.00112	0.00074	0.0000353731
101	**103**	CU-35	2606.0	1.5532	1.0242	0.0000076819	0.01941	0.01280	0.0006145483
113	**114**	CU-35	128.0	0.0763	0.0503	0.0000003773	0.00095	0.00063	0.0000301850
115	**116**	CU-35	154.0	0.0918	0.0605	0.0000004540	0.00115	0.00076	0.0000363164
117	**118**	CU-35	11.0	0.0066	0.0043	0.0000000324	0.00008	0.00005	0.0000025940
119	**120**	CU-35	64.0	0.0381	0.0252	0.0000001887	0.00048	0.00031	0.0000150925

Table 39 - Line data for feeder R220 (on 5 MVA base)

From	To	Type	Length (m)	R (ohm)	X (ohm)	B (mho)	R (pu)	X (pu)	B (pu)
124	**125**	CU-35	570.0	0.3397	0.2240	0.0000016802	0.00425	0.00280	0.0001344177
126	**127**	CU-35	2061.5	1.2287	0.8102	0.0000060768	0.01536	0.01013	0.0004861440
127	**128**	CU-35	10.0	0.0060	0.0039	0.0000000295	0.00007	0.00005	0.0000023582
129	**130**	CU-35	366.0	0.2181	0.1438	0.0000010789	0.00273	0.00180	0.0000863103
131	**57**	CU-35	86.0	0.0513	0.0338	0.0000002535	0.00064	0.00042	0.0000202806
132	**133**	CU-35	14.0	0.0083	0.0055	0.0000000413	0.00010	0.00007	0.0000033015
132	**134**	CU-35	1238.0	0.7378	0.4865	0.0000036493	0.00922	0.00608	0.0002919458
135	**136**	CU-35	455.0	0.2712	0.1788	0.0000013412	0.00339	0.00224	0.0001072983
137	**138**	CU-35	30.0	0.0179	0.0118	0.0000000884	0.00022	0.00015	0.0000070746
137	**139**	CU-35	378.0	0.2253	0.1486	0.0000011143	0.00282	0.00186	0.0000891402
139	**140**	CU-35	350.0	0.2086	0.1376	0.0000010317	0.00261	0.00172	0.0000825372
1	**2**	CU-95	37.0	0.0081	0.0132	0.0000001194	0.00010	0.00017	0.0000095483
2	**3**	CU-95	340.0	0.0748	0.1217	0.0000010968	0.00094	0.00152	0.0000877414
3	**5**	CU-95	126.0	0.0277	0.0451	0.0000004064	0.00035	0.00056	0.0000325159
5	**7**	CU-95	465.0	0.1023	0.1665	0.0000015000	0.00128	0.00208	0.0001199993
7	**9**	CU-95	304.0	0.0669	0.1088	0.0000009806	0.00084	0.00136	0.0000784511
9	**11**	CU-95	256.0	0.0563	0.0916	0.0000008258	0.00070	0.00115	0.0000660641
11	**12**	CU-95	174.0	0.0383	0.0623	0.0000005613	0.00048	0.00078	0.0000449030
135	**73**	CU-95	854.0	0.1879	0.3057	0.0000027548	0.00235	0.00382	0.0002203858
131	**132**	CU-95	2148.0	0.4726	0.7690	0.0000069290	0.00591	0.00961	0.0005543193
64	**135**	CU-95	6257.0	1.3765	2.2400	0.0000201838	0.01721	0.02800	0.0016147001
29997	**1**	XLPE-240	27.0	0.0041	0.0292	0.0000044956	0.00005	0.00036	0.0003596495

Table 40 - Line data for feeder R260 (on 5 MVA base)

From	To	Type	Length (m)	R (ohm)	X (ohm)	B (mho)	R (pu)	X (pu)	B (pu)
254	**255**	AAAC-35	100.0	0.1071	0.0393	0.0000002942	0.00134	0.00049	0.0000235343
255	**256**	AAAC-35	94.0	0.1007	0.0369	0.0000002765	0.00126	0.00046	0.0000221222
255	**257**	AAAC-35	320.0	0.3427	0.1258	0.0000009414	0.00428	0.00157	0.0000753098
257	**258**	AAAC-35	8.0	0.0086	0.0031	0.0000000235	0.00011	0.00004	0.0000018827
257	**259**	AAAC-35	247.0	0.2645	0.0971	0.0000007266	0.00331	0.00121	0.0000581297
259	**260**	AAAC-35	446.0	0.4777	0.1753	0.0000013120	0.00597	0.00219	0.0001049630
260	**262**	AAAC-35	377.0	0.4038	0.1482	0.0000011091	0.00505	0.00185	0.0000887243
262	**264**	AAAC-35	87.0	0.0932	0.0342	0.0000002559	0.00116	0.00043	0.0000204748
296	**297**	AAAC-35	48.0	0.0514	0.0189	0.0000001412	0.00064	0.00024	0.0000112965
300	**301**	AAAC-35	376.0	0.4027	0.1478	0.0000011061	0.00503	0.00185	0.0000884890
290	**291**	ACSR-16	157.5	0.1997	0.0665	0.0000004576	0.00250	0.00083	0.0000366073
296	**298**	ACSR-16	698.0	0.8851	0.2946	0.0000020279	0.01106	0.00368	0.0001622345
298	**299**	ACSR-16	25.0	0.0317	0.0106	0.0000000726	0.00040	0.00013	0.0000058107
298	**300**	ACSR-16	1318.0	1.6712	0.5562	0.0000038292	0.02089	0.00695	0.0003063396
300	**302**	ACSR-16	495.0	0.6277	0.2089	0.0000014381	0.00785	0.00261	0.0001150517
302	**303**	ACSR-16	218.0	0.2764	0.0920	0.0000006334	0.00346	0.00115	0.0000506692
304	**305**	ACSR-16	110.0	0.1395	0.0464	0.0000003196	0.00174	0.00058	0.0000255670
304	**401**	ACSR-16	192.0	0.2435	0.0810	0.0000005578	0.00304	0.00101	0.0000446261
306	**307**	ACSR-16	865.0	1.0968	0.3650	0.0000025131	0.01371	0.00456	0.0002010499
401	**306**	ACSR-16	981.0	1.2439	0.4140	0.0000028501	0.01555	0.00517	0.0002280115
250	**373**	ACSR-35	117.0	0.1253	0.0460	0.0000003442	0.00157	0.00057	0.0000275351
252	**254**	ACSR-35	466.0	0.4991	0.1831	0.0000013709	0.00624	0.00229	0.0001096698
254	**378**	ACSR-35	241.0	0.2581	0.0947	0.0000007090	0.00323	0.00118	0.0000567177
267	**268**	ACSR-35	28.0	0.0300	0.0110	0.0000000824	0.00037	0.00014	0.0000065896
267	**269**	ACSR-35	384.0	0.4113	0.1509	0.0000011296	0.00514	0.00189	0.0000903717
269	**270**	ACSR-35	41.0	0.0439	0.0161	0.0000001206	0.00055	0.00020	0.0000096491
269	**271**	ACSR-35	1007.5	1.0790	0.3959	0.0000029639	0.01349	0.00495	0.0002371081
271	**274**	ACSR-35	523.0	0.5601	0.2055	0.0000015386	0.00700	0.00257	0.0001230844
274	**276**	ACSR-35	626.0	0.6704	0.2460	0.0000018416	0.00838	0.00308	0.0001473247
276	**289**	ACSR-35	626.0	0.6704	0.2460	0.0000018416	0.00838	0.00308	0.0001473247
289	**290**	ACSR-35	197.0	0.2110	0.0774	0.0000005795	0.00264	0.00097	0.0000463626
289	**293**	ACSR-35	318.0	0.3406	0.1250	0.0000009355	0.00426	0.00156	0.0000748391
293	**295**	ACSR-35	564.0	0.6040	0.2217	0.0000016592	0.00755	0.00277	0.0001327334
295	**309**	ACSR-35	826.5	0.8852	0.3248	0.0000024314	0.01106	0.00406	0.0001945110
306	**308**	ACSR-35	252.0	0.2699	0.0990	0.0000007413	0.00337	0.00124	0.0000593064
373	**252**	ACSR-35	892.0	0.9553	0.3506	0.0000026241	0.01194	0.00438	0.0002099259
378	**267**	ACSR-35	414.0	0.4434	0.1627	0.0000012179	0.00554	0.00203	0.0000974320
221	**222**	CU-16	165.0	0.2102	0.0688	0.0000004563	0.00263	0.00086	0.0000365010
223	**224**	CU-16	284.0	0.3618	0.1184	0.0000007853	0.00452	0.00148	0.0000628260

Table 41 - Line data for feeder R260 (on 5 MVA base)

From	To	Type	Length (m)	R (ohm)	X (ohm)	B (mho)	R (pu)	X (pu)	B (pu)
225	**226**	CU-16	10.0	0.0127	0.0042	0.0000000277	0.00016	0.00005	0.0000022122
226	**227**	CU-16	182.0	0.2319	0.0759	0.0000005033	0.00290	0.00095	0.0000402617
264	**265**	CU-16	5.0	0.0064	0.0021	0.0000000138	0.00008	0.00003	0.0000011061
271	**272**	CU-16	365.0	0.4650	0.1522	0.0000010093	0.00581	0.00190	0.0000807447
272	**273**	CU-16	1008.0	1.2842	0.4203	0.0000027874	0.01605	0.00525	0.0002229881
274	**275**	CU-16	527.0	0.6714	0.2198	0.0000014573	0.00839	0.00275	0.0001165821
276	**277**	CU-16	220.0	0.2803	0.0917	0.0000006084	0.00350	0.00115	0.0000486680
277	**278**	CU-16	1197.0	1.5250	0.4991	0.0000033100	0.01906	0.00624	0.0002647984
278	**279**	CU-16	852.0	1.0854	0.3553	0.0000023560	0.01357	0.00444	0.0001884781
278	**280**	CU-16	91.0	0.1159	0.0379	0.0000002516	0.00145	0.00047	0.0000201309
280	**281**	CU-16	63.0	0.0803	0.0263	0.0000001742	0.00100	0.00033	0.0000139368
282	**283**	CU-16	83.0	0.1057	0.0346	0.0000002295	0.00132	0.00043	0.0000183611
282	**284**	CU-16	236.0	0.3007	0.0984	0.0000006526	0.00376	0.00123	0.0000522075
284	**285**	CU-16	80.0	0.1019	0.0334	0.0000002212	0.00127	0.00042	0.0000176975
293	**294**	CU-16	1436.0	1.8295	0.5988	0.0000039709	0.02287	0.00749	0.0003176696
327	**328**	CU-16	113.0	0.1440	0.0471	0.0000003125	0.00180	0.00059	0.0000249977
333	**334**	CU-16	58.0	0.0739	0.0242	0.0000001604	0.00092	0.00030	0.0000128307
335	**336**	CU-16	550.0	0.7007	0.2294	0.0000015209	0.00876	0.00287	0.0001216701
336	**337**	CU-16	699.0	0.8905	0.2915	0.0000019329	0.01113	0.00364	0.0001546317
359	**363**	CU-16	381.0	0.4854	0.1589	0.0000010536	0.00607	0.00199	0.0000842842
360	**426**	CU-16	119.0	0.1516	0.0496	0.0000003291	0.00190	0.00062	0.0000263250
363	**364**	CU-16	119.0	0.1516	0.0496	0.0000003291	0.00190	0.00062	0.0000263250
363	**365**	CU-16	1018.0	1.2969	0.4245	0.0000028150	0.01621	0.00531	0.0002252003
372	**326**	CU-16	115.0	0.1465	0.0480	0.0000003180	0.00183	0.00060	0.0000254401
203	**204**	CU-35	10.0	0.0060	0.0039	0.0000000295	0.00007	0.00005	0.0000023582
206	**207**	CU-35	10.0	0.0060	0.0039	0.0000000295	0.00007	0.00005	0.0000023582
208	**209**	CU-35	870.0	0.5185	0.3419	0.0000025645	0.00648	0.00427	0.0002051638
209	**210**	CU-35	467.0	0.2783	0.1835	0.0000013766	0.00348	0.00229	0.0001101282
209	**213**	CU-35	36.0	0.0215	0.0141	0.0000001061	0.00027	0.00018	0.0000084895
210	**211**	CU-35	261.0	0.1556	0.1026	0.0000007694	0.00194	0.00128	0.0000615492
210	**212**	CU-35	52.0	0.0310	0.0204	0.0000001533	0.00039	0.00026	0.0000122627
215	**216**	CU-35	243.0	0.1448	0.0955	0.0000007163	0.00181	0.00119	0.0000573044
217	**218**	CU-35	12.0	0.0072	0.0047	0.0000000354	0.00009	0.00006	0.0000028298
219	**220**	CU-35	72.0	0.0429	0.0283	0.0000002122	0.00054	0.00035	0.0000169791
247	**248**	CU-35	746.0	0.4446	0.2932	0.0000021990	0.00556	0.00366	0.0001759221
250	**251**	CU-35	55.0	0.0328	0.0216	0.0000001621	0.00041	0.00027	0.0000129701
252	**253**	CU-35	420.0	0.2503	0.1651	0.0000012381	0.00313	0.00206	0.0000990446
260	**261**	CU-35	215.0	0.1281	0.0845	0.0000006338	0.00160	0.00106	0.0000507014
262	**263**	CU-35	16.0	0.0095	0.0063	0.0000000472	0.00012	0.00008	0.0000037731
264	**375**	CU-35	274.0	0.1633	0.1077	0.0000008077	0.00204	0.00135	0.0000646148

Table 42 - Line data for feeder R260 (on 5 MVA base)

From	To	Type	Length (m)	R (ohm)	X (ohm)	B (mho)	R (pu)	X (pu)	B (pu)
266	**375**	CU-35	214.0	0.1275	0.0841	0.0000006308	0.00159	0.00105	0.0000504656
266	**377**	CU-35	339.0	0.2020	0.1332	0.0000009993	0.00253	0.00167	0.0000799432
273	**382**	CU-35	370.0	0.2205	0.1454	0.0000010907	0.00276	0.00182	0.0000872536
280	**383**	CU-35	334.0	0.1991	0.1313	0.0000009846	0.00249	0.00164	0.0000787641
284	**286**	CU-35	1371.0	0.8171	0.5388	0.0000040414	0.01021	0.00674	0.0003233099
286	**288**	CU-35	540.0	0.3218	0.2122	0.0000015918	0.00402	0.00265	0.0001273431
286	**385**	CU-35	752.0	0.4482	0.2955	0.0000022167	0.00560	0.00369	0.0001773370
290	**292**	CU-35	120.0	0.0715	0.0472	0.0000003537	0.00089	0.00059	0.0000282985
295	**387**	CU-35	784.0	0.4673	0.3081	0.0000023110	0.00584	0.00385	0.0001848833
302	**399**	CU-35	176.0	0.1049	0.0692	0.0000005188	0.00131	0.00086	0.0000415044
309	**310**	CU-35	1761.0	1.0496	0.6921	0.0000051910	0.01312	0.00865	0.0004152799
310	**311**	CU-35	25.0	0.0149	0.0098	0.0000000737	0.00019	0.00012	0.0000058955
310	**312**	CU-35	53.0	0.0316	0.0208	0.0000001562	0.00039	0.00026	0.0000124985
312	**313**	CU-35	1388.0	0.8272	0.5455	0.0000040915	0.01034	0.00682	0.0003273189
312	**370**	CU-35	104.0	0.0620	0.0409	0.0000003066	0.00077	0.00051	0.0000245253
313	**314**	CU-35	605.0	0.3606	0.2378	0.0000017834	0.00451	0.00297	0.0001426714
313	**315**	CU-35	295.0	0.1758	0.1159	0.0000008696	0.00220	0.00145	0.0000695671
315	**316**	CU-35	18.5	0.0110	0.0073	0.0000000545	0.00014	0.00009	0.0000043627
315	**317**	CU-35	200.0	0.1192	0.0786	0.0000005896	0.00149	0.00098	0.0000471641
317	**318**	CU-35	50.0	0.0298	0.0197	0.0000001474	0.00037	0.00025	0.0000117910
317	**319**	CU-35	704.0	0.4196	0.2767	0.0000020752	0.00524	0.00346	0.0001660176
319	**320**	CU-35	45.5	0.0271	0.0179	0.0000001341	0.00034	0.00022	0.0000107298
319	**321**	CU-35	260.0	0.1550	0.1022	0.0000007664	0.00194	0.00128	0.0000613133
321	**322**	CU-35	845.0	0.5036	0.3321	0.0000024909	0.00630	0.00415	0.0001992683
321	**323**	CU-35	178.0	0.1061	0.0700	0.0000005247	0.00133	0.00087	0.0000419761
323	**324**	CU-35	145.0	0.0864	0.0570	0.0000004274	0.00108	0.00071	0.0000341940
323	**325**	CU-35	520.0	0.3099	0.2044	0.0000015328	0.00387	0.00255	0.0001226267
327	**329**	CU-35	445.0	0.2652	0.1749	0.0000013118	0.00332	0.00219	0.0001049401
329	**330**	CU-35	109.0	0.0650	0.0428	0.0000003213	0.00081	0.00054	0.0000257044
329	**413**	CU-35	175.0	0.1043	0.0688	0.0000005159	0.00130	0.00086	0.0000412686
331	**332**	CU-35	91.0	0.0542	0.0358	0.0000002682	0.00068	0.00045	0.0000214597
331	**333**	CU-35	506.0	0.3016	0.1989	0.0000014916	0.00377	0.00249	0.0001193252
333	**335**	CU-35	396.0	0.2360	0.1556	0.0000011673	0.00295	0.00195	0.0000933849
335	**338**	CU-35	380.0	0.2265	0.1493	0.0000011201	0.00283	0.00187	0.0000896118
338	**339**	CU-35	1637.0	0.9757	0.6433	0.0000048255	0.01220	0.00804	0.0003860382
338	**348**	CU-35	288.0	0.1716	0.1132	0.0000008490	0.00215	0.00141	0.0000679163
339	**340**	CU-35	93.0	0.0554	0.0365	0.0000002741	0.00069	0.00046	0.0000219313
339	**341**	CU-35	300.0	0.1788	0.1179	0.0000008843	0.00224	0.00147	0.0000707462
341	**419**	CU-35	202.0	0.1204	0.0794	0.0000005954	0.00150	0.00099	0.0000476357
341	**421**	CU-35	303.0	0.1806	0.1191	0.0000008932	0.00226	0.00149	0.0000714536

Table 43 - Line data for feeder R260 (on 5 MVA base)

From	To	Type	Length (m)	R (ohm)	X (ohm)	B (mho)	R (pu)	X (pu)	B (pu)
343	**344**	CU-35	458.0	0.2730	0.1800	0.0000013501	0.00341	0.00225	0.0001080058
343	**345**	CU-35	823.5	0.4908	0.3236	0.0000024275	0.00614	0.00405	0.0001941982
345	**346**	CU-35	694.0	0.4136	0.2727	0.0000020457	0.00517	0.00341	0.0001636594
345	**347**	CU-35	1647.0	0.9816	0.6473	0.0000048550	0.01227	0.00809	0.0003883964
348	**349**	CU-35	100.0	0.0596	0.0393	0.0000002948	0.00075	0.00049	0.0000235821
348	**423**	CU-35	100.0	0.0596	0.0393	0.0000002948	0.00075	0.00049	0.0000235821
350	**351**	CU-35	420.0	0.2503	0.1651	0.0000012381	0.00313	0.00206	0.0000990446
350	**352**	CU-35	96.0	0.0572	0.0377	0.0000002830	0.00072	0.00047	0.0000226388
352	**353**	CU-35	59.0	0.0352	0.0232	0.0000001739	0.00044	0.00029	0.0000139134
352	**354**	CU-35	110.0	0.0656	0.0432	0.0000003243	0.00082	0.00054	0.0000259403
354	**355**	CU-35	417.0	0.2485	0.1639	0.0000012292	0.00311	0.00205	0.0000983372
354	**357**	CU-35	392.0	0.2336	0.1541	0.0000011555	0.00292	0.00193	0.0000924416
355	**424**	CU-35	90.0	0.0536	0.0354	0.0000002653	0.00067	0.00044	0.0000212238
357	**358**	CU-35	242.0	0.1442	0.0951	0.0000007134	0.00180	0.00119	0.0000570686
357	**359**	CU-35	100.0	0.0596	0.0393	0.0000002948	0.00075	0.00049	0.0000235821
359	**360**	CU-35	911.0	0.5430	0.3580	0.0000026854	0.00679	0.00448	0.0002148325
360	**361**	CU-35	91.0	0.0542	0.0358	0.0000002682	0.00068	0.00045	0.0000214597
365	**367**	CU-35	193.0	0.1150	0.0758	0.0000005689	0.00144	0.00095	0.0000455134
365	**428**	CU-35	193.0	0.1150	0.0758	0.0000005689	0.00144	0.00095	0.0000455134
367	**368**	CU-35	165.0	0.0983	0.0648	0.0000004864	0.00123	0.00081	0.0000389104
367	**369**	CU-35	1912.0	1.1396	0.7514	0.0000056361	0.01424	0.00939	0.0004508888
370	**371**	CU-35	50.0	0.0298	0.0197	0.0000001474	0.00037	0.00025	0.0000117910
370	**372**	CU-35	50.0	0.0298	0.0197	0.0000001474	0.00037	0.00025	0.0000117910
372	**327**	CU-35	657.0	0.3916	0.2582	0.0000019367	0.00489	0.00323	0.0001549341
373	**374**	CU-35	809.0	0.4822	0.3179	0.0000023847	0.00603	0.00397	0.0001907788
375	**376**	CU-35	95.0	0.0566	0.0373	0.0000002800	0.00071	0.00047	0.0000224029
378	**379**	CU-35	573.0	0.3415	0.2252	0.0000016891	0.00427	0.00281	0.0001351252
379	**380**	CU-35	98.0	0.0584	0.0385	0.0000002889	0.00073	0.00048	0.0000231104
379	**381**	CU-35	239.0	0.1424	0.0939	0.0000007045	0.00178	0.00117	0.0000563611
383	**282**	CU-35	321.0	0.1913	0.1262	0.0000009462	0.00239	0.00158	0.0000756984
383	**384**	CU-35	38.0	0.0226	0.0149	0.0000001120	0.00028	0.00019	0.0000089612
385	**287**	CU-35	32.0	0.0191	0.0126	0.0000000943	0.00024	0.00016	0.0000075463
385	**386**	CU-35	368.0	0.2193	0.1446	0.0000010848	0.00274	0.00181	0.0000867819
387	**296**	CU-35	3088.0	1.8404	1.2136	0.0000091027	0.02301	0.01517	0.0007282137
387	**388**	CU-35	432.0	0.2575	0.1698	0.0000012734	0.00322	0.00212	0.0001018745
388	**389**	CU-35	140.0	0.0834	0.0550	0.0000004127	0.00104	0.00069	0.0000330149
388	**390**	CU-35	329.0	0.1961	0.1293	0.0000009698	0.00245	0.00162	0.0000775849
390	**391**	CU-35	241.0	0.1436	0.0947	0.0000007104	0.00180	0.00118	0.0000568327
390	**392**	CU-35	82.0	0.0489	0.0322	0.0000002417	0.00061	0.00040	0.0000193373
392	**393**	CU-35	63.0	0.0375	0.0248	0.0000001857	0.00047	0.00031	0.0000148567

Table 44 - Line data for feeder R260 (on 5 MVA base)

From	To	Type	Length (m)	R (ohm)	X (ohm)	B (mho)	R (pu)	X (pu)	B (pu)
392	**394**	CU-35	250.0	0.1490	0.0983	0.0000007369	0.00186	0.00123	0.0000589551
394	**395**	CU-35	180.0	0.1073	0.0707	0.0000005306	0.00134	0.00088	0.0000424477
394	**396**	CU-35	270.0	0.1609	0.1061	0.0000007959	0.00201	0.00133	0.0000636715
396	**397**	CU-35	38.0	0.0226	0.0149	0.0000001120	0.00028	0.00019	0.0000089612
396	**398**	CU-35	211.0	0.1258	0.0829	0.0000006220	0.00157	0.00104	0.0000497581
399	**304**	CU-35	577.0	0.3439	0.2268	0.0000017009	0.00430	0.00283	0.0001360684
399	**400**	CU-35	291.0	0.1734	0.1144	0.0000008578	0.00217	0.00143	0.0000686238
401	**402**	CU-35	3837.0	2.2869	1.5079	0.0000113105	0.02859	0.01885	0.0009048433
402	**403**	CU-35	18.0	0.0107	0.0071	0.0000000531	0.00013	0.00009	0.0000042448
402	**404**	CU-35	445.0	0.2652	0.1749	0.0000013118	0.00332	0.00219	0.0001049401
404	**405**	CU-35	505.0	0.3010	0.1985	0.0000014886	0.00376	0.00248	0.0001190894
404	**408**	CU-35	78.0	0.0465	0.0307	0.0000002299	0.00058	0.00038	0.0000183940
405	**406**	CU-35	382.0	0.2277	0.1501	0.0000011260	0.00285	0.00188	0.0000900834
405	**407**	CU-35	75.0	0.0447	0.0295	0.0000002211	0.00056	0.00037	0.0000176865
408	**409**	CU-35	88.0	0.0524	0.0346	0.0000002594	0.00066	0.00043	0.0000207522
408	**412**	CU-35	23.0	0.0137	0.0090	0.0000000678	0.00017	0.00011	0.0000054239
409	**410**	CU-35	99.0	0.0590	0.0389	0.0000002918	0.00074	0.00049	0.0000233462
409	**411**	CU-35	108.0	0.0644	0.0424	0.0000003184	0.00080	0.00053	0.0000254686
413	**414**	CU-35	919.0	0.5477	0.3612	0.0000027090	0.00685	0.00451	0.0002167190
413	**415**	CU-35	2548.0	1.5186	1.0014	0.0000075109	0.01898	0.01252	0.0006008707
415	**416**	CU-35	594.0	0.3540	0.2334	0.0000017510	0.00443	0.00292	0.0001400774
415	**417**	CU-35	610.0	0.3636	0.2397	0.0000017981	0.00454	0.00300	0.0001438505
417	**331**	CU-35	100.0	0.0596	0.0393	0.0000002948	0.00075	0.00049	0.0000235821
417	**418**	CU-35	196.0	0.1168	0.0770	0.0000005778	0.00146	0.00096	0.0000462208
419	**342**	CU-35	396.0	0.2360	0.1556	0.0000011673	0.00295	0.00195	0.0000933849
419	**420**	CU-35	144.0	0.0858	0.0566	0.0000004245	0.00107	0.00071	0.0000339582
421	**343**	CU-35	2800.0	1.6688	1.1004	0.0000082537	0.02086	0.01376	0.0006602974
421	**422**	CU-35	19.0	0.0113	0.0075	0.0000000560	0.00014	0.00009	0.0000044806
423	**350**	CU-35	400.0	0.2384	0.1572	0.0000011791	0.00298	0.00197	0.0000943282
424	**356**	CU-35	405.0	0.2414	0.1592	0.0000011938	0.00302	0.00199	0.0000955073
424	**425**	CU-35	125.0	0.0745	0.0491	0.0000003685	0.00093	0.00061	0.0000294776
426	**362**	CU-35	946.0	0.5638	0.3718	0.0000027886	0.00705	0.00465	0.0002230862
426	**427**	CU-35	133.0	0.0793	0.0523	0.0000003921	0.00099	0.00065	0.0000313641
428	**429**	CU-35	195.0	0.1162	0.0766	0.0000005748	0.00145	0.00096	0.0000459850
428	**432**	CU-35	1368.0	0.8153	0.5376	0.0000040325	0.01019	0.00672	0.0003226025
429	**430**	CU-35	81.0	0.0483	0.0318	0.0000002388	0.00060	0.00040	0.0000191015
429	**431**	CU-35	163.0	0.0971	0.0641	0.0000004805	0.00121	0.00080	0.0000384387
432	**366**	CU-35	1300.0	0.7748	0.5109	0.0000038321	0.00969	0.00639	0.0003065667
432	**433**	CU-35	64.0	0.0381	0.0252	0.0000001887	0.00048	0.00031	0.0000150925
201	**202**	CU-95	17.0	0.0037	0.0061	0.0000000548	0.00005	0.00008	0.0000043871

Table 45 - Line data for feeder R260 (on 5 MVA base)

From	To	Type	Length (m)	R (ohm)	X (ohm)	B (mho)	R (pu)	X (pu)	B (pu)
202	**203**	CU-95	9.0	0.0020	0.0032	0.0000000290	0.00002	0.00004	0.0000023226
203	**205**	CU-95	10.0	0.0022	0.0036	0.0000000323	0.00003	0.00004	0.0000025806
205	**206**	CU-95	536.0	0.1179	0.1919	0.0000017290	0.00147	0.00240	0.0001383218
206	**208**	CU-95	57.0	0.0125	0.0204	0.0000001839	0.00016	0.00026	0.0000147096
208	**214**	CU-95	714.0	0.1571	0.2556	0.0000023032	0.00196	0.00320	0.0001842570
214	**215**	CU-95	15.0	0.0033	0.0054	0.0000000484	0.00004	0.00007	0.0000038709
215	**217**	CU-95	150.0	0.0330	0.0537	0.0000004839	0.00041	0.00067	0.0000387094
217	**219**	CU-95	87.0	0.0191	0.0311	0.0000002806	0.00024	0.00039	0.0000224515
219	**221**	CU-95	150.0	0.0330	0.0537	0.0000004839	0.00041	0.00067	0.0000387094
221	**223**	CU-95	108.0	0.0238	0.0387	0.0000003484	0.00030	0.00048	0.0000278708
223	**225**	CU-95	75.0	0.0165	0.0269	0.0000002419	0.00021	0.00034	0.0000193547
225	**228**	CU-95	150.0	0.0330	0.0537	0.0000004839	0.00041	0.00067	0.0000387094
228	**229**	CU-95	301.0	0.0662	0.1078	0.0000009710	0.00083	0.00135	0.0000776770
228	**230**	CU-95	150.0	0.0330	0.0537	0.0000004839	0.00041	0.00067	0.0000387094
230	**231**	CU-95	81.0	0.0178	0.0290	0.0000002613	0.00022	0.00036	0.0000209031
230	**232**	CU-95	139.0	0.0306	0.0498	0.0000004484	0.00038	0.00062	0.0000358708
232	**233**	CU-95	67.0	0.0147	0.0240	0.0000002161	0.00018	0.00030	0.0000172902
232	**234**	CU-95	154.0	0.0339	0.0551	0.0000004968	0.00042	0.00069	0.0000397417
234	**235**	CU-95	585.0	0.1287	0.2094	0.0000018871	0.00161	0.00262	0.0001509668
234	**236**	CU-95	105.0	0.0231	0.0376	0.0000003387	0.00029	0.00047	0.0000270966
236	**237**	CU-95	116.0	0.0255	0.0415	0.0000003742	0.00032	0.00052	0.0000299353
236	**238**	CU-95	703.0	0.1547	0.2517	0.0000022677	0.00193	0.00315	0.0001814183
238	**239**	CU-95	35.0	0.0077	0.0125	0.0000001129	0.00010	0.00016	0.0000090322
238	**240**	CU-95	412.0	0.0906	0.1475	0.0000013290	0.00113	0.00184	0.0001063220
240	**241**	CU-95	143.0	0.0315	0.0512	0.0000004613	0.00039	0.00064	0.0000369030
240	**242**	CU-95	203.5	0.0448	0.0729	0.0000006564	0.00056	0.00091	0.0000525158
242	**243**	CU-95	208.0	0.0458	0.0745	0.0000006710	0.00057	0.00093	0.0000536771
242	**244**	CU-95	494.5	0.1088	0.1770	0.0000015952	0.00136	0.00221	0.0001276121
244	**245**	CU-95	81.0	0.0178	0.0290	0.0000002613	0.00022	0.00036	0.0000209031
244	**246**	CU-95	186.0	0.0409	0.0666	0.0000006000	0.00051	0.00083	0.0000479997
246	**247**	CU-95	337.0	0.0741	0.1206	0.0000010871	0.00093	0.00151	0.0000869672
246	**250**	CU-95	96.0	0.0211	0.0344	0.0000003097	0.00026	0.00043	0.0000247740
247	**249**	CU-95	80.0	0.0176	0.0286	0.0000002581	0.00022	0.00036	0.0000206450
29997	**201**	XLPE-240	32.0	0.0048	0.0346	0.0000053281	0.00006	0.00043	0.0004262513

The load at each MV node is considered to be associated to the rated power of the connected MV/LV transformer. From this rule are excluded the zero injection nodes and the generation nodes. The active power (MW) and reactive power (MVAr), based on the transformer MVA, the % loading and the load power factor (PF), are given as:

$$P(MW) = \frac{MVA \cdot (Loading\,\%) \cdot PF}{100}$$

$$Q(MVAr) = \frac{MVA \cdot (Loading\,\%) \cdot \sqrt{1 - PF^2}}{100}$$

Noisy measurements are generated by adding Gaussian error to the true measurements as follows:

$$z_i^{meas} = z_i^{true} + rand \times \sigma_i$$

where z_i^{meas} is the measured or assumed value, z_i^{true} is the true value (obtained from a load-flow solution), $rand$ is a $\mathcal{N}(0,1)$ random number, and σ_i is the standard deviation of the measurement error. Assuming that $\mu_i = z_i^{true}$ is the mean value of the ith measurement, then a $\pm 3\sigma_i$ deviation around the mean covers about 99.7% of the Gaussian curve. Hence, for a given % of maximum measurement error about the mean μ_i, standard deviation σ_i is given by [5]:

$$\sigma_i = \frac{\mu_i \times error\%}{300} = \frac{z_i^{true} \times error\%}{300}$$

We assume an error 1% for voltage measurements, 3% for power flow and injection measurements, 15% for load injection measurements, and 0.5% for CB pseudo measurements. As higher weights indicate more accurate measurements, the past data will be given lower weights and recent data are given higher weights. A gross error on the ith measurement is simulated as:

$$z_i^{meas} = z_i^{true} \pm b_i \sigma_i$$

where multiplier b_i? 3.

The measurement system consists of:

- 55 V magnitude measurements at slack bus and DG nodes (*near real-time*)
- 2 pairs of P/Q flow measurements (*real-time*), at all lines originating at the slack bus
- 54 pairs of P/Q injection measurements (*near real-time*) at DG sites.
- 137 pairs of P/Q loads (*pseudo*) at MV nodes
- 182 pairs of P/Q zero injections (*perfect*)

According to the above measurement configuration, the measurement redundancy $r = \frac{m}{n} = 1.07$, where $m = 805$ is the total number of measurements, $N = 374$ is the total number of nodes and $n = 2N - 1 = 747$ is the number of states. This redundancy is low and the error filtering capability of the state estimator will be also low. To zero injections are assigned much larger confidence than regular measurements.

APPENDIX C. Measurement model

The measurement vector includes the branch active and reactive power flows, the bus active and reactive power injections, the bus voltage magnitudes, the circuit breaker active and reactive power flows and statuses, and circuit breaker operational constraints. For a system containing N buses and M circuit breakers, the state vector will have $(2N+3M-1)$ elements: N bus voltage magnitudes, $(N-1)$ phase angles, M circuit breaker active power flows, M circuit breaker reactive power flows, and M circuit breaker statuses, where the phase angle of the reference bus is set equal to 0. The state vector x, assuming that bus 1 is chosen as the reference, will have the following form:

$$x^T = \left[\delta_2 \text{K}\ \delta_N\ \ V_1\ V_2 \text{K}\ V_N\ \ P_{cb,1}\ P_{cb,2} \text{K}\ P_{cb,M}\ \ Q_{cb,1}\ Q_{cb,2} \text{K}\ Q_{cb,M}\ \ s_{cb,1}\ s_{cb,2} \text{K}\ s_{cb,M}\ \right]$$

In order to construct the measurement model of the state estimation problem, we assume the general two-port π-model for a transmission line connecting buses i and j, as shown in Figure 79. For branch $i-j$, its series admittance is defined as $y_{ij} = g_{ij} + jb_{ij}$ and the admittance of the shunt branch connected at bus i is defined as $y_{sij} = g_{sij} + jb_{sij}$. A shunt capacitor or reactor at bus i is defined by $y_i = g_i + j\,b_i$. Load and generation at bus i are modeled as equivalent complex power injections, $\tilde{S}_{Gi}$ and $\tilde{S}_{Di}$, respectively, and therefore have no effect on the network model. Exceptions are constant impedance type loads which are included as shunt admittances for the corresponding buses. The bus voltage phasors at buses i and j are $\tilde{V}_i = V_i \angle \delta_i$ and $\tilde{V}_j = V_j \angle \delta_j$.

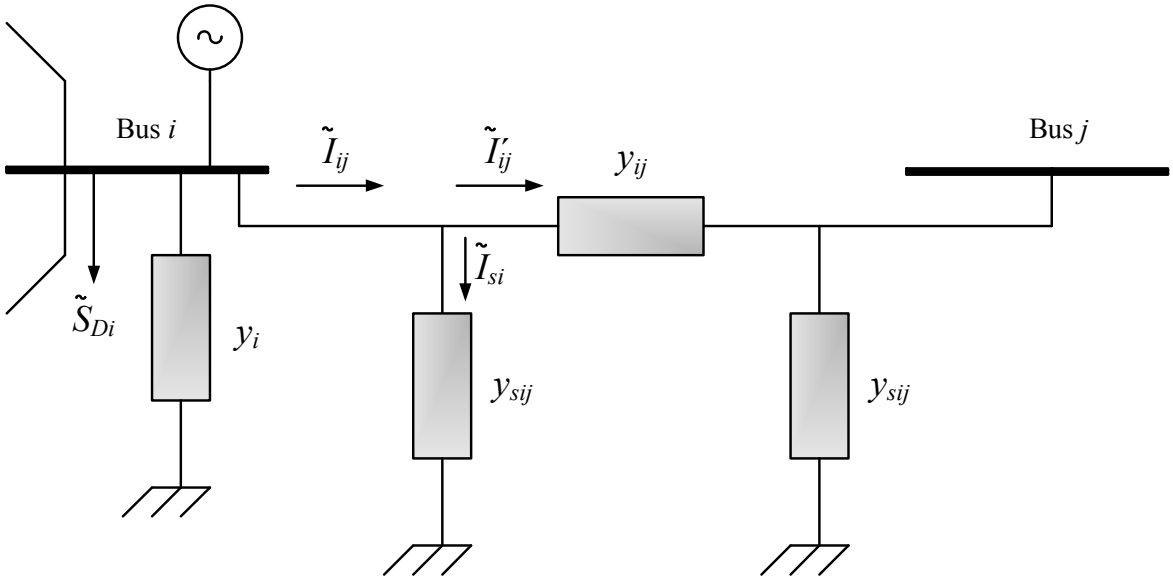

Figure 79 - Two-port π-model of a network branch

The expressions for each of the above types of measurements are given below:

- Real power injection at bus i:

$$P_i = V_i^2 \sum_{j \in a(i)} \left(g_{ij} + g_{sij}\right) + V_i^2 g_i - V_i \sum_{j \in a(i)} V_j \left(g_{ij}\cos\delta_{ij} + b_{ij}\sin\delta_{ij}\right)$$

- Reactive power injection at bus i:

$$Q_i = -V_i^2 \sum_{j \in a(i)} \left(b_{ij} + b_{sij}\right) - V_i^2 b_i - V_i \sum_{j \in a(i)} V_j \left(g_{ij}\sin\delta_{ij} - b_{ij}\cos\delta_{ij}\right)$$

- Real power flow from bus i to bus j:

$$P_{ij} = V_i^2 \left(g_{ij} + g_{sij}\right) - V_i V_j \left(g_{ij}\cos\delta_{ij} + b_{ij}\sin\delta_{ij}\right)$$

- Reactive power flow from bus i to bus j:

$$Q_{ij} = -V_i^2 \left(b_{ij} + b_{sij}\right) - V_i V_j \left(g_{ij}\sin\delta_{ij} - b_{ij}\cos\delta_{ij}\right)$$

- Operational constraints for circuit breaker $i-j$:

$$0_{s_{ij}\delta_{ij}} \equiv 0 = s_{ij}\delta_{ij}, \qquad 0_{s_{ij}V_{ij}} \equiv 0 = s_{ij}V_{ij}$$

$$0_{(1-s_{ij})P_{ij}} \equiv 0 = (1-s_{ij})P_{cb,ij}, \qquad 0_{(1-s_{ij})Q_{ij}} \equiv 0 = (1-s_{ij})Q_{cb,ij}$$

where $a(i)$ is the set of buses connected to bus i, $P_{cb,ij}$ and $Q_{cb,ij}$ are the real and reactive flows on circuit breaker $i-j$, respectively, s_{ij} is the status of circuit breaker $i-j$, $\delta_{ij} = \delta_i - \delta_j$ and $V_{ij} = V_i - V_j$.

The structure of the measurement Jacobian matrix H will be as follows:

$$H = \begin{bmatrix} \frac{\partial P_i}{\partial \delta} & \frac{\partial P_i}{\partial V} & 0 & 0 & 0 \\ \frac{\partial P_{ij}}{\partial \delta} & \frac{\partial P_{ij}}{\partial V} & 0 & 0 & 0 \\ \frac{\partial Q_i}{\partial \delta} & \frac{\partial Q_i}{\partial V} & 0 & 0 & 0 \\ \frac{\partial Q_{ij}}{\partial \delta} & \frac{\partial Q_{ij}}{\partial V} & 0 & 0 & 0 \\ 0 & \frac{\partial V_i}{\partial V} & 0 & 0 & 0 \\ 0 & 0 & \frac{\partial P_{cb,ij}}{\partial P_{cb}} & 0 & 0 \\ 0 & 0 & 0 & \frac{\partial Q_{cb,ij}}{\partial Q_{cb}} & 0 \\ \frac{\partial 0_{s_{ij}\delta_{ij}}}{\partial \delta} & 0 & 0 & 0 & \frac{\partial 0_{s_{ij}\delta_{ij}}}{\partial s_{cb}} \\ 0 & \frac{\partial 0_{s_{ij}V_{ij}}}{\partial V} & 0 & 0 & \frac{\partial 0_{s_{cb}V_{ij}}}{\partial s_{cb}} \\ 0 & 0 & \frac{\partial 0_{(1-s_{ij})P_{cb,ij}}}{\partial P_{cb}} & 0 & \frac{\partial 0_{(1-s_{ij})P_{cb,ij}}}{\partial s_{cb}} \\ 0 & 0 & 0 & \frac{\partial 0_{(1-s_{ij})Q_{cb,ij}}}{\partial Q_{cb}} & \frac{\partial 0_{(1-s_{ij})Q_{cb,ij}}}{\partial s_{cb}} \\ 0 & 0 & 0 & 0 & \frac{\partial s_{ij}}{\partial s_{cb}} \end{bmatrix}$$

The expressions of partial derivatives for the real (P_{ij}) and reactive (Q_{ij}) flow on transmission line $i-j$, the real (P_i) and reactive (Q_i) injection at bus i, the magnitude (V_i) at bus i, the real ($P_{cb,ij}$) and reactive ($Q_{cb,ij}$) flow on circuit breaker $i-j$, and the circuit breaker operational constraints and status ($0_{s_{ij}\delta_{ij}}$, $0_{s_{ij}V_{ij}}$, $0_{(1-s_{ij})P_{ij}}$, $0_{(1-s_{ij})Q_{ij}}$, and s_{ij}), with respect to state variables (bus voltage angles and magnitudes, real and reactive power flows through circuit breakers, and circuit breaker statuses), are given by the following equations:

- Elements corresponding to real power injection measurements:

$$\frac{\partial P_i}{\partial \delta_i} = V_i \sum_{m \in a(i)} V_j \left(g_{ij} \sin \delta_{ij} - b_{ij} \cos \delta_{ij} \right)$$

$$\frac{\partial P_i}{\partial \delta_j} = -V_i V_j \left(g_{ij} \sin \delta_{ij} - b_{ij} \cos \delta_{ij} \right)$$

$$\frac{\partial P_i}{\partial V_i} = 2V_i \sum_{m \in a(i)} \left(g_{ij} + g_{sij} \right) + 2V_i g_i - \sum_{m \in a(i)} V_j \left(g_{ij} \cos \delta_{ij} + b_{ij} \sin \delta_{ij} \right)$$

$$\frac{\partial P_i}{\partial V_j} = -V_i \left(g_{ij} \cos \delta_{ij} + b_{ij} \sin \delta_{ij} \right)$$

$$\frac{\partial P_i}{\partial P_{cb,ij}} = 0, \qquad \frac{\partial P_i}{\partial Q_{cb,ij}} = 0, \qquad \frac{\partial P_i}{\partial s_{ij}} = 0$$

- Elements corresponding to reactive power injection measurements:

$$\frac{\partial Q_i}{\partial \delta_i} = -V_i \sum_{m \in a(i)} V_j \left(g_{ij} \cos \delta_{ij} + b_{ij} \sin \delta_{ij} \right)$$

$$\frac{\partial Q_i}{\partial \delta_j} = V_i V_j \left(g_{ij} \cos \delta_{ij} + b_{ij} \sin \delta_{ij} \right)$$

$$\frac{\partial Q_i}{\partial V_i} = -2V_i \sum_{m \in a(i)} \left(b_{ij} + b_{sij} \right) - 2V_i b_i - \sum_{m \in a(i)} V_j \left(g_{ij} \sin \delta_{ij} - b_{ij} \cos \delta_{ij} \right)$$

$$\frac{\partial Q_i}{\partial V_j} = -V_i \left(g_{ij} \sin \delta_{ij} - b_{ij} \cos \delta_{ij} \right)$$

$$\frac{\partial Q_i}{\partial P_{cb,ij}} = 0, \qquad \frac{\partial Q_i}{\partial Q_{cb,ij}} = 0, \qquad \frac{\partial Q_i}{\partial s_{ij}} = 0$$

- Elements corresponding to real power flow measurements:

$$\frac{\partial P_{ij}}{\partial \delta_i} = V_i V_j \left(g_{ij} \sin \delta_{ij} - b_{ij} \cos \delta_{ij} \right)$$

$$\frac{\partial P_{ij}}{\partial \delta_j} = -V_i V_j \left(g_{ij} \sin \delta_{ij} - b_{ij} \cos \delta_{ij} \right)$$

$$\frac{\partial P_{ij}}{\partial V_i} = -V_j \left(g_{ij} \cos \delta_{ij} + b_{ij} \sin \delta_{ij} \right) + 2V_i \left(g_{ij} + g_{sij} \right)$$

$$\frac{\partial P_{ij}}{\partial V_j} = -V_i \left(g_{ij} \cos \delta_{ij} + b_{ij} \sin \delta_{ij} \right)$$

$$\frac{\partial P_{ij}}{\partial P_{cb,ij}}=0, \qquad \frac{\partial P_{ij}}{\partial Q_{cb,ij}}=0, \qquad \frac{\partial P_{ij}}{\partial s_{ij}}=0$$

- Elements corresponding to reactive power flow measurements:

$$\frac{\partial Q_{ij}}{\partial \delta_i}=-V_i V_j\left(g_{ij}\cos\delta_{ij}+b_{ij}\sin\delta_{ij}\right)$$

$$\frac{\partial Q_{ij}}{\partial V_i}=-V_j\left(g_{ij}\sin\delta_{ij}-b_{ij}\cos\delta_{ij}\right)-2V_i\left(b_{ij}+b_{sij}\right)$$

$$\frac{\partial Q_{ij}}{\partial V_j}=-V_i\left(g_{ij}\sin\delta_{ij}-b_{ij}\cos\delta_{ij}\right)$$

$$\frac{\partial Q_{ij}}{\partial P_{cb,ij}}=0, \qquad \frac{\partial Q_{ij}}{\partial Q_{cb,ij}}=0, \qquad \frac{\partial Q_{ij}}{\partial s_{ij}}=0$$

- Elements corresponding to voltage magnitude measurements:

$$\frac{\partial V_i}{\partial V_i}=1, \qquad \frac{\partial V_i}{\partial V_j}=0, \qquad \frac{\partial V_i}{\partial \delta_i}=0, \qquad \frac{\partial V_i}{\partial \delta_j}=0$$

$$\frac{\partial V_i}{\partial P_{cb,ij}}=0, \qquad \frac{\partial V_i}{\partial Q_{cb,ij}}=0, \qquad \frac{\partial V_i}{\partial s_{ij}}=0$$

- Elements corresponding to circuit breaker pseudo measurements $0_{s_{ij}\delta_{ij}}$:

$$\frac{\partial 0_{s_{ij}\delta_{ij}}}{\partial V_i}=0, \qquad \frac{\partial 0_{s_{ij}\delta_{ij}}}{\partial V_j}=0, \qquad \frac{\partial 0_{s_{ij}\delta_{ij}}}{\partial \delta_i}=s_{ij}, \qquad \frac{\partial 0_{s_{ij}\delta_{ij}}}{\partial \delta_j}=-s_{ij}$$

$$\frac{\partial 0_{s_{ij}\delta_{ij}}}{\partial P_{cb,ij}}=0, \qquad \frac{\partial 0_{s_{ij}\delta_{ij}}}{\partial Q_{cb,ij}}=0, \qquad \frac{\partial 0_{s_{ij}\delta_{ij}}}{\partial s_{ij}}=\delta_{ij}=\delta_i-\delta_j$$

- Elements corresponding to circuit breaker pseudo measurements $0_{s_{ij}V_{ij}}$:

$$\frac{\partial 0_{s_{ij}V_{ij}}}{\partial V_i}=s_{ij}, \qquad \frac{\partial 0_{s_{ij}V_{ij}}}{\partial V_j}=-s_{ij}, \qquad \frac{\partial 0_{s_{ij}V_{ij}}}{\partial \delta_i}=0, \qquad \frac{\partial 0_{s_{ij}V_{ij}}}{\partial \delta_j}=0$$

$$\frac{\partial 0_{s_{ij}V_{ij}}}{\partial P_{cb,ij}}=0, \qquad \frac{\partial 0_{s_{ij}V_{ij}}}{\partial Q_{cb,ij}}=0, \qquad \frac{\partial 0_{s_{ij}V_{ij}}}{\partial s_{ij}}=V_{ij}=V_i-V_j$$

- Elements corresponding to circuit breaker pseudo measurements $0_{(1-s_{ij})P_{ij}}$:

$$\frac{\partial 0_{(1-s_{ij})P_{ij}}}{\partial V_i}=0, \quad \frac{\partial 0_{(1-s_{ij})P_{ij}}}{\partial V_j}=0, \quad \frac{\partial 0_{(1-s_{ij})P_{ij}}}{\partial \delta_i}=0, \quad \frac{\partial 0_{(1-s_{ij})P_{ij}}}{\partial \delta_j}=0$$

$$\frac{\partial 0_{(1-s_{ij})P_{ij}}}{\partial P_{cb,ij}}=(1-s_{ij}), \quad \frac{\partial 0_{(1-s_{ij})P_{ij}}}{\partial Q_{cb,ij}}=0, \quad \frac{\partial 0_{(1-s_{ij})P_{ij}}}{\partial s_{ij}}=-P_{ij}$$

- Elements corresponding to circuit breaker pseudo measurements $0_{(1-s_{ij})Q_{ij}}$:

$$\frac{\partial 0_{(1-s_{ij})Q_{ij}}}{\partial V_i}=0, \quad \frac{\partial 0_{(1-s_{ij})Q_{ij}}}{\partial V_j}=0, \quad \frac{\partial 0_{(1-s_{ij})Q_{ij}}}{\partial \delta_i}=0, \quad \frac{\partial 0_{(1-s_{ij})Q_{ij}}}{\partial \delta_j}=0$$

$$\frac{\partial 0_{(1-s_{ij})Q_{ij}}}{\partial P_{cb,ij}}=0, \quad \frac{\partial 0_{(1-s_{ij})Q_{ij}}}{\partial Q_{cb,ij}}=(1-s_{ij}), \quad \frac{\partial 0_{(1-s_{ij})Q_{ij}}}{\partial s_{ij}}=-Q_{ij}$$

- Elements corresponding to circuit breaker status measurements:

$$\frac{\partial s_{ij}}{\partial V_i}=0, \quad \frac{\partial s_{ij}}{\partial V_j}=0, \quad \frac{\partial s_{ij}}{\partial \delta_i}=0, \quad \frac{\partial s_{ij}}{\partial \delta_j}=0$$

$$\frac{\partial s_{ij}}{\partial P_{cb,ij}}=0, \quad \frac{\partial s_{ij}}{\partial Q_{cb,ij}}=0, \quad \frac{\partial s_{ij}}{\partial s_{ij}}=1$$

APPENDIX D. State estimation quality indices

The state estimation quality indices related to accuracy and performance of the state estimation methodology are described in [57], [58]. These indices express the deviations of the estimated network quantities with regard to their true values. Let define by *L* and *N* the number of network branches and buses respectively.

Accuracy – It is desired that estimated quantities be as close as possible to their true values. Accuracy KPIs are defined by choosing a power flow solution quantity of interest and defining a norm-like calculation on the difference between the "true" value (derived from the power flow solution) and the "estimated" value (derived from the state estimation solution) or the "measured" value (derived from measuring devices or forecasting tools).

– KPIs which measure the accuracy of active (*Pf*) and reactive (*Qf*) branch power flows:

1-norm	$\sum_{j=1}^{L}\left\|Pf_j^{true}-Pf_j^{est}\right\|$	
2-norm (Euclidean norm)	$\sum_{j=1}^{L}\left(Pf_j^{true}-Pf_j^{est}\right)^2$	$\sum_{j=1}^{L}\left(Qf_j^{true}-Qf_j^{est}\right)^2$
infinity norm	$\max_{j=1,K,L}\left\|Pf_j^{true}-Pf_j^{est}\right\|$	$\max_{j=1,K,L}\left\|Qf_j^{true}-Qf_j^{est}\right\|$

– KPIs which measure the accuracy of active (*Pi*) and reactive (*Qi*) bus power injections:

1-norm	$\sum_{j=1}^{N}\left\|Pi_j^{true}-Pi_j^{est}\right\|$	$\sum_{j=1}^{N}\left\|Qi_j^{true}-Qi_j^{est}\right\|$
2-norm (Euclidean norm)	$\sum_{j=1}^{N}\left(Pi_j^{true}-Pi_j^{est}\right)^2$	$\sum_{j=1}^{N}\left(Qi_j^{true}-Qi_j^{est}\right)^2$
infinity norm	$\max_{j=1,K,N}\left\|Pi_j^{true}-Pi_j^{est}\right\|$	$\max_{j=1,K,N}\left\|Qi_j^{true}-Qi_j^{est}\right\|$

– The norm KPI of the error of the state estimate captures the effect of both voltage magnitude and angle errors:

$$Macc_V=\left\|\overline{V}^{error}\right\|_2=\left(\sum_{j=1}^{N}\left|\overline{V}_j^{true}-\overline{V}_j^{est}\right|^2\right)^{\frac{1}{2}}$$

where $\overline{V}_j^{true}$ and $\overline{V}_j^{est}$ is the true and estimated complex phasor voltage at the jth bus.

– Error Estimation Index (EEI):

$$EEI = \sum_{i=1}^{N} \left(\frac{z_i^{true} - z_i^{est}}{\sigma_i} \right)^2$$

– KPIs which determine the ability of the state estimator to accurately discern active and reactive power flow and injection measurements:

$$PIP_f = \frac{\sum_{j=1}^{L} \left(Pf_j^{true} - Pf_j^{est} \right)^2}{\sum_{j=1}^{L} \left(Pf_j^{true} - Pf_j^{meas} \right)^2} \qquad PIQ_f = \frac{\sum_{j=1}^{L} \left(Qf_j^{true} - Qf_j^{est} \right)^2}{\sum_{j=1}^{L} \left(Qf_j^{true} - Qf_j^{meas} \right)^2}$$

$$PIP_i = \frac{\sum_{j=1}^{N} \left(PI_j^{true} - PI_j^{est} \right)^2}{\sum_{j=1}^{N} \left(PI_j^{true} - PI_j^{meas} \right)^2} \qquad PIQ_i = \frac{\sum_{j=1}^{N} \left(QI_j^{true} - QI_j^{est} \right)^2}{\sum_{j=1}^{N} \left(QI_j^{true} - QI_j^{meas} \right)^2}$$

For good estimation, the estimate of each flow will lie closer to the true than will the measured value and the entire metric will be less than one.

Performance – The performance of the estimator determines its capability to provide a stable solution in reasonable and predictable time to be used by other applications in the control center. The following KPIs quantify the performance of the state estimator to converge.

$$Mconv_{obj} = \left| 1 - \frac{J^{k_{term}}}{J^{k_{term}-1}} \right|$$

$$Mconv_V = \max_{i \in N} \left| 1 - \frac{V_i^{k_{term}}}{V_i^{k_{term}-1}} \right|$$

$$Mconv_\delta = \max_{i \in N} \left| \delta_i^{k_{term}} - \delta_i^{k_{term}-1} \right|$$

where k_{term} denotes the terminal iteration of the state estimation algorithm

The metric $Mconv_{obj}$ measures the relative change in objective function value J at the last iteration, while the metric $Mconv_V$ and $Mconv_\delta$ measure the largest final relative change in bus voltage magnitude and angle, respectively, over the network buses. Note that $Mconv_\delta$ uses the absolute difference to avoid problems when the angle is near zero, which will occur near the system reference bus.

References

1. A. Monticelli, State Estimation in Electric Power Systems: A Generalized Approach, Boston: Kluwer Academic Publishers, 1999.
2. A. Abur and A. G. Exposito, Power System State Estimation – Theory and Implementation, New York, Marcel Dekker, Inc., 2004.
3. V. Thornley, N. Jenkins, and S. White, “State estimation applied to active distribution networks with minimal measurements”, in Proc. 5-th PSCC Conf., Liege, Aug. 2005.
4. I. Cobelo, A. Shafiu, N. Jenkins, and G. Strbac, “State estimation of networks with distributed generation”, Euro. Trans. Electr. Power, vol. 17, pp. 21–36, 2007.
5. R. Singh, B. C. Pal, and R. A. Jabr, “Choice of estimator for distribution system state estimation”, IET Gener. Transm. Distrib., vol. 3, no. 7, pp. 666–678, 2009.
6. K. Samarakoon, J. Wu, J. Ekanayake, N. Jenkins, “Use of delayed smart meter measurements for distribution state estimation”, IEEE PES General Meeting, 2011, pp. 1–6.
7. G. N. Korres, N. D. Hatziargyriou, P. J. Katsikas, “State estimation in multi-microgrids”, European Transactions on Electrical Power, Special Issue: Microgrids and Energy Management, Vol. 21, No. 2, pp. 1178-1199, March 2011.
8. H. Wang, N. N. Schulz, “Using AMR data for load estimation for distribution system analysis”, Electric Power Systems Research, vol. 76, pp. 336–342, 2006.
9. M. Wache, D. C. Murray, “Application of synchrophasor measurements for distribution networks”, IEEE PES General Meeting, 2011, pp. 1–4.
10. M. Paolone, A. Borghetti, C. A. Nucci, “On the measurement of synchrophasors in active distribution power networks”, IEEE PES ISGT Europe, 2011.
11. G. N. Korres, N. M. Manousakis, State estimation and bad data processing for systems including PMU and SCADA measurements, Electr. Power Syst. Res. 81 (2011) 1514–1524.
12. M. Z. Degefa, R. J. Millar, M. Koivisto, M. Humayun, M. Lehtonen, “Load flow analysis framework for active distribution networks based on smart meter reading system”, Engineering, vol. 5, pp. 1–8, Oct. 2013.
13. H. Ku-Long, Y.-Y. Hsu, and Y. Chien-Chuen, "Short term load forecasting using a multilayer neural network with an adaptive learning algorithm," IEEE Trans. Power Syst., vol. 7, pp. 141-149, 1992.
14. V. Miranda, J. Krstulovic, H. Keko, C. Moreira, and J. Pereira, “Reconstructing missing data in state estimation with autoencoders,” IEEE Trans. Power Syst., vol. 27, no. 2, pp. 604–611, May 2012.
15. P. N. Pereira Barbeiro, J. Krstulovic, H. Teixeira, J. Pereira, F. J. Soares, J. P. Iria, “State Estimation in Distribution Smart Grids Using Autoencoders”, PEOCO2014 - 2014 IEEE 8th International Power Engineering and Optimization Conference, Langkawi, The Jewel of Kedah, Malaysia. 24-25 March 2014.

16. S. Haykin, Neural Networks: A Comprehensive Foundation: Prentice Hall PTR, 1998.
17. G. E. Hinton, and R. R. Salakhutdinov, “Reducing the Dimensionality of Data with Neural Networks,” Science, vol. 313, no. 5786, pp. 504-507, July 28, 2006.
18. I. T. Jollife, Principal component analysis, New York: Springer, 2002.
19. N. Japkowicz, S. J. Hanson, and M. A. Gluck, “Nonlinear Autoassociation Is Not Equivalent to PCA,” Neural Computation, vol. 12, no. 3, pp. 531-545, 2000/03/01, 2000.
20. B. Golomb, and T. Sejnowski, "Sex Recognition from Faces Using Neural Networks," Applications of Neural Networks, A. Murray, ed., pp. 71-92: Springer US, 1995.
21. G. W. Cottrell, P. Munro, and D. Zipser, “Learning Internal Representations from Gray-Scale Images: An Example of Extensional Programming,” in Proc. 9th Annu. Conf. Cognitive Science Society, Seattle, WA, 1987.
22. M. K. Fleming, and G. W. Cottrell, “Categorization of faces using unsupervised feature extraction,” in IJCNN International Joint Conference on Neural Networks, 1990, pp. 65-70 vol.2.
23. S. Narayanan, R. J. Marks, II, J. L. Vian, J. J. Choi, M. A. El-Sharkawi, and B. B. Thompson, “Set constraint discovery: missing sensor data restoration using autoassociative regression machines,” in IJCNN '02. Proceedings of the 2002 International Joint Conference on Neural Networks, 2002, pp. 2872-2877.
24. J. Krstulovic, V. Miranda, A. J. A. Simoes Costa, and J. Pereira, “Towards an Auto-Associative Topology State Estimator,” Power Systems, IEEE Transactions on, vol. 28, no. 3, pp. 3311-3318, 2013.
25. B. B. Thompson, R. J. Marks, and M. A. El-Sharkawi, “On the contractive nature of autoencoders: application to missing sensor restoration,” in Neural Networks, 2003. Proceedings of the International Joint Conference on, 2003, pp. 3011-3016 vol.4.
26. V. Miranda, A. R. G. Castro, and S. Lima, “Diagnosing Faults in Power Transformers With Autoassociative Neural Networks and Mean Shift,” Power Delivery, IEEE Transactions on, vol. 27, no. 3, pp. 1350-1357, 2012.
27. V. Miranda, and N. Fonseca, “EPSO - best-of-two-worlds meta-heuristic applied to power system problems,” in Evolutionary Computation, 2002. CEC '02. Proceedings of the 2002 Congress on, 2002, pp. 1080-1085.
28. V. Miranda, and N. Fonseca, “EPSO - evolutionary particle swarm optimization, a new algorithm with applications in power systems,” in IEEE/PES Transmission and Distribution Conference and Exhibition, Asia Pacific, 2002, pp. 745-750.
29. A. G. Madureira, and J. A. Peças Lopes, “Coordinated voltage support in distribution networks with distributed generation and microgrids,” IET Renewable Power Generation, vol. 3, no. 4, pp. 439-454, 2009.
30. G.N. Korres, G.C. Contaxis, "Identification and Updating of Minimally Dependent Sets of Measurements in State Estimation", IEEE Trans. Power Syst., vol. 6, no. 3, pp. 999-1005, Aug. 1991.

31. M. Shahidehpour, Y. Wang, Communication and Control in Electric Power Systems: Applications of Parallel and Distributed Processing, Wiley–IEEE Press, New Jersey, 2003, July.
32. M. M. Nordman, M. Lehtonen, “Distributed agent-based state estimation for electrical distribution networks”, IEEE Trans. on Power Syst., vol. 20, no. 2, pp. 652–658, May 2005.
33. A. Gomez-Exposito, A. Abur, A. de la Villa Jaen, C. Gomez-Quiles, A multilevel state estimation paradigm for smart grids, in: Proc. of the IEEE 99 (June (6)) (2011) 952–976.
34. A. Gomez-Exposito, A. de la Villa Jaen, C. Gomez-Quiles, P. Rousseaux, T. Van Cutsem, A taxonomy of multi-area state estimation methods, Electr. Power Syst. Res. 81 (2011) 1060–1069.
35. G. N. Korres, “A distributed multi-area state estimation”, IEEE Trans. on Power Syst., vol. 26, vol. 1, pp. 73–84, Feb. 2011.
36. L. Xie, D.-H. Choi, S. Kar, and H. V. Poor, Fully distributed state estimation for wide-area monitoring systems, IEEE Trans. Smart Grid 3 (February (3)) (2012) 1154–1169.
37. G. N. Korres, A. A. Tzavellas, E. Galinas, “A distributed implementation of multi-area power system state estimation on a cluster of computers”, Electric Power Systems Research, Vol. 102, pp. 20–32, 2013.
38. yWorks GmbH. The diagramming company. www.yworks.com, 2009.
39. George Karypis and Vipin Kumar. METIS A Software Package for Partitioning Unstructured Graphs, Partitioning Meshes, and Computing Fill-Reducing Orderings of Sparse Matrices Version 4.0, 1998.
40. Bruce Hendrickson and Robert W. Leland. The Chaco User's Guide _ Version 2.0, 1995.
41. Chris Walshaw. The serial JOSTLE librairy user guide : Version 3.0, 2002.
42. François Pellegrini. Scotch and LibScotch 5.1 User's Guide, 2008.
43. RF Fowler and C Greenough. RALPAR - RAL Mesh Partitioning Program: Version 2.0, 1997.
44. A. Abur, H. Kim, and M. Celik, “Identifying the unknown circuit breaker statuses in power networks,” IEEE Trans. Power Syst., vol.10, pp. 2029–2035, Nov. 1995.
45. K. A. Clements and A. S. Costa, “Topology error identification using normalized Lagrange multipliers,” IEEE Trans. on Power Syst., vol. 13, no. 2, pp. 347–353, May 1998.
46. A. Monticelli, “Testing equality constraints hypothesis in weighted least squares state estimators,” IEEE Trans. Power Syst., vol. 15, no. 3, pp. 950–954, Aug. 2000.
47. J. M. C. Pereira, “A state estimation approach for distribution networks considering uncertainties and switching”, Doctoral dissertation, FEUP, Portugal, July 2001.

48. G. N. Korres, P. J. Katsikas, "Identification of circuit breaker statuses in WLS state estimator", IEEE Trans. on Power Systems, Vol. 17, No. 3, pp. 818-825, August 2002.

49. E. M. Lourenço, A. J. A. Simões Costa, and K. A. Clements, "Bayesian based hypothesis testing for topological error identification in generalized state estimation," IEEE Trans. Power Syst., vol. 19, no. 2, pp. 1206–1215, May 2004.

50. E. Caro, A. J. Conejo, A. Abur, "Breaker status identification," IEEE Trans. Power Syst., vol. 25, no.2, pp. 694–702, May 2010.

51. R. Singh, E. Manitsas, B. C. Pal, G. Strbac, "A recursive Bayesian approach for identification of network configuration changes in distribution system state estimation", IEEE Trans. Power Syst., vol. 25, no. 3, pp. 668–675, Aug. 2010.

52. G. N. Korres, N. M. Manousakis, "A state estimation algorithm for monitoring topology changes in distribution systems", Panel Session for State Estimation in Distribution Network, 2012 PES General Meeting, 22-26 July 2012, San Diego, CA, USA, pp. 1-7.

53. A. Shafiu, N. Jenkins, G. Strbac, "Measurement location for state estimation of distribution networks with generation", Proc. Inst. Elect. Eng., Gen., Transm., Distrib., vol. 152, no. 2, pp. 240–246, Mar. 2005.

54. R. Singh, B. C. Pal, R. B. Vinter, "Measurement placement in distribution system state estimation", IEEE Trans. Power Syst., vol. 24, no. 2, pp. 668–675, May 2009.

55. R. D. Zimmerman, C. E. Murillo-Sanchez, and R. J. Thomas, "Matpower: Steady-state operations, planning and analysis tools for power systems research and education", IEEE Transactions on Power Systems, vol. 26, no. 1, pp. 12-19, Feb. 2011.

56. PTI Load Flow Data Format. [Online]. Available: https://www.ee.washington.edu/research/pstca/formats/pti.txt

57. "Metrics for determining the impact of phasor measurements on power system state estimation", KEMA, 2006.

58. P. C. Vide, F. P. M. Barbosa, J. A. B. Carvalho, "Metric indices for performance evaluation of a mixed measurement based state estimator", Power Engineering and Electrical Engineering, Vol. 11, No. 2, 2013.

59. C. Gouveia, D. Rua, F. Ribeiro, C. L. Moreira, and J. A. P. Lopes, "INESC porto experimental smart grid: Enabling the deployment of EV and DER," in PowerTech (POWERTECH), 2013 IEEE Grenoble, 2013, pp. 1-6.

60. A. A. Augusto, J. Pereira, and V. Miranda, "Selection of the most relevant measurements for state estimation under information theoretic criteria," in PMAPS 2014, Durham, England, 2014.